Resolution of enantiomers of chiral compounds using crystallization processes: from fundamental studies to process development

Dissertation

zur Erlangung des akademischen Grades

Doktoringenieurin

(Dr.-Ing.)

von M.Sc., Francesca, Cascella

geb. am 3. April 1991 in Barletta

genehmigt durch die Fakultät für Verfahrens- und Systemtechnik der Otto-von-Guericke-Universität Magdeburg

Promotionskommission:	Prof. Dr.-Ing., Andreas, Seidel-Morgenstern
	Prof. Dr., Adrian Evan, Flood
	Dr., Gérard, Guillamot
	apl. Prof. Dr. rer. nat., Heike, Lorenz

eingereicht am: 27. Mai 2021

Promotionskolloquium am: 1. Oktober 2021

Abstract

Chirality appears as a unifying characteristic of our macroscopic and microscopic environment. The fact that the biomolecules of living organisms are chiral has profound implications on the application of chiral bioactive compounds, such as pharmaceuticals, agrochemicals or flavors and fragrances. It is known that the enantiomers of bioactive molecules can exhibit different biological activity. This leads, in some cases, to harmful consequences for the living system. Therefore, the isolation of single enantiomers of chiral molecules is of major concern within the pharmaceutical, food and agrochemical sectors and has increasingly received attention within the scientific community. Among the known methods exploitable for the resolution of chiral compounds, crystallization-based processes are considered simple, cost-efficient and industrially scalable. The selective crystallization of single enantiomers from a supersaturated solution at eutectic composition is known as preferential crystallization. When applied on conglomerate forming systems, this technique allows producing a single enantiomer starting from a solution at racemic composition.

This thesis provides results of a comprehensive experimental study on the applicability of crystallization processes for the production of pure enantiomers of pharmaceutically relevant compounds. The thesis presents results of investigations carried out with three chiral model compounds. The study includes the experimental determination of the solid-liquid equilibria, such as binary melt phase diagrams and ternary solubility phase diagrams, as well as investigations on the solid-state properties of the model compounds. Based on the determined specific fundamental thermodynamic and kinetic properties, different variants of the preferential crystallization processes have been designed and performed. Various experimental conditions have been applied and crystallizer configurations have been exploited, such as a single stirred tank, a coupled configuration using two stirred tanks and a continuously operating tubular fluidized bed crystallizer. The crystallization processes have been evaluated and compared in terms of their productivity and yield, as well as of the chiral purity of the products collected.

The overall goal of the thesis was to identify and assess advantageous and limiting compound specific characteristics for the selection of crystallization conditions to achieve efficiently enantioseparation.

Kurzzusammenfassung

Chiralität tritt als gemeinsames Merkmal unserer makroskopischen und mikroskopischen Umgebung auf. Die Tatsache, dass Biomoleküle lebender Organismen chiral sind, hat tiefgreifende Auswirkungen auf die Anwendung chiraler bioaktiver Verbindungen wie Pharmazeutika, Agrochemikalien sowie Aromen und Duftstoffe. Es ist bekannt, dass Enantiomere bioaktiver Moleküle unterschiedliche biologische Aktivitäten haben können. Dies führt in einigen Fällen zu schädlichen Folgen für den lebenden Organismus. Daher ist die Isolierung einzelner Enantiomere chiraler Moleküle im Pharma-, Lebensmittel- und Agrochemiesektor von großer Bedeutung und hat in der Wissenschaft zunehmend an Beachtung gewonnen. Unter den bekannten Verfahren, die zur Trennung chiraler Verbindungen verwendet werden können, werden kristallisationsbasierte Verfahren als einfach, kostengünstig und industriell skalierbar angesehen. Die selektive Kristallisation einzelner Enantiomere aus einer übersättigten Lösung mit eutektischer Zusammensetzung ist als Bevorzugte Kristallisation bekannt. Angewandt auf konglomerat-bildende Systeme ermöglicht diese Technik die Gewinnung des gewünschten Enantiomers durch Animpfen aus einer Lösung mit racemischer Zusammensetzung.

Diese Arbeit liefert eine umfassende experimentelle Studie zur Anwendbarkeit von Kristallisationsverfahren zur Gewinnung von reinen Enantiomeren pharmazeutisch relevanter Verbindungen. Experimentelle Untersuchungen wurden anhand von drei chiralen Modellverbindungen durchgeführt. Diese umfassten die experimentelle Bestimmung der Fest-flüssig-Gleichgewichte, d.h. der binären Schmelzphasendiagramme und der ternären Löslichkeitsphasendiagramme, sowie die Untersuchung der Festkörpereigenschaften der Modellverbindungen. Basierend auf experimentell bestimmten grundlegenden thermodynamischen und kinetischen Informationen wurden verschiedene Varianten von Bevorzugten Kristallisationsprozessen entworfen und durchgeführt. Unterschiedliche experimentelle Bedingungen wurden für Kristallisationsprozesse unter Einsatz eines einzelnen Rührkessels, zweier gekoppelter Rührkessel und eines kontinuierlich betriebenen rohrförmigen Wirbelschichtkristallisators realisiert. Die Kristallisationsprozesse wurden hinsichtlich der erzielten Produktivität, Ausbeute sowie der chiralen Reinheit der erhaltenen Produkte bewertet und miteinander verglichen.

Ziel der Arbeit war es, vorteilhafte und limitierende substanzspezifische Eigenschaften für die Auswahl der Kristallisationsbedingungen und Prozesskonfigurationen zu identifizieren und zu bewerten, um eine effiziente Enantiomerentrennung zu ermöglichen.

Contents

Chapter 1. Introduction

1.1 Isolation of pure enantiomers: needs and state of the art

The chiral nature of the biological molecules has profound implications in the field of agrochemistry, food chemistry, flavors and fragrances and in particular for the pharmaceutical industry. The fact that different configurations of a chiral pharmaceutical ingredient can have different pharmacological and toxicological activities when they interact with the biological environment is widely recognized.[1] In the past, analytical techniques were not as developed as they are today and drugs were used in their racemic form for the treatment of diseases.[2] The tragedy associated with the case of the Thalidomide has stimulated for the years afterward the research to move from racemates to single enantiomers.[3] In fact, in the late 1980s,[4] the regulatory authorities have issued strict requirements on new drugs, that only enantiopure drugs must be marketed and each enantiomer should be studied separately for its biological activity. The methods currently known to isolate pure enantiomers are mainly based on two strategies, *i.e.* the asymmetric synthesis and the resolution methods. The asymmetric synthesis enables the production of pure enantiomeric form of a chiral molecule by means of chiral reagents, substrates or catalysts.[5–8] Although great progress has been made in synthetic chemistry, asymmetric synthetic routes remain expensive and with low overall yield. Consequently, the applicability of selective reactions for the production of pure enantiomers on an industrial scale is still limited.[9] For this reason, scientific interest has been directed in developing novel technologies and using cost-efficient, straightforward and widely applicable enantioselective separation processes. The exploitation of the modern technologies

makes the resolution techniques effective at both analytical and industrial scale, therefore they are better applicable on an industrial level. Over the last decade, various resolution techniques have been applied to a remarkable range of chiral molecules. Four main resolution methods can be identified, namely kinetic resolution, chromatographic methods, membrane-based separations and crystallization methods.

Kinetic resolution

In kinetic resolution, both enantiomers of a racemic substrate react in an asymmetric environment at different rates, to give the enantiomeric products.[10,11] The racemate is subjected to a reaction using a chiral agent and one of the enantiomers of the racemate reacts more quickly than the other. An intrinsic limitation of this approach is that the maximum yield of one enantiomeric product can never exceed 50 %. In order to overcome this limitation, a re-iterative process of enantiomeric separation, racemization, and kinetic resolution can be performed, hence allowing the conversion of a racemic mixture into a single enantiomer through an *in situ* racemization. This combinatorial process is defined as dynamic kinetic resolution.[11–13]

Chromatographic methods

Chromatographic methods can be classified as direct and indirect. The first type exploits either a chiral stationary phase or a chiral mobile phase. The difference in stability between the diastereomeric complexes leads to a difference in retention time between the enantiomers. In the indirect approach, diastereomeric compounds are formed prior to the separation procedure. In these compounds, the enantiomers are covalently bonded to a chiral reagent. These diastereomers have different physical and chemical properties and can therefore usually be separated on a routine, non-chiral stationary phase.[14,15] The instrumentation improvements and the increasing choice of commercially available chiral stationary phases have enabled the large development of the chromatographic resolution. The chromatographic techniques for chiral separation include, gas chromatography,[16–18] supercritical fluid chromatography,[19] liquid chromatography,[20,21] thin layer chromatography[22,23] and simulated moving bed chromatography.[24,25] A major drawback of those methods is that chromatographic processes are expensive and therefore there is an interest in developing alternative technologies.

Membranes

The membrane-based separation methods can be classified as direct methods, using enantioselective chiral membranes and assisted-methods, in which a non-enantioselective membrane separation is combined with other chiral recognition approaches such as enzymatic resolution.[26,27] In direct membrane-based separation methods, the enantioselective membrane acts as a technical tool, which enables the resolution of enantiomers. The membrane is able to resolve optical isomers due to the chiral properties such as chiral recognition sites.[28]

Crystallization methods

Resolution by crystallization is considered as a simple and economic technique since it does not involve particularly sophisticated technologies. The selection, design and optimization of crystallization techniques require knowledge regarding the solid–liquid equilibria of the chiral system which have to be determined experimentally.[29] Productive modes of operation can be identified from the specific type of phase diagram.[30] Organic chiral molecules are classified into conglomerates, racemic compound forming systems and solid solutions and the selection of their resolution technique depends upon the type of crystalline enantiomeric system. One way to perform the resolution of enantiomers *via* crystallization is performing the so-called classical resolution, using a foreign chiral element, *i.e.* the resolving agent, to form diastereomers.[31,32] Those are then separated by achiral methods and finally decomposed to yield the pure enantiomers. A direct crystallization approach consists in the selective crystallization of one enantiomeric form of the chiral molecule from a solution containing both of the enantiomers at racemic or enriched composition without the need for any chiral auxiliary.[33,34] Preferential crystallization is a direct method, which can be applied when the chiral molecule crystallizes in two mechanically separable enantiomeric forms. The basic underlying idea of this technique is that crystallization can enable the separation due to differences in the crystallization kinetics of the enantiomers. By seeding a supersaturated solution with the desired enantiomer, the growth of crystals of the desired molecule and its consumption from the liquid phase occur, while the impurity only starts crystallizing when its supersaturation level is sufficiently high to start nucleation, the so-called entrainment effect.

1.2 Objective and structure of the thesis

Motivated by the relevance and the need for chiral resolutions as well as by the fundamental role of solid-liquid equilibria in the crystallization technology, the present thesis intends to extend the knowledge of the fundamental properties and the crystallization behavior of chiral systems, which are relevant for the pharmaceutical industry. The thesis provides a systematic investigation on the applicability of preferential crystallization as technique to isolate pure enantiomers of chiral molecules. The studied compounds are of particular relevance for the pharmaceutical industry, being one an active pharmaceutical ingredient marketed for cough remedies and the other a precursor of a drug, which is largely marketed. The thesis covers the main steps related to the development of crystallization processes for enantioseparation purposes. Starting from the determination of the fundamental properties of the studied chiral systems, such as solubility, metastability in chosen solvents as well as their solid-state properties, the crystallization runs have been designed choosing appropriate supersaturation conditions. In particular, a range of experimental conditions have been applied and different crystallizer configurations have been exploited for the experimental resolution runs, *i.e.* a single stirred tank, a coupled configuration for the so-called coupled preferential crystallization and dissolution approach as well as a tubular fluidized bed crystallizer. The thesis addresses not only the fundamental investigations for designing crystallization processes, but also a range of application-oriented aspects such as monitoring methodologies and the performance assessment of the resolution runs. A description of appropriate crystallization monitoring technologies is provided and the control strategies of the resolution runs are discussed. These have been evaluated in terms of chosen key performance indicators, such as purity of the product collected, as well as productivity and yield, which have been properly defined depending on the type of crystallizer and crystallization approach used. Furthermore, the thesis provides a preliminary investigation on the fundamental technical aspects related to the exploitation of tubular fluidized bed crystallizer in a continuous operation mode.

The thesis is structured as follows:

Chapter 2 provides the fundamental concepts of chirality, crystallization, solid-liquid equilibria as well as an overview of the role of enantiomers in the pharmaceutical industry. A description of the definition of supersaturation as the driving force as well as a graphical representation of its variation during the crystallization process is given. The chapter also describes possible configurations of crystallizers exploitable for resolution purposes.

Focus is set on the applicability of stirred tanks and fluidized bed crystallizers, which have been subjects of the experimental studies. **Chapter 3** provides detailed information on the methods, crystallization setups and experimental conditions used in the present work. The calculation of the essential supersaturation ratio is explained in depth with the aid of graphical representations. Furthermore, a description of the calculation of productivity and yield depending on the configuration of crystallizer exploited is given. The results of the experiments and their interpretation are discussed in **chapter 4**. The chapter is divided in two sections, one for each chiral compound studied and organized based on the increasing complexity of the configuration of crystallizers exploited. In particular, the first section, 4.1, is dedicated to a chiral precursor of the drug Clopidogrel. The experimental investigation covers thermodynamic and resolution aspects, which have not previously investigated for this system. The thermodynamic fundamental properties related to the solid-liquid equilibria of this chiral intermediate are described. Furthermore, a feasibility study on the application of direct crystallization processes for resolution purposes is provided, based on two different crystallization approaches exploited for the first time for this system. Section 4.2 presents the experimental results related to the API guaifenesin, which has been the subject of previous investigations in our laboratories. Compared to the first system studied, a larger investigation has been carried out on guaifenesin, exploiting an additional crystallizer configuration as well as a larger variation of experimental conditions. A qualitative summary of the findings of the two studied systems is given in **chapter 5**. The final section of chapter 5 addresses a further resolution methodology, which is applicable to other enantiomeric systems and is explained in detail in a subsequent section of the thesis. The conclusions and the future research perspectives related to the topics of the thesis are given in **chapter 6.** Finally, the last section, the **annex,** returns to the experimental investigation, describing the novel resolution method mentioned in chapter 5, experimentally applied to the chiral system methionine.

Chapter 2. Theoretical background

The present chapter will provide the fundamental concepts necessary to understand the relevance of the topic addressed in the thesis and the methods used in the experimental work, which will be described in the next chapters. The definition of enantiomers and their significant role in human life as well as in the pharmaceutical industry will be explained in the first part of the chapter. The attention will be then devoted to the description of the crystallization as a physical process as well as to the solid-liquid equilibria of the known crystalline enantiomeric systems. An overview of the resolution methods will be provided with a focus on the crystallization techniques. Finally, the various crystallizer configurations that are mostly exploited for the resolution of pharmaceutically relevant molecules will be described.

2.1 Chirality

The origin of the word chiral is the Greek word *cheir*, which means “hand”. Chirality is a geometrical property of those molecules which are non-superimposable with their mirror image. Chirality manifests itself in both molecules and crystals.[35] The first observation of chiral crystals is attributed to Louis Pasteur (1848). He observed that by the evaporation of a dilute solution of sodium ammonium tartrate racemate, the crystals formed were hemihedral (Figure 2.1a).[36] Such property of the crystals was first called *dissymmetry*. The term *chirality* was coined by Lord Kelvin in his Baltimore lectures given in 1884 and 1893.[37] At a molecular level, chirality can occur due to the presence of at least one asymmetric

carbon, generating left-hand and right-hand versions of the same molecule. The two non-superimposable mirror-image forms of chiral molecules are called enantiomers.

2.1.1 Nomenclature of enantiomers

In order to differentiate enantiomers, different nomenclatures are used. Usually organic molecules are classified as levorotatory (-)-isomers or dextrorotatory (+)-isomers depending on whether they rotate a linear polarized light to the left (-) or to the right (+). An equimolar mixture (50/50) of the two enantiomers of a chiral compound is called a racemic mixture (racemate) and has sign (±), meaning that it does not exhibit optical activity. The second method of differentiation of enantiomers derives from the knowledge of the Cahn–Ingold–Prelog (CIP) sequence rules. It is currently the one recommended by the International Union of Pure and Applied Chemistry (IUPAC) to attribute the absolute configuration of organic molecules.[38]

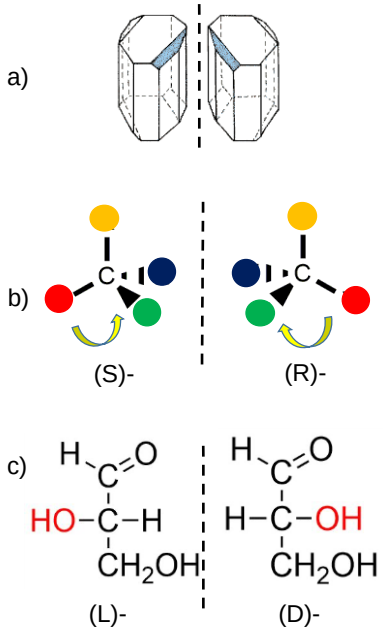

Figure 2. 1 Pair of hemihedral crystals of sodium ammonium tartrate (a). Assignment of the absolute configuration for a fictitious pair of enantiomers with yellow functional group having highest priority and blue functional group lowest priority (b). 2-D Fisher projections for the glyceraldehyde molecule: D (L) enantiomer is represented with the -OH functional group projecting to the right (left) side (c).

Based on the priority assigned to the substituents connected to the stereo-center from 1 (highest priority) to 4 (lowest priority), if the sense of rotation is clockwise and the substituent with lowest priority is the farthest from the observer, the configuration at the stereo-center is considered *(R)*- (from Latin: *Rectus*=right). On the other hand, if the sense of rotation is anti-clockwise, the configuration at the stereo-center is considered *(S)*- (from Latin: *Sinister*=left),[39] as illustrated in Figure 2.1b. In biochemistry, monosaccharides and amino acids are depicted with the L- / D- nomenclature, which derives from the well-known Fisher projections. One aligns a given molecule with the carbon in the highest oxidation state superiorly. At chiral center closest to the bottom, if the substituent (*e.g.* OH) projects to left, the molecule is a L-isomer (Figure 2.1c).[40]

2.1.2 Crystalline enantiomeric systems

Chiral molecules at the crystalline solid state can show different packing of enantiomers within the crystal lattice. Three different categories of enantiomeric systems have been defined by Roozeboom (1899),[41] by the observation of the melting point of the chiral molecules at different enantiomeric compositions, as illustrated in Figure 2.2.[42]

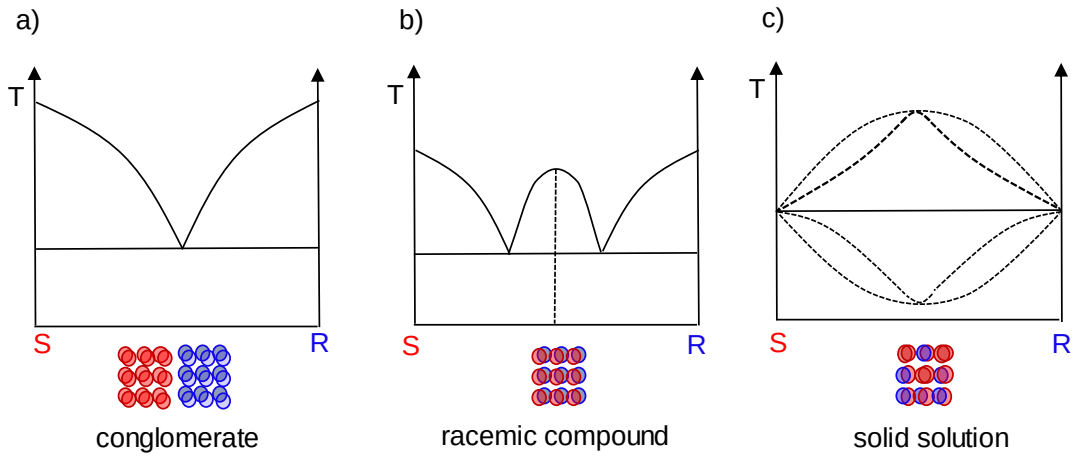

Figure 2. 2 Binary melt phase diagrams of the three known enantiomeric systems: (a) conglomerate, (b) racemic compound and (c) solid solutions. Red and blue full circles represent the two enantiomers within the crystal lattice.

A conglomerate forming system is an equimolar mixture of the two mechanically separable crystalline enantiomers of a compound. This mixture exhibits a characteristic melt phase diagram with lowest melting point at the racemic composition and higher melting point

moving towards the enantiopure composition. Hence, one eutectic at racemic composition is expected for such enantiomeric system (Figure 2.2a). When the two enantiomers coexist in the same unit cell of the crystal lattice in 1:1 ratio in an ordered structure, the system is called racemic compound and exhibits two eutectic points at deviating compositions (Figure 2.2b). Solid solutions are mixtures in which the two enantiomers coexist in the same unit cell in a non-stoichiometric and disordered ratio (also called mixed crystals) (Figure 2.2c). A prerequisite for the enantiomeric resolution *via* preferential crystallization (PC) starting from a solution at racemic composition is that the enantiomeric system belongs to the first category, *i.e.* conglomerate forming systems. Racemic compound forming systems can be resolved *via* PC only if one of the two enantiomers is present in sufficient excess.[43] While solid solutions, at some preconditions, can be resolved *via* fractional crystallization, which consists in several crystallization steps to ensure a certain initial enantiomeric excess.[42,44]

2.1.3 Detection of a conglomerate

Several experimental techniques allow the determination of the enantiomeric solid-state systems. In case of chiral morphology, shape recognition can be used to observe the dissymmetry of two enantiomeric crystals. Pasteur is the pioneer of this method, exploiting tweezers to separate the chiral crystals of sodium ammonium tartrate. Based on the first systematic classification of the enantiomeric systems done by Roozeboom,[41] by observing the melting point of enantiomeric mixtures, the investigation of the melting binary phase diagram is an applicable method to detect conglomerates. However, it is necessary that the system remains stable over the melting event and does not undergo decomposition close to the melting point. Differential Scanning Calorimetry, (DSC) and X-ray Powder Diffraction, (XRPD) can be used for this purpose. The latter, provides fundamental information on the crystal lattice; in fact, it is one of the pivotal techniques used in crystallization. Superimposable XRPD patterns of the racemate and the pure enantiomer of a chiral molecule suggest that the system might be a conglomerate. While, if the two patterns are not identical, further investigations (*i.e.* by means of DSC) are needed in order to determine whether the system is a racemic compound forming system or it forms solid solutions. Another technique applicable for detection of conglomerates is Second Harmonic Generation (SHG). However, it is defined as prescreening technique and it is not error-free.[33] The intensity of the SHG signal relies on the symmetry class to which the

studied system belongs. Centrosymmetric space groups are SHG inactive, while non-centrosymmetric space groups generate a positive SHG signal. As the majority of racemic compounds is known to crystallize in centrosymmetric space groups, they are not expected to exhibit any SHG activity. On the other hand, conglomerate forming systems, which crystallize in a special category of non-centrosymmetric space groups, named the chiral space groups are expected to exhibit a SHG signal.[45–47] Not only solid-state techniques are used to detect conglomerates. Investigations on the solubility ternary phase diagrams are of a special interest for this purpose. The isothermal solubility method, although time consuming, offers not only a screening of conglomerate but also a useful set of data necessary in designing a preferential crystallization process. In case of conglomerates, a V-shaped solubility isotherm with a higher solubility in correspondence of the racemic composition should be observed. Other applicable routes in detecting a conglomerate consist in the comparison of spectroscopic analyses such as Raman, IR or solid-state NMR spectra.

2.1.4 Enantiomers in drug molecules

Chirality is nowadays a top-class subject for academic research as well as for process development in the pharmaceutical, food and agricultural industry.[48] The building blocks of living organisms are made of ordered asymmetric macromolecular units, left-handed amino acids and right-handed sugars, which are able to interact selectively with optical isomers. As enantiomers of drugs can have greatly different affinities at receptor sites, metabolized at different rates, and have different affinities for tissues and protein binding sites,[49] a number of possible scenarios derives from the difference of interaction of the enantiomers in the biological environment. One enantiomer can be more potent than the other as for the case of the Methadone, used as pain reliever, whose *(R)*- enantiomer is more potent than the *(S)*- enantiomer.[50] Examples of adverse activity of the unwanted enantiomers are well known as for the case of the Thalidomide.[51,52] Furthermore, the administration of enantiomers leads to less complex clinical pharmacokinetics than what occurs with the administration of the racemate form, such as smaller doses of medication, simpler and more selective pharmacodynamics profile, less complex pharmacodynamics profile.[53] In view of above, regulatory authorities demands not only that chiral drugs are administered in an optically pure form but also an assessments of the activity of each

enantiomer is required when it comes to the developments of new chiral drugs as a single enantiomer.[54,55]

2.2 Fundamentals of crystallization

2.2.1 Thermodynamics: solutions and solubility

Crystallization is described as a phase change in which a crystalline product is obtained either from a gaseous state or from a condensed state such as molten, amorphous solid state or a solution. Solutions are made up of two or more components of which one is the solvent and the other is the solute(s).[56] There is a variety of ways to express the composition of a solution. If we consider the simple system of a solvent and a solute, its composition may be expressed in terms of mass fraction, mole fraction, or a variety of concentration units. At a given temperature, there is a maximum amount of solute completely soluble in a given amount of solvent. When this maximum is reached, the solution is defined as saturated. The amount of solute required to make a saturated solution at a given condition is called *solubility.* In the majority of cases the solubility increases with increasing temperature, although this feature varies widely from compound to compound.[57]

2.2.2 Supersaturation and metastability

A saturated solution represents the equilibrium condition between the solute in solid state and the solid in solvated state, at a specific temperature. In order for the crystallization event to occur, it is necessary to perturbate such condition, bringing the system out of its equilibrium state. The resulting system is a solution containing more solute than the amount represented by the equilibrium condition, hence exhibiting *supersolubility*; such solution is defined as supersaturated. There are several ways to create supersaturation, depending on the shape of the solubility curve as a function of the temperature. Generally, if the substance exhibits a strong temperature dependency as for the case of many salts and organic substances, the supersaturation is created by cooling.[58] In case of a low temperature dependency as for the sodium chloride in water,[59,60] evaporative crystallization as well as vacuum crystallization might be appropriate. Another way to create supersaturation is the addition of an antisolvent to the saturated solution and it can

be done in combination to either of the two aforementioned operations to reach higher yield.[59] The supersaturation, *S(T)*, is quantified by the difference between the chemical potential of the system in the current state and the chemical potential of the system in the reference (equilibrium) state. As the chemical potential of a system is not easily accessible, the usage of the concentration is preferred, as expressed in Eq. 2.1

$$S(T) = \frac{C}{C^*} \tag{2.1}$$

Where *C* is concentration at the current state, or initial state for the initial supersaturation, and *C** is the concentration at the reference state, or equilibrium state. The two states are schematically represented in Figure 2.3, for a fictitious case of cooling crystallization.

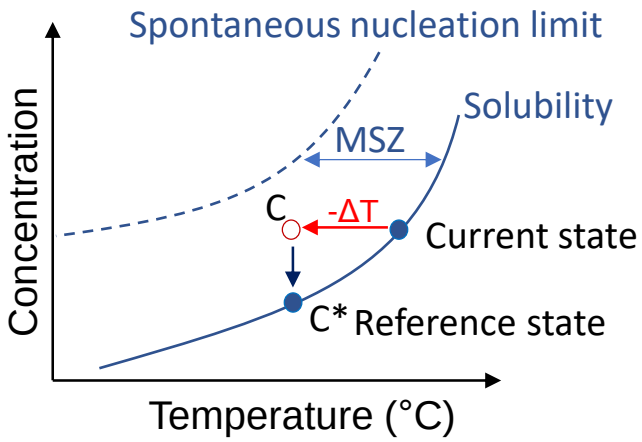

Figure 2. 3 Phase diagram for a case of cooling crystallization. The metastable zone is defined between the solubility and nucleation limit. C and C* represent the two states of the system, which allow quantification of the initial supersaturation ratio.

As shown, the extent of the cooling is done in such a way that the system remains within the so-called metastable zone, where the spontaneous nucleation is improbable for a limited amount of time; however, in the presence of seed crystals, growth is favored.[61] Such region is bounded by two limits, the solubility curve and the nucleation curve, and its width is influenced by a variety of factors such as saturation temperature, rate of supersaturation generation, impurity level, mixing and solution history.[62] By cooling further the solution, hence increasing the supersaturation, the system might exit the metastable zone where spontaneous and uncontrolled nucleation will occur. As the control over the nucleation and growth is crucial to achieve desired properties of the product crystals,

however challenging, understanding the generation of nuclei in solution is fundamental in the contest of industrial crystallization.

2.2.3 Nucleation

A supersaturated solution is a necessary but not sufficient condition to cause crystallization from solution. In order for the crystallization event to take place, the formation of nuclei or solid bodies as center of crystallization must occur.[63] Such formation can be spontaneous or it can be artificially induced. A proper nomenclature allows distinguishing the various ways to induce a nucleation event. The formation of nuclei in absence of any crystalline surface of the solid is defined as *primary nucleation*. This can proceed *homogeneously* when the compound nucleates spontaneously without the interplay of any substrate, which is a rare event since dust particles or reactor walls generally cannot be avoided, or *heterogeneously* if the compound nucleates in the presence of a substrate such as dust particles in solution, which is the majority of primary nucleation events. For a homogeneous nucleation, only clusters having critical size, namely r* will survive and grow, while the crystals with lower size will dissolve. The value of the r* corresponds to the maximum of the total free energy of the nucleation process, ΔG_T. The total free energy is the result of two energetic contributions: an energy cost represented by the surface energy, ΔG_S, and an energy gain, represented by the volume free energy, ΔG_V, as shown in Figure 2.4a. The first increases with the size, as a result of the fact that the molecules need to overcome the surface tension, σ, to create a new surface. On the other hand, the second contribution decreases because when more molecules go to the bulk phase, the system reaches a lower energetic level. As a results of those two contributions, the total free energy presents a maximum, which represents the energetic barrier to create stable clusters within the solution. The surface free energy prevails at low radius of the cluster ($r<r^*$), leading to an initial increase of the total free energy. At higher size of the cluster ($r>r^*$), the growth becomes energetically favored with respect to creation of new surface, therefore the bulk free energy prevails over the surface free energy. Such description of the primary, homogeneous nucleation event is defined as Classical Nucleation Theory (CNT).

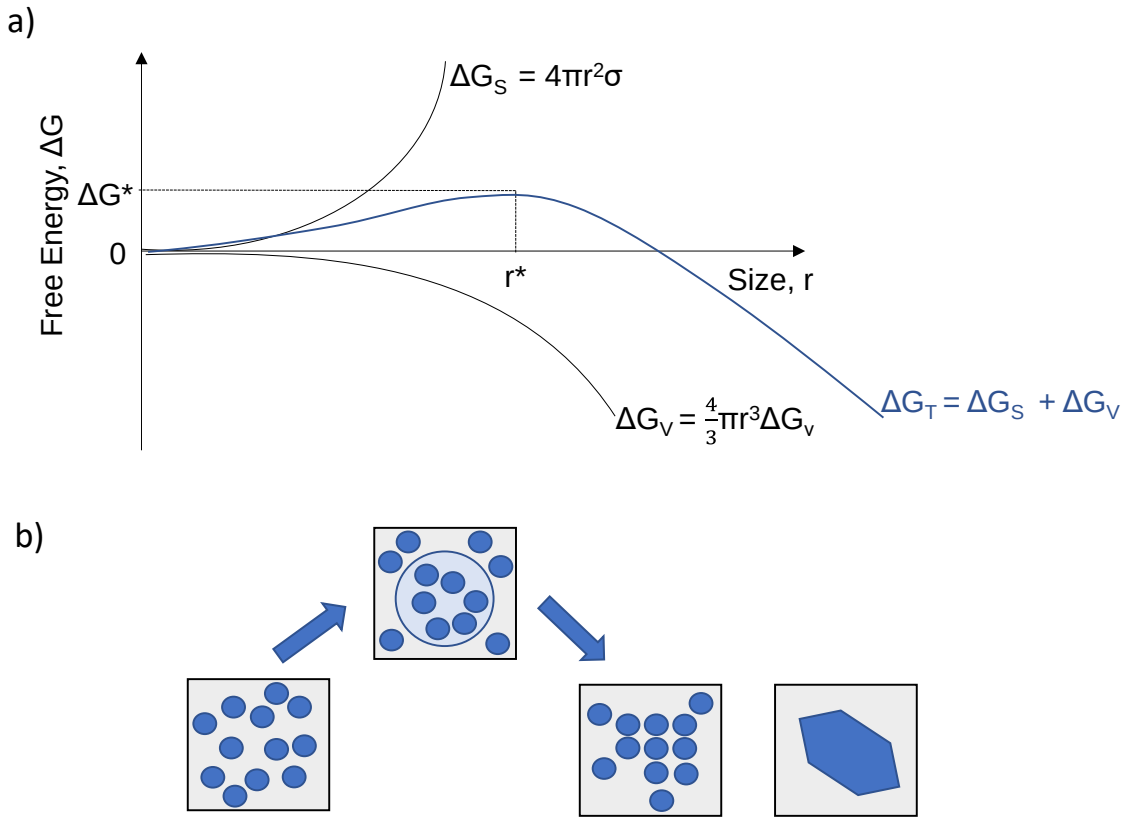

Figure 2. 4 Free Energy diagram for a homogeneous nucleation process (a) and representation of the two-step nucleation model (b).

Nucleation can also occur after the breakage of an existing macroscopic crystal due to the collision with the stirrer or any other surface within the solution. In this case, the event is defined as *secondary nucleation*. When nuclei are formed, their behavior within the supersaturated solution will depend on their size: due to the fluctuation of supersaturation and temperature within the crystallizer, the smaller crystals will not survive as result of the so-called Gibbs-Thomson effect.

However, several limitations of the CNT have been experimentally proved concerning the formation of critical nuclei, as well as the initial cluster shape and subsequent growth. A two-step nucleation theory has been then proposed, for a crystallization from solution, suggesting that in the first stage of nucleation the molecules aggregate to form a fractal cluster and in a second stage, a re-arrangement of the initial aggregate leads to the formation of more compact and ordered structures (Figure 2.4b).[64–66] A clear understanding of the nucleation behavior is an ongoing debate within the crystallization

community. The main challenges rely in the difficulty to experimentally perform monitoring and characterization of the formation of nuclei in solution. However, much interest has been devoted to this field,[67,68] and hopefully in the nearfuture new findings will contribute to explain some of the questions raised in the next chapters.

2.3 Phase rule

A phase is an entity of a material system, which is uniform in chemical composition and physical state. Examples of phases are, oxygen in gaseous state (pure phase), a mixture of oxygen, nitrogen and carbon dioxide (mixed phase); mixtures of two or more miscible liquids or solids are also a one-phase system.[60] For a system at thermodynamic equilibrium, J.W. Gibbs derived an equation that relates the number of independent components *N*, number of phases, *P*, and degree of freedom, *F*, of a system, (Eq. 2.2).

$$P + F = N + 2 \qquad (2.2)$$

Three variables can be considered in a system; temperature, pressure and concentration. The degree of freedom represents the number of the aforementioned variable that can be changed in a system without varying the number of phases. Based on the number of independent component *N*, a system is named unary *N=1*, binary, *N=2*, ternary *N=3* and so on. The number 2 in the Eq. 2.2 represents the two physical variables, temperature and pressure. A system is named univariant, when only one variable can be altered without change the number of phases present, (*F=1*), bivariant when the variable that can be changed are two (*F=2*), invariant when none of the variable can be independently changed without having a change of the number of phases (*F=0*). A graphical representation of the phases in equilibrium in a system is called phase diagram. It is usually represented by plotting a thermodynamic property of a system as a function of a variable such as temperature, pressure or concentration (mole fraction) and so on. It allows to identify the phases that occur and coexist at different conditions and represent the thermodynamic foundation of all crystallization processes.

2.3.1 Solid-liquid equilibria of a binary system

Let us consider a system composed of two components A and B, (*N=2*) at constant pressure. For such a system, the phase rule will be defined as expressed in Eq. 2.3.

$$P + F = 3 \qquad (2.3)$$

This expression means that the maximum number of phases that can exists are three, leaving no degree of freedom (*F=0*); therefore, temperature and composition cannot be changed independently without having a change in the number of phases. This condition occurs at the eutectic point, x_{eu} in Figure 2.5, where all three phases s_A, s_B and l_{AB} are present and the state of the system is named an invariant state, since *F=0*.

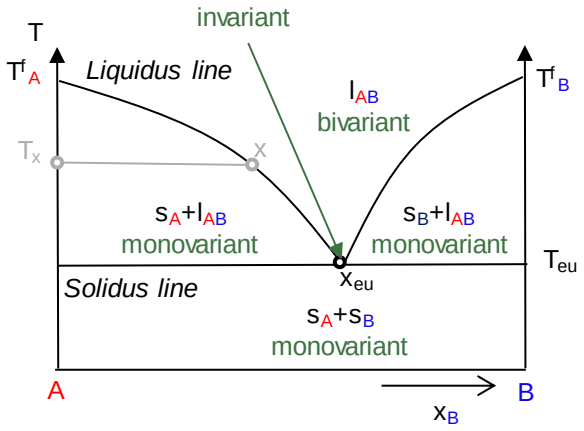

Figure 2. 5 Binary melt phase diagram for two components A and B. Solid and liquid phases within the phase regions are defined by s and l. T^f_A (T^f_B) is the melting temperature of the pure component A (B).

Below the solidus line (Figure 2.5), two phases are stable represented by A and B in the solid state. In this region the composition of the components cannot be changed as they remain pure, therefore one variable is fixed leaving one degree of freedom (*F=1*). Hence, in this region the system is in a monovariant state. In the region between the solidus and liquidus line, two phases are stable, the solid phase of one component (s_A or s_B) and a liquid phase containing both components A and B (l_{AB}). By arbitrarily choosing one temperature, T_x in Figure 2.5, in order to describe the state of the system only one composition can be defined. Therefore, the degree of freedom of the system equals one (*F=1*) and the system is in monovariant state. Above the liquidus line, by choosing one temperature, no composition is fixed in order to describe the state of the system and only one phase is stable (l_{AB}), hence the system is in bivariant state (*F=2*). The system described above refers to two components A and B, which are completely immiscible at the solid state and miscible at the liquid phase. In a chiral system, such property of immiscibility at the solid state is characteristic of a conglomerate forming system, where

A and B correspond to the two enantiomers and the single eutectic x_{eu} is located at the racemic mixture (Figure 2.6a).

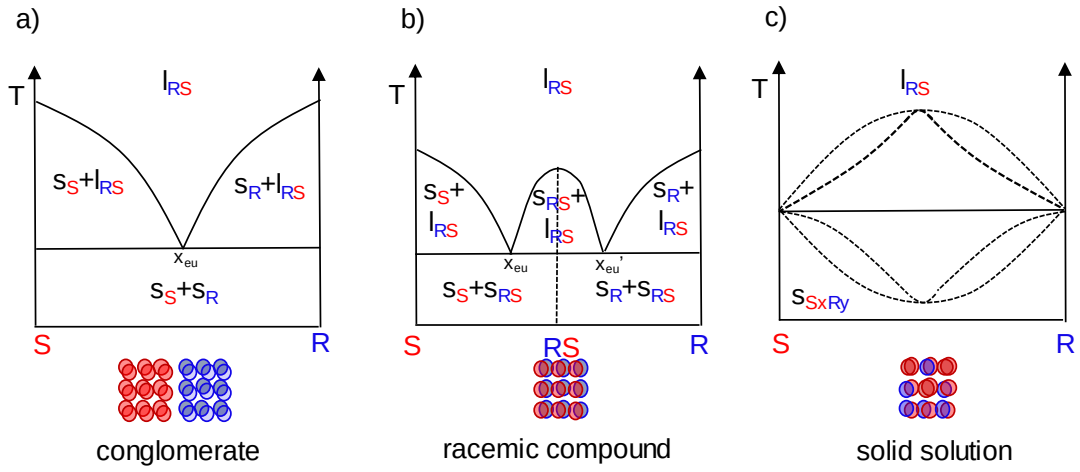

Figure 2. 6 Melt binary phase diagram for a conglomerate (a), racemic compound forming system (b) and solid solutions of an arbitrary chiral system (c). A code color for the two components identifies the enantiomers R and S, s and l identify the phases in equilibrium within each region.

In the case of a racemic compound forming system, the application of the phase rule leads to an additional phase region below the liquidus line at composition $x_{eu}<x<x_{eu'}$. In this two-phase region, a solid phase, s_{RS}, which is a mixture of both of enantiomers incorporated into the crystal lattice, and a liquid phase are in equilibrium (Figure 2.6b). Systems in which the enantiomers are completely miscible at both the solid and the liquid state at any composition are called solid solutions. When the melting point remains unvaried over the composition range, thus the liquidus line is flat, the solid solution is called ideal. On the other hand, as the enantiomers arrange randomly within the crystal lattice (mixed crystals), the liquidus line within the melt binary phase diagram can exhibit a minimum or a maximum melting point (Figure 2.6c).

2.3.2 Solid-liquid equilibria of a ternary system

A mixture of two components A and B in the presence of a solvent constitutes a ternary system. A phase diagram for a ternary system requires a representation in three dimensions as three axes are required to depict the relative concentration of each component and one axes to depict the temperature. Figure 2.7a shows such three-

dimensional representation. Considering the three-dimensional phase diagram illustrated in Figure 2.7a, each face of the prism represents a binary phase diagram between two of the components of the system.[60] The face of the prism representing the binary phase diagram between a pure component A or B and the solvent allows determining the solubility of A and B respectively for the specific temperature, while the face of the prism representing the binary phase diagram between A and B allows to determine composition at the eutectic.

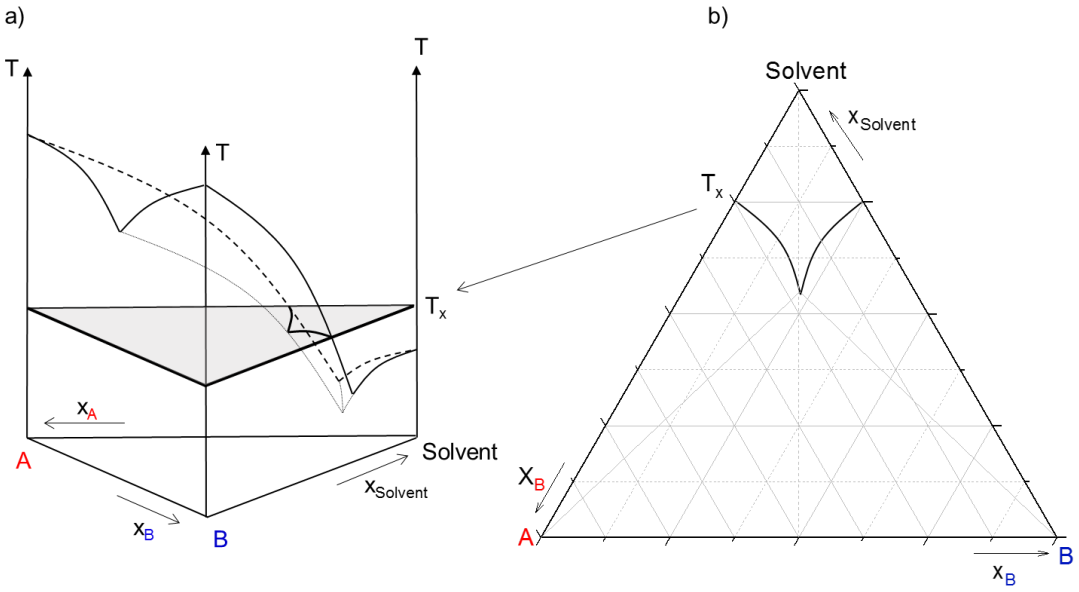

Figure 2. 7 Three-dimensional (a) and two-dimensional (b) phase diagram for a ternary system, A, B and a generic solvent. Shaded isothermal section represents the solubility isothermal ternary phase diagram for a specific temperature, T_x.[60]

The resulting solubility ternary phase diagram can then be represented in two dimensions as illustrated in Figure 2.7b. Each vertex of the triangle constitutes a pure component and the continuous black line within the ternary phase diagram corresponds to the isothermal solubility line at a certain temperature, T_x. A typical mixture of two enantiomers in a generic solvent represents a ternary system and the representation of the solubility ternary phase diagrams depends on the type of enantiomeric systems as shown in Figure 2.8. Conglomerate forming systems exhibit the highest solubility at the eutectic (racemic) composition and show a V-shaped form of the solubility isotherm, symmetrical with respect to the racemate-solvent line (Figure 2.8a). Within the ternary phase diagram of a conglomerate forming system, the thermodynamic stable phases can be identified as

follows: above the eutectic composition, only one liquid phase is thermodynamically stable, consisting of a solution that contains both enantiomers dissolved in the solvent.

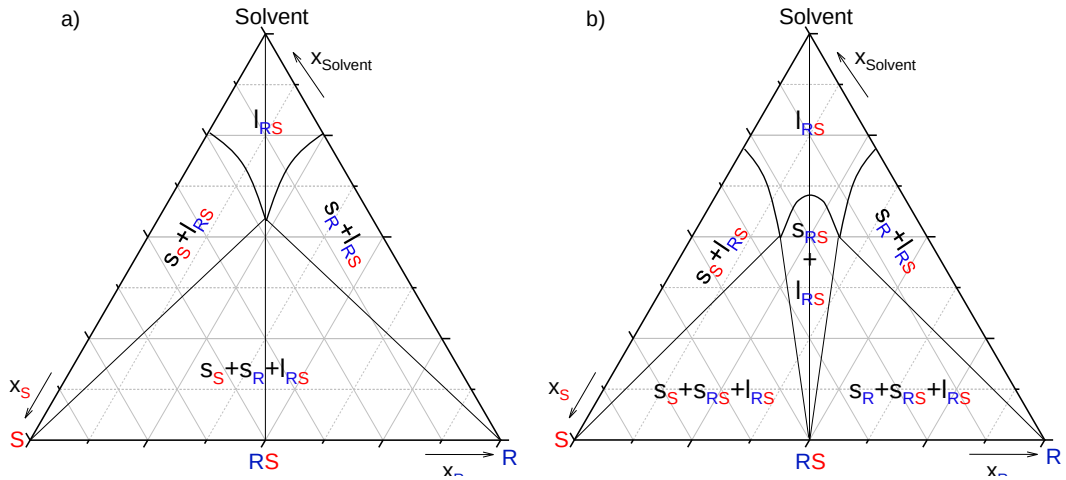

Figure 2. 8 Ternary phase diagrams for a conglomerate forming system (a) and a racemic compound forming system (b). A code color identifies the two components R and S, while s and l represent the phases in equilibrium within each region.

Below the V-shaped solubility isotherms, the 2-phase domains between the axes and the equilibrium tie lines consist of a saturated solution phase of varying composition and a solid pure enantiomer phase, *(S)*- or *(R)*- respectively for the 2-phase region located on the left and right side of the ternary phase diagram in Figure 2.8a. In the corresponding 3-phase domain, two solid phases represented by both pure enantiomers, and a saturated solution of eutectic (racemic) composition coexist in equilibrium. For a racemic compound forming system (Figure 2.8b), two different scenarios are possible for the 2-phase domains, one consisting of a saturated solution with a racemic solid phase and one consisting of a saturated solution and one of the pure enantiomers as solid in equilibrium. In the corresponding 3-phase domain a mixture of two solid phases, pure *(S)*- or *(R)*- enantiomer and the racemic compound *(RS)*- coexist with a saturated solution of eutectic composition.

2.3.3 Theoretical determination of solid-liquid equilibria

Considering a system of two enantiomers in a solvent, which are not chemically dissociated in liquid state and are fully immiscible at the solid state, *i.e.* a conglomerate

system, the relation between the melting point of the components and the composition of the mixture is expressed by the well-known Schröder-van Laar equation in a simplified version (Eq. 2.4).[42]

$$\ln(x) = \frac{\Delta H_A^f}{R}\left(\frac{1}{T_A^f} - \frac{1}{T^f}\right) \tag{2.4}$$

Where, x is the mass fraction of the enantiomer in excess in the mixture, ΔH_A^f is the enthalpy of fusion of the pure enantiomer in *J mol*$^{-1}$, R is the gas constant in *J mol*$^{-1}$ *K*$^{-1}$, T_A^f is the fusion temperature of the pure enantiomer in *K* and T^f is the fusion temperature of the studied mixture in *K*. The enthalpy of fusion of the mixture and the pure enantiomer are experimentally determined, *e.g.* from the DSC thermograms. Eq. 2.4 is representative for ideal mixtures, where interaction between pair of *homo*-components are equivalent with the interaction between *hetero*-components. As for most of the real solutions, the assumption of ideality is unjustified, discrepancy between the experimental data and the theoretical data can be observed. The deviation from the ideal behavior is described by the activity coefficient γ, (Eq. 2.5), which is equal to one in case of ideal solutions.

$$\ln(\gamma x) = \frac{\Delta H_A^f}{R}\left(\frac{1}{T_A^f} - \frac{1}{T^f}\right) \tag{2.5}$$

A reliable estimation of the activity coefficient can be achieved using predictive models such as the UNIFAC group contribution method.[69,70]

For racemic compound forming systems Eq. 2.4 is only applicable at composition $x_{eu}<x<1$. For $x_{rac}<x<x_{eu}$, where the solid phase consists of a pure racemic compound, the liquidus line can be calculated using the Prigogine and Defay equation (Eq. 2.6).

$$ln4x(1-x) = \frac{2\Delta H_{Rac}^f}{R}\left(\frac{1}{T_{Rac}^f} - \frac{1}{T^f}\right) \tag{2.6}$$

Where, ΔH_{Rac}^f and T_{Rac}^f are respectively the enthalpy of fusion in *J mol*$^{-1}$ and the fusion temperature in K of the racemic compound, T^f is the melting point of the mixture and x is the mass fraction of the more abundant enantiomer in the mixture.

2.3.4 Experimental determination of solid-liquid equilibria

The understanding of the phases in equilibrium is crucial for a successful crystallization process; therefore, the determination of the solid-liquid equilibria is an important requirement at the first stage of the process development. Binary phase diagrams are usually built from the data collected by calorimetric techniques. Nowadays, DSC is a

powerful experimental technique that allows not only to detect pure enantiomeric systems but also to systematically measure the melting points of several mixtures at various enantiomeric compositions. Solubility ternary phase diagrams can be determined *via* polythermal and isothermal methods. Polythermal methods can be informative in the first stage of the solubility investigation, as they provide, thanks to the modern technologies, a large number of results in a relative short time.[71] However, one may find lack of reproducibility in such data, as the equilibration of the system might not be reached during the experiments. On the other hand, although, elaborative and time consuming, the isothermal method provides accurate solubility data.[60] A further investigation *via* XRPD analysis can provide information about the solid state in equilibrium with the saturated solution, hence allowing to discriminate the presence of polymorphs or solvates of the studied system.

2.4 Provision of pure enantiomers

Several concepts of provision and separation of enantiomers have been addressed in the last decades and are summarized in a non-exhaustive manner in Scheme 2.1. Generally enantiomerically pure compounds are obtained either from chiral starting materials generated by a reaction *via* asymmetric synthesis or chiral resolution. Synthetic routes exploit an enantiomerically pure substrate, reagent solvent or catalyst as starting material, yielding two asymmetric synthetic pathways. The use of chiral auxiliaries in asymmetric synthesis has found wide applications. Chiral auxiliaries are molecules capable of temporarily binding to the starting compound, thus inducing chirality in one or more steps of a synthetic route.[72] Although most of the available chiral auxiliaries are derived from compounds of natural origin, their addition and removal from the synthetic route represents a limitation in terms of costs and yield.[73] Asymmetric synthesis can be performed also by exploiting a small amount of chiral catalyst in form of metal-ligand complex, chiral organo-ligands or biocatalysts. Pioneering works on metal-ligand complexes are recognized to Noyori and colleagues for their investigations on the asymmetric hydrogenation with Rh complex of BINAP.[74] Despite the tremendous progress achieved, the number of highly selective reactions that supply pure enantiomers on an industrially relevant scale is still limited. Therefore, there is a great interest in developing and using processes of separation of racemates.[73] An extensive effort has been devoted towards chromatographic separation techniques such as thin layer chromatography (TLC), gas chromatography (GC), supercritical fluid chromatography (SFC), and above all

high-performance liquid chromatography (HPLC).[75,76] The tunability of the characteristics of both the fluid mobile phase and the stationary phase , allows coverage of a wide spectrum of possible requirements in the separation problem. However, much interest has been devoted in alternative technologies, due to the high costs of the chromatographic processes.

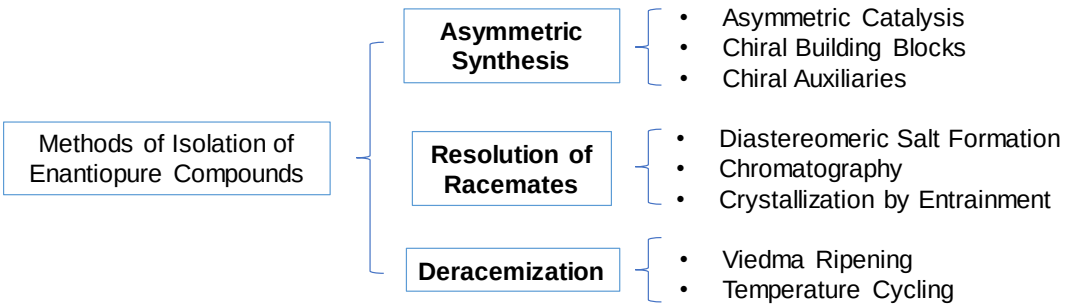

Scheme 2. 1 Scheme of selected experimental methods to isolate pure enantiomers**.**

2.4.1 Crystallization-based separation technologies

The classical method used in the manufacturing of an Active Pharmaceutical Ingredient (API) is called classical resolution. It consists in the usage of suitable chiral resolving agents to provide diastereomeric salts, which have different solubility in solution, therefore they are separable *via* crystallization.[77] A direct crystallization of the preferred enantiomer from a racemic solution, without the usage of an auxiliary is possible exploiting the so-called preferential crystallization. The principle of this technique is known from 1866, when one of Pasteur's students accomplished a resolution of enantiomers by providing seed crystals of single enantiomer in a supersaturated solution of the racemate.[78,79] A systematic application of this process was possible only in the 20th century with Jacques.[80] More recent novel techniques, deracemization processes such as Viedma ripening and temperature cycling, combine the racemization process with the crystallization process.[81–83] The racemization in solution enables the total spontaneous resolution of the system. The conversion of the unwanted enantiomer in racemate, enables an increase of the overall yield of the process, compared to 50% achievable with preferential crystallization.

2.4.2 Principle of preferential crystallization (PC) resolution processes

From an experimental point of view, a typical PC process of a conglomerate forming system starts with the creation of a solution at racemic composition saturated at certain temperature (Figure 2.9a). Then, in order to induce crystallization from the solution, a certain supersaturation degree is generated thus placing the system within the metastable region. The supersaturation degree must be chosen in a way that the supersaturated solution remains clear and no spontaneous nucleation should be expected (Figure 2.9b). As in the present work the supersaturation of the PC runs was generated by cooling, the stage represented in Figure 2.9b refers to a cooling PC process. After creating the supersaturation, seed crystals of the pure enantiomer are introduced into the system, hence triggering the selective crystallization of the preferred enantiomer. As the crystallization proceeds, the mother liquor is depleted with respect to the preferred enantiomer while the counter-enantiomer remains in the solvated metastable state (Figure 2.9c). After a certain time from the seeding, the spontaneous nucleation of the unwanted enantiomer is likely to happen; therefore, the process must be interrupted so that the solid collected product remains uncontaminated (Figure 2.9d). Usually the interruption of the process is carried out *via* solid-liquid separation of the suspension obtained and washing of the crystals, in order to remove traces of mother liquor in the solid.

Due to the stochastic nature of the nucleation of the counter-enantiomer, its determination remains a challenging aspect of the resolution process. Purity of the components (solute and solvent) as well as experimental conditions such as cooling rate, stirring rate or inner wall of the crystallizer, influence the occurrence of such event. An indirect determination of the nucleation of the unwanted enantiomer is given by the usage of on-line or in-line analytic tools such as polarimeter and densitometer as explained in the experimental section of this thesis.

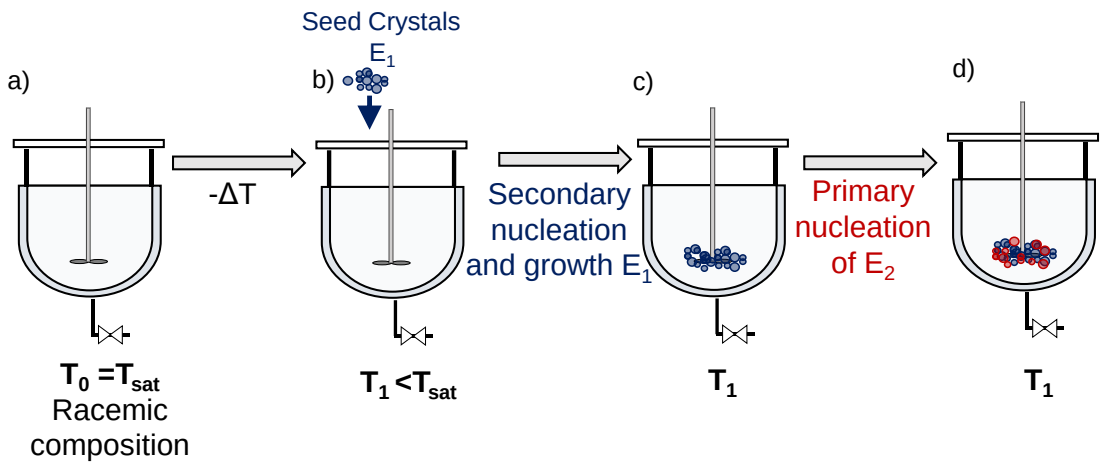

Figure 2. 9 Schematic representation of the main stages of a cooling isothermal preferential crystallization (PC) process.

2.4.3 Thermodynamic description of the supersaturation degree

Let us consider the ternary phase diagram of a generic system composed of two enantiomers in a generic solvent (Figure 2.10). The starting point of a PC process would be point A, located in correspondence of the saturation (higher) temperature, which corresponds to a supersaturated solution at racemic composition. By seeding the supersaturated solution with pure crystals of the preferred enantiomer, *i.e. (R)*- enantiomer in Figure 2.10, the composition of the mother liquor will change as a result of the depletion of the preferred enantiomer from the solution. The line RAr in Figure 2.10 represents the change of the composition of the mother liquor upon seeding. Specifically, the composition of the mother liquor will displace up to the metastable solubility curve of the *(R)*-enantiomer, which is no longer limited to CE but it is extended within the metastable region until point r. As the preferred *(R)*- enantiomer crystallizes during the process, an alteration of the degree of supersaturation of the unseeded enantiomer will occur. The supersaturation degree of the counter-enantiomer is defined as the distance between the point, which describes the solution composition achieved and the prolongation of the solubility isotherm of the counter-enantiomer (C'E) at crystallization temperature. Specifically the system passes from Y to W, and the segments YX and WZ in Figure 2.10 are representative of the respective variation of the supersaturation degree during the process.

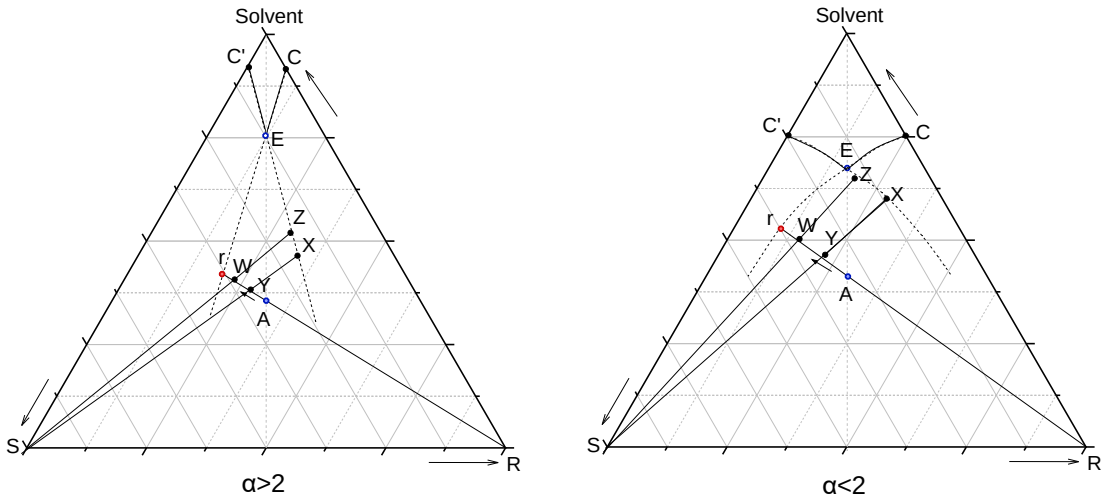

Figure 2. 10 Schematic representation of the supersaturation degree of the unseeded *(S)*-enantiomer during a preferential crystallization process for two generic ternary systems characterized by α> 2 (left) and α< 2 (right). C and C´ merely refer to the graphical points within the illustration rather than to the concentration values.

Upon seeding, two possible case scenarios can take place depending on the shape of the solubility isotherms of the system. Given *α*, the ratio of solubility between the solution at racemic composition and the solution containing only pure enantiomer at the same temperature (Meyerhoffer coefficient), the risk of spontaneous nucleation of the counter-enantiomer will depend on the value of this parameter (Eq. 2.7).

$$\alpha(T) = \frac{C(T)_{Racemate}}{C(T)_{Enantiomer}} \tag{2.7}$$

For *α*>2, meaning that the racemate is much more soluble than the enantiomers, as the crystallization proceeds, the degree of the supersaturation of the counter-enantiomer increases, in fact WZ>YX (Figure 2.10, left). As a consequence, the risk of spontaneous nucleation of the unseeded enantiomer increases during the development of the process. For the case *α*<2 (Figure 2.10, right), WZ<YX, meaning that the degree of the supersaturation of the counter-enantiomer decreases. As a result, the solution becomes more stable as the preferred enantiomer crystallizes, making the spontaneous nucleation of the counter-enantiomer less likely to occur. From the description above, one sees that in order to perform an optimal resolution, without having contamination of the counter-enantiomer, systems belonging to the case *α*<2 are preferred.

2.5 Crystallization as unit operation technique

Crystallization activities extend back in history as far as the writings of man. The crystallization of salts by evaporation of naturally occurring solutions, such as seawater or natural brines, can be found through ages of early civilization, therefore, it is considered as one of the oldest known engineering operation unit. The usefulness of this technique has led man to develop increasingly sophisticated procedures, from the mere production of salt, dating back to the prehistoric era, to the first purification process *via* recrystallization, performed by Biringuccio in 1550, up to modern crystallization techniques, extensively exploited in many fields of industry and academia.[84,85] Today, crystalline products are present in every aspect of life. In fact, crystallization is used as separation and purification technique within the food, chemical and pharmaceutical industry.[86] The properties of such products and ultimately their success in the market strictly depend on the characteristics of the crystals, such as purity, size, color, morphology, shear diversity. Skills and knowledge of basics of chemistry, material science and chemical engineering are brought together to design products with required specification, making crystallization a fascinating intertwining of disciplines, indeed still referred to as more an art rather than a science.[25]

2.5.1 Crystal engineering

In the pharmaceutical industry, crystallization is often used as final step in the manufacturing of APIs, in fact more than 90% of the small molecule drugs are delivered in solid form. Solid-state properties such as crystal polymorphic form and morphology must be accurately determined as they can impact the bio-performance of the administered drug,[87] making the screening of polymorphs, co-crystals and solvates a fundamental investigation in this area. Polymorphism is the ability of a compound to exist in two or more crystalline phases. A variety of physical-chemical properties changes from one polymorph to another, such as solubility, melting point and dissolution rates, causing differences in the bioavailability of the drug.[88,89] A change of physicochemical properties of a molecule can also occur as a result of co-crystal formation. Co-crystals are molecular compounds of two multicomponent systems, which are solid at room temperature, kept together by non-covalent interactions. In the pharmaceutical industry, co-crystal formation, using molecules accepted by the regulatory authorities, is widely used to enhance and tailor the physicochemical stability of a pharmaceutically active component. When one of

the components is liquid at room temperature and is a solvent, the system is called a solvate. Particular attention is devoted to the hydrates, not only for the excellent ability of the water to form hydrogen bonding which enhance the stability of the solvate, but also for their occurrence in the formulation of creams and gels.[90,91]

2.5.2 Process development: batch and continuous operation

The implementation of crystallization in the pharmaceutical industry has traditionally been as a batch operation, specifically when the production rate is low.[92] Commonly, stirred tanks are used for either cooling, evaporative or reaction crystallization, requiring a rather simple maintenance and less capital investment compared to the continuous crystallizers. The possibility to adjust specific experimental features, such as the seeding procedure allows exploiting such crystallizers for various experimental conditions and various systems. However, a batch-to-batch variability of the isolated material in terms of crystal size, degree of crystallinity and purity is usually observed. Although batch is still the most common operation mode, the exploitation of semi-continuous and continuous crystallizers can provide more consistent product properties, higher control of the product attributes over the process, as well as a cost reduction.[93] A type of crystallizer applicable for continuous operation is the Mixed Suspension Mixed Product Removal (MSMPR).[94] Advantages in the employment of the MSMPR include an easy maintenance, an easy control of the temperature and a homogeneous mixing within the crystallizer. The latter allows to minimize the variation of residence time hence increasing the homogeneity of the solid properties. The applicability of the MSMPR has been demonstrated on a number of pharmaceutical molecules such as glutamic acid,[95] paracetamol[96] and aminobenzoic acid.[97] Another type of reactor has been used in the continuous production of APIs, namely Plug Flow Reactor (PFR), consisting in a tubular reactor in which the content flows at constant velocity. As the system inside a PFR has a short residence time, they are preferred in case of systems with fast kinetics. Also in this case, a number of reported cases demonstrate the applicability of such crystallizers, as for the case of glutamic acid and ketoconazole.[98-99]

2.5.3 Crystallization in single and coupled stirred tanks

At present, there have been a number of successful enantiomeric resolutions using various crystallizer configurations and operation modes. Common stirred tanks in batch

mode have been used as in the case of guaifenesin enantiomers,[100] asparagine,[101] 2-cloro mandelic acid,[102] and methionine.[103] From those studies it emerges that monitoring of the process is a crucial aspect to take into account for a successful resolution.[104] Optical analytic tools, such as FBRM, FTIR and turbidity probes, as well as the usage of the polarimeter for optical rotation signal of the mother liquor, are necessary to ensure a good control of the depletion of the preferred enantiomer from the mother liquor and avoid contamination during the process. Such issue is the main drawback of batch processes, as the enantiomeric excess of mother liquor cannot be renewed up to racemic values without interrupting the process. Continuous approaches constitute a valid alternative to keep the mother liquor at racemic composition. Stirred tanks in a coupled configuration have received major attention in the last decades, as they not only allow to minimize the increase of the supersaturation with respect of the counter-enantiomer in the mother liquor, but also they enable the simultaneous production of both enantiomers into the two tanks. As the preferential crystallization of the enantiomers in each tank proceeds, the crystal free mother liquor is exchanged between the two tanks keeping the supersaturation with respect of the counter-enantiomer low, hence avoiding its spontaneous nucleation. The experimental development and exhaustive models have been realized by Elsner *et al.* for the case of the resolution of threonine and asparagine enantiomer in water in two coupled crystallizers.[105,106] The concept of coupled configuration can be used in an alternative operation mode, as also reported in the present work for the model compound guaifenesin and CPG-intermediate, named coupled preferential crystallization and dissolution (CPCD), which has been applied in other works for the resolution of pharmaceutical molecules such as guaifenesin,[107] threonine[108] and omeprazole.[109]

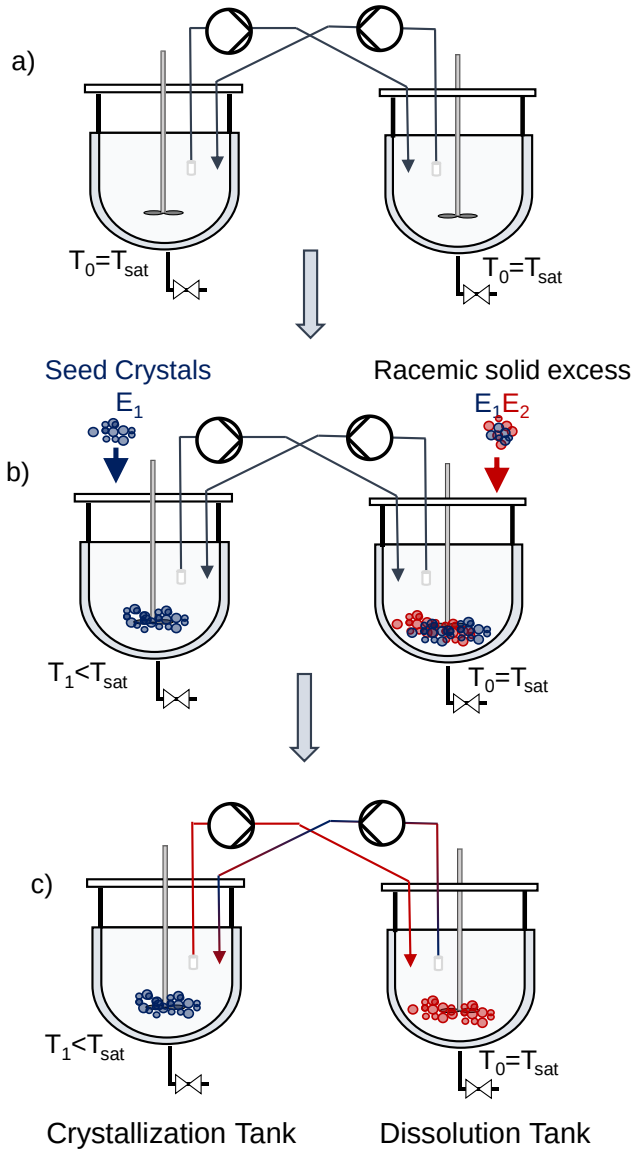

Figure 2. 11 Schematic representation of the main stages of a coupled preferential crystallization and dissolution (CPCD) process.

The process exploits two stirred tanks coupled *via* an external loop. After feeding a racemic solution saturated at a certain temperature into the two tanks (Figure 2.11a), one tank, namely the crystallization tank, is cooled to crystallization temperature while the other tank, namely the dissolution tank, is kept at saturation temperature and it is filled with an excess of racemic solid phase, which remains suspended in the saturated solution. (Figure 2.11b). After seeding the crystallization tank with homochiral crystals of pure enantiomer, the exchange between the two tanks is activated (Figure 2.11c). As the

crystallization of the seeded enantiomer proceeds, the mother liquor within the crystallization tank, slightly depleted with respect of the preferred enantiomer, is transported to the dissolution tank. Due to such depletion, the selective dissolution of the preferred enantiomer from the solid excess is therefore triggered yielding to a refreshment of the mother liquor up to racemic composition. By keeping the mother liquor close to racemic composition, the supersaturation of the counter-enantiomer within the crystallization tank is reduced, allowing to run the process for longer time respect to a PC in a single stirred tank. Moreover, the selective dissolution of one enantiomer in the dissolution tank, allows enriching the solid excess with respect of the unwanted enantiomer, hence enhancing the applicability of such configuration for the production of the two pure enantiomers of a chiral compound.

2.5.4 Crystallization in fluidized bed crystallizers

Alternatives to the stirred tanks are the fluidized bed crystallizers, known for their advantages of ensuring robust control of the process, stable crystal growth as well as the adjustability of the crystal size of the isolated product with volumetric flow rate within the crystallizer. The upward flow of mother liquor carries the smallest nuclei to the upper part and then out of the tubular crystallizer, hence minimizing the risk of contamination from the counter-enantiomer. In a fluidized bed crystallizer, the particles are less prone to attrition and breakage than in stirred tank crystallizers and tend to segregate according to their size. Larger and heavier particles populate at the bottom of the crystallizer and the smaller particles accumulate at the top of the bed. The complexity of the hydrodynamic behavior of the particles within the crystallizer makes the application of such configuration in pharmaceutical crystallization a challenging task.[110] Nonetheless, a number of APIs have been successfully resolved as for the case of the ortho and para isomers of amino benzoic acid, and asparagine.[111-112]

2.5.5 Performance assessment of enantioselective crystallization processes

While demonstrating the feasibility of a given process is an important first step for process development, the evaluation of the performances of the process using Key Performance Indicators (KPIs) is a decisive requirement in manufacturing. In the recent years, a large number of variants of enantioselective crystallization processes have been reported;

however, only few of them have systematically addressed the performance assessment of the processes using chosen KPIs. A comprehensive overview of the evaluation of the KPIs for the enantioselective crystallization processes present in literature has been provided by Köllges *et al*.[113] It can be seen that a direct comparison among the processes is a challenging task, since the resolution processes are applied on different target substances, which exhibit different thermodynamics and kinetics. Moreover, in order to generate a representative indicator of the studied process, a number of parameters and constraints (*e.g.* related to the crystallization technique used, as well as the configuration of the crystallizer exploited) should be considered in defining the chosen KPI. Particularly relevant for enantioseparation processes are productivity and chiral purity, which have been used as KPIs already in a number of previous works.[105,112,114] While the enantiomeric purity can be directly measured *via* enantioselective HPLC, the productivity is calculated taking into account the mass of the product collected, the volume (either of the crystallizer or of the solution) and the time of the process. In the present thesis, together with the two aforementioned KPIs, the yield of the process was evaluated as well. Details on the definition of the chosen KPIs are provided in the next chapter.

Chapter 3. Experimental description

The following chapter will describe the technical aspects of the experimental work performed for the present thesis. In the first section, the chiral molecules studied and the solvent used will be listed. Afterwards, the devices and the methods used to determine the thermodynamics and kinetics of two of the model compounds studied will be described. An in depth elucidation of the calculation of the supersaturation ratio will be provided using the system guaifenesin in water as example, with an emphasis to the conversion from ternary to Cartesian coordinates. The setups and the rational approaches used for the resolution of the chiral molecules will be explained with a focus on the process monitoring through selected analytic devices. The calculation of chosen performance indicators namely purity, productivity and yield of the resolution processes will be defined for the various configurations. Finally, the techniques used for the characterization at the solid-state as well as in solution will be explained.

3.1 Materials

Racemic and enantiopure *(R)*- 2-(benzylideneamino)-2-(2-chlorophenyl) acetamide, here named clopidogrel (CPG) intermediate, were provided by Syncom BV Pharmaceuticals and used without further treatment. The chiral purity of the enantiomeric material has been determined by HPLC and resulted between 96 and >99%. Racemic guaifenesin, guaiacol glycerol ether, was purchased from TCI Deutschland GmbH. The chemical purity of the substance was above 98 % and was used without previous treatment. Enantiopure guaifenesin was produced *via* single batch PC as well as CPCD in water and

isopropanol.[100,107] DL- and L-methionine reagent grade, ≥ 98% (HPLC) was purchased from Sigma Aldrich. The solvents used in the present work, isopropanol, ethanol, acetone, ethyl acetate and acetonitrile were HPLC grade and a milli-Q system Merck Millipore, Milli-Q Advantage was used to produce Millipore water.

3.2 Fundamental investigations

3.2.1 Isothermal solubility measurements

Isothermal solubility measurements were carried out for two chiral model compounds, *i.e.* CPG-intermediate in acetonitrile and guaifenesin in various organic solvents. The measurements consisted of preparing suspensions of the chiral system in a chosen solvent at various enantiomeric compositions in sealed vials. Vials equipped with a magnetic stirrer were immersed in a water bath within double-jacketed vessels connected to a thermostat. Especially, sealed vials of 8 mL volume were used for CPG-intermediate in acetonitrile, due to a limited availability of the material, while for the guaifenesin system 20 mL volume vials were used. A Pt-100 probe was used to monitor the temperature with the time. Several temperatures were investigated between 10 and 50 °C for CPG-intermediate in acetonitrile, while the solubility of guaifenesin in organic solvents was determined in the temperature range between 10 and 60 °C. The suspensions were thermostated over 48 h under continuous stirring in order to ensure a homogeneous mixing. The equilibration and the achievement of the saturation concentration was verified by observing the variation of the concentration with the time and a gravimetric analysis allowed to determine the concentration of the saturated solutions. A sample of 1 mL of the equilibrated solution was withdrawn and filtrated; hence, the saturated concentrations were derived as expressed by Eq. 3.1, where m_{solute} is the mass of the solute that remained after complete evaporation of the solvent. Several repetitions were performed in order to determine the standard deviations of the final concentration values.

$$C_{sat}\,(T) = \frac{m_{solute}}{m_{solute} + m_{solvent}} \tag{3.1}$$

3.2.2 Multiple reactor system Crystalline Particle Vision®

A multiple reactor system, Crystalline Particle Vision (Technobis, The Netherlands) was exploited for the polythermal determination of the solubility of the model compounds CPG-

intermediate in acetonitrile and guaifenesin in isopropanol, as well as for the determination of their metastable zone width (MSZW). Various suspensions of the substances in the chosen solvent were prepared in 6 mL vials equipped with a top stirrer and then placed in the multiple reactor system. The clear point and the cloud point of the solutions have been determined through the turbidity signal given by the multiple reactor system. Furthermore, images of the solutions during the experiments were recorded using the integrated camera of the device, which allowed accurate detection of the disappearance of crystals close to saturation point as well as their nucleation during the cooling ramps. The instrument allowed the setting of several temperature programs, one for each sample, therefore a fast screening of the nucleation point as a function of the cooling rate as well as a function of the concentration of the samples has been carried out for the determination of the metastable region.

3.2.3 Metastable zone determination

The metastable zone width of two of the model compounds studied were determined using the so-called Nývlt method.[115,116] Samples at various concentration between 20 °C and 50 °C for the system CPG-intermediate in acetonitrile and between 20 °C and 40 °C for guaifenesin in isopropanol were prepared and located into the multiple reactor Crystalline, described above. The samples were heated until the complete dissolution of crystals was observed. Afterwards, the samples were cooled using a controlled cooling ramp for each sample. Cooling programs between 0.5 K/h and 100 K/h and between 0.5 K/h and 10 K/h were applied respectively for the CPG-intermediate system and for the guaifenesin system. The cloud point, at various saturation concentration and at various cooling rates has been determined by direct observation of the formation of crystals during the cooling ramps using the integrated camera of the Crystalline device. Given the saturation temperature, T_{sat}, and the cloud point of each solution for each cooling ramp, T_{cloud}, the difference between the two temperatures has been calculated. The resulting T_{sat}-T_{cloud}=$\Delta T_{max,}$ represents the maximum subcooling achievable without having the occurrence of spontaneous nucleation, at a chosen cooling rate and initial concentration of the solution. By plotting the ΔT_{max} as a function of the cooling rate for each concentration, the extrapolation of the ΔT_{max} to a fictitious zero cooling rate allowed the determination of the limit of the metastable region for each concentration investigated, hence the primary nucleation curve of the studied system (Nývlt method).

3.2.4 Calculation of supersaturation in single batch PC

In the present work, the driving force for PC experiments in a single tank has been defined in terms of the initial supersaturation ratio, (*S(T)*), taking into account the mass fraction of the desired enantiomer *(x_i)*, as expressed in Eq. 3.2.[117]

$$S(T) = \frac{x_{i,0}}{x_{i,sat}(T, x_{i,0})} \tag{3.2}$$

The supersaturation ratio can be defined as the ratio between the concentration of the system in the current state and its equilibrium concentration.[116] In the present work, the current state and reference state refer to the initial condition of the system, *i.e.* at the initial composition. In fact, in Eq. 3.2 the current state is defined by $x_{i,0}$, which is the mass fraction of the preferred enantiomer in the initial state, *i.e.* at saturation conditions at the initial saturation temperature. While the so-called reference state or equilibrium state is represented by $x_{i,sat,}(T,x_{i,0})$ which is dependent on the current temperature, *T*, and the initial state, $x_{i,0}$. The reference state, $x_{i,sat,}(T,x_{i,0})$, can be identified in Figure 3.1 as the intersection between the prolongation of the solubility isotherm at the crystallization temperature within the metastable region (metastable solubility), represented by the dashed black line in Figure 3.1, and the tie line connecting the corner of pure (seeded) enantiomer and the current state, $x_{i,0,}$ which is represented by the blue line in Figure 3.1.

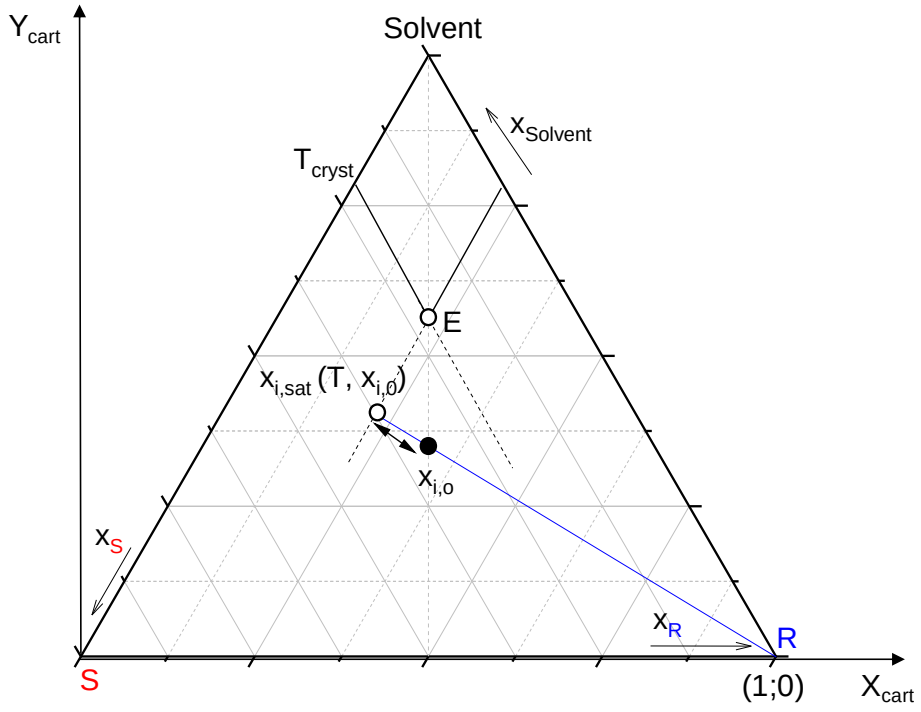

Figure 3. 1 Representation of the initial state ($x_{i,o}$), and reference state ($x_{i,sat}(T,x_{i,o})$) for a ternary system of two enantiomers in a generic solvent during a preferential crystallization process at temperature T_{cryst}. The black arrow between the two states represents the driving force of the process.

In order to determine the reference state, ($x_{i,sat,}(T,x_{i,0})$ in Figure 3.1), a conversion of the composition of the system at the initial saturation point (Figure 3.1, full black dot) and the solubility isotherm at crystallization temperature (Figure 3.1, continuous black line) from the ternary coordinates to the orthogonal, Cartesian, coordinates was necessary. The derivation of the equations reported below was taken from ref [118].

The terms of Eq. 3.2 have been calculated as described in the following steps:

1. Conversion of the solubility isotherm at the chosen crystallization temperature, from the ternary coordinates to Cartesian coordinates using Eq. 3.3 and Eq. 3.4.[118]

$$X_{cart}(T_{cryst}) = x_i(T_{cryst}) + (0.5 * x_{solvent}(T_{cryst})) \quad (3.3)$$

$$Y_{cart}(T_{cryst}) = \sin(60°) * x_{solvent}(T_{cryst}) \quad (3.4)$$

Where, $x_i(T_{cryst})$ and $x_{solvent}(T_{cryst})$ are the mass fraction of the more abundant enantiomer in the mixture and the solvent respectively, taken from the solubility data at crystallization temperature.

2. Cartesian representation of Y_{cart} (T_{cryst}) as a function of X_{cart} (T_{cryst}) and data fitting with a linear regression.

As a clarifying example, Figure 3.2 illustrates the graphical representation of the solubility isotherm in Cartesian coordinates for the system guaifenesin in water, at various enantiomeric composition and at a chosen crystallization temperature, T_{cryst}=25 °C. This representation has been used in the present thesis for the calculation of the supersaturation ratio of the PC run in single stirred tank.

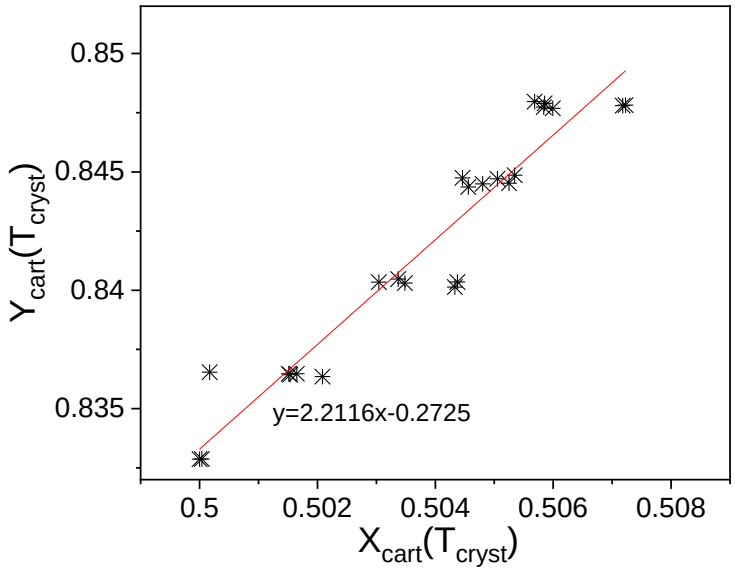

Figure 3. 2 Cartesian representation of the experimentally determined solubility data of guaifenesin in water at various enantiomeric compositions at the chosen crystallization temperature. The Cartesian coordinates X_{cart} (T_{cryst}) and Y_{cart} (T_{cryst}) have been calculated as explained in step 1.

The resulting solubility isotherm converted in Cartesian coordinates corresponds to Eq. 3.5:

$$y = 2.2116x - 0.2725 \quad (3.5)$$

3. Conversion of the solubility of the system at initial saturation temperature and racemic composition in Cartesian coordinate using Eq. 3.6 and Eq. 3.7.

$$X_{cart}(T_{0,sat}) = x_i(T_{0,sat}) + (0.5 * x_{solvent}(T_{0,sat})) \quad (3.6)$$

$$Y_{cart}(T_{0,sat}) = \sin(60°) * x_{solvent}(T_{0,sat}) \quad (3.7)$$

For this step, the mass fraction of one enantiomer $x_i\ (T_{0,sat})$ and the mass fraction of the solvent $x_{solvent}\ (T_{0,sat})$ in the initial state of the system, *i.e.* at saturation temperature and racemic composition, have been used.

4. Representation of the tie line connecting the solubility point at initial saturation temperature having Cartesian coordinates (X_{cart} ($T_{0,sat}$);Y_{cart} ($T_{0,sat}$)) and the pure enantiomer corner of the ternary phase diagram having Cartesian coordinates (1;0) and fitting with linear regression.

In Figure 3.3, one can see the graphical representation of the tie line of the system guaifenesin in water in Cartesian coordinates at a chosen initial state, *i.e.* initial saturation concentration, used for the calculation of the supersaturation ratio of the PC run in single stirred tank.

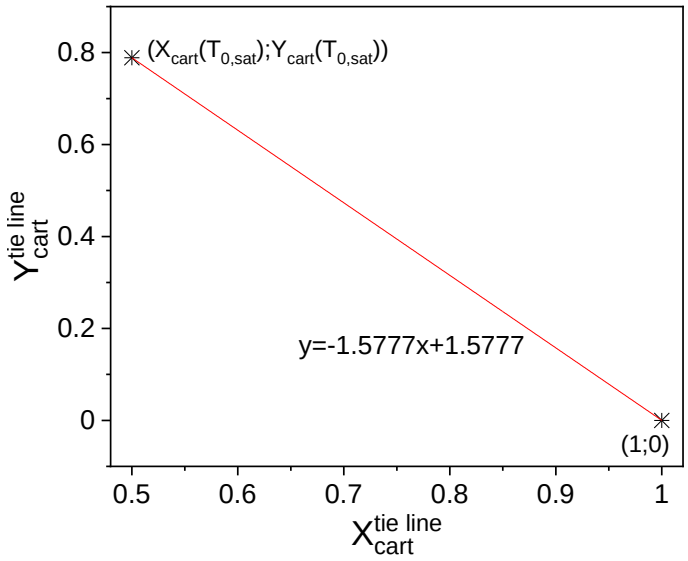

Figure 3. 3 Cartesian representation of the tie line having coordinates (X_{cart} ($T_{0,sat}$);Y_{cart} ($T_{0,sat}$)), (1;0) for the system guaifenesin in water at a chosen initial saturation temperature.

The converted tie line corresponds to Eq. 3.8

$$y = -1.5777x + 1.5777 \quad (3.8)$$

5. Determination of the intersection point between the prolongation within the metastable region of the solubility isotherm at crystallization temperature and the tie line obtained at step 4.

Such intersection point has been calculated by solving equation 3.5 obtained by the regression in step 2 and equation 3.8 obtained in step 4.

6. Conversion of the intersection point having coordinate ($X_{cart}^{intersec}$, $Y_{cart}^{intersec}$) in ternary coordinates, using Eq. 3.9 and Eq. 3.10.

$$x_{solvent}^{intersec} = \frac{Y_{cart}^{intersec}}{\sin(60°)} \tag{3.9}$$

$$x_i^{intersec} = X_{cart}^{intersec} - \left(0.5 * x_{solvent}^{intersec}\right) = x_{i,sat}(T, x_{i,0}) \tag{3.10}$$

7. Knowing the value of the mass fraction of the desired enantiomer at the initial state, $x_{i,0}$ and the mass fraction of the desired enantiomer at the reference state $x_i^{intersec}$ which can be defined as $x_{i,\,sat}(T, x_{i,0})$, the supersaturation ratio is calculated by the ratio of the these two terms (Eq. 3.2).

3.3 Crystallization setups

In the present section, the setups used for the crystallization runs are described and schematically represented. The various configuration of crystallizers used are represented and the various components used for the process monitoring are specified. For each configuration, a detailed explanation of the terms used in the determination of the performance indicators, productivity and yield of the resolution process is given.

3.3.1 Single batch stirred tank setup

PC experiments in a single tank were performed in a 450 mL double-jacketed stirred tank. The vessel was connected to a thermostat (Lauda, Proline RP 845, Ecoline RE104 or Julabo) and a Pt-100 probe was used to monitor the temperature of the solution during the process. The stirred tank was linked to a polarimeter and a densitometer. A thermostated tube-in-tube configuration was used in order to avoid the crystallization of the solution pumped from the crystallizer to the analytics (Figure 3.4). A process control system PCS7 (Siemens) was connected to the electrical parts of the analytic components, hence enabling the monitoring of the analytic signals. The single stirred tank has been exploited for the single batch PC runs of CPG-intermediate in acetonitrile and guaifenesin

in isopropanol and in water. In addition to the resolution runs, the single stirred tank setup has been exploited for the production of seed crystals of pure enantiomers of guaifenesin *via* recrystallization, which have been used for the PC experiments in tubular fluidized bed crystallizer, as explained in section 3.3.5.

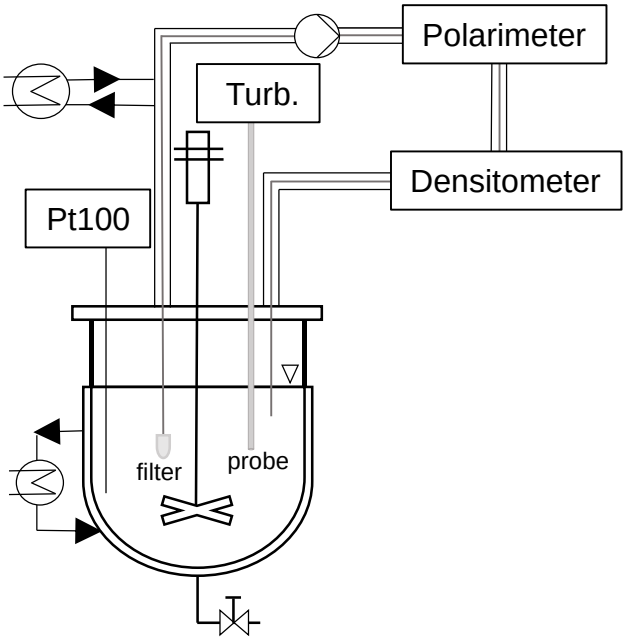

Figure 3. 4 Schematic representation of the single batch stirred tank setup used for PC experiments. On-line densitometer, polarimeter and in-line turbidity meter (Turb.), as well as the single units of the setup such as stirrer, thermostat, filter, Pt-100 and peristaltic pump are indicated in detail.

At the end of the resolution processes in single stirred tank, after removing completely the suspension from the crystallizer, a solid-liquid separation was performed *via* vacuum filtration and the crystals were washed with ice-cold solvent. The remaining solid phase was dried and weighed in order to determine the performance parameters. The yield, *Y %*, was calculated according to Eq. 3.11:

$$Yield\,\% = \frac{\left(m_{product} * Pu_{product}\right) - m_{seed}}{m_{product}^{theoretical} * 0.5} * 100 \qquad (3.11)$$

Where $m_{product}$ is the mass of the collected product, $Pu_{product}$ is the purity given by the HPLC analysis, m_{seed} is the mass of the seed crystals invested in the crystallization process and $m_{product}^{theoretical}$ is the mass of product theoretically achievable considering the solubility at the

initial saturation temperature and the solubility at the crystallization temperature. The productivity, *Pr (g/h/L)*, was calculated according to Eq. 3.12:

$$\mathrm{Pr}\left(\frac{g}{h*L}\right)=\frac{\left(m_{product}\ *Pu_{product}\right)-m_{seeds}}{t_{production}\ *V_{crystallizer}} \tag{3.12}$$

Where $t_{production}$ is the time from the seeding until the end of the process and $V_{crystallizer}$ is the volume of the crystallizer.

3.3.2 Coupled batch stirred tank setup

Experiments of coupled preferential crystallization and dissolution (CPCD) were carried out in two double-jacketed stirred tanks of 450 mL each equipped with Teflon coated propeller type stirrers (stirring rate 200 rpm). The vessels were connected with each other using a thermostated tube-in-tube configuration. Two gear pumps (Tuthill, D-Series, $\dot{V}$ =0-30 mL/min) were used to transport the crystals-free solution between the left tank and the right tank at a certain flow rate, while the two mass-flow meters/controllers (Bronkhorst Maettig GmbH, mini Cori-Flow M14) enabled a precise control of the exchange rate. Each tank was linked to a polarimeter and a densitometer *via* peristaltic pumps.

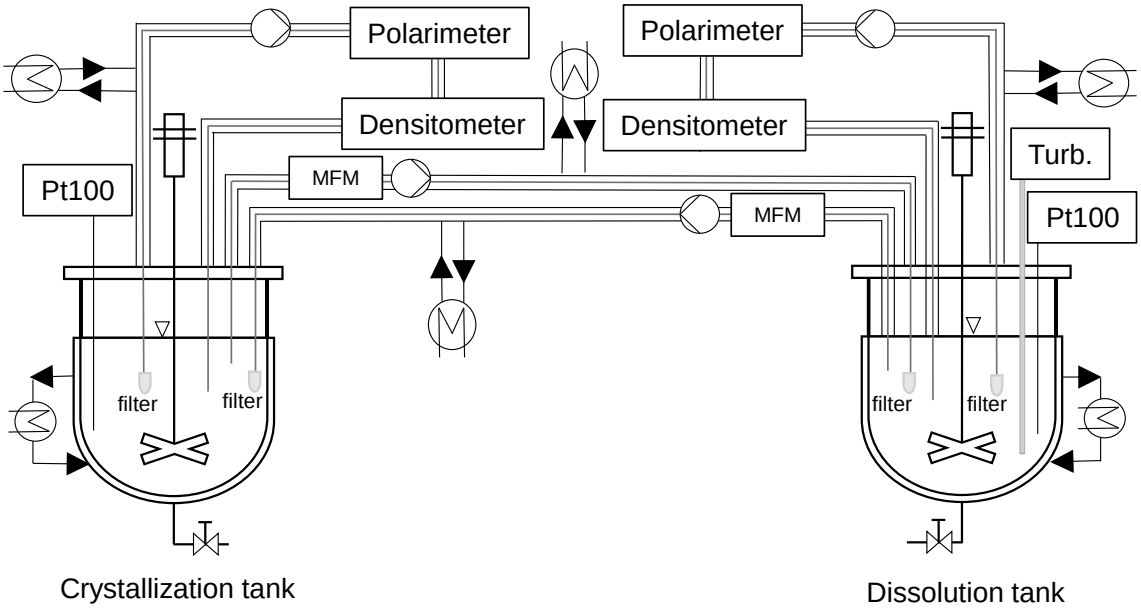

Figure 3. 5 Schematic representation of the coupled batch stirred tank setup used for CPCD experiments. On-line densitometer, polarimeter and in-line turbiditymeter (Turb.), as well as the single units of the setup such as stirrers, thermostats, filters, Pt-100 probes, peristaltic pumps and mass-flow-meters (MFM) are indicated in detail.

The turbidity probe was used to monitor the depletion of suspension density from the racemate solid excess present in the dissolution tank. Implementation and monitoring of the experimental conditions were possible using the process control system PCS 7 (Siemens). The coupled stirred tanks were used for the CPCD runs for CPG-intermediate in acetonitrile and the system guaifenesin in isopropanol. Productivity and yield values for the CPCD process have been calculated using Eq. 3.13 and Eq. 3.14 for the crystallization tank and Eq. 3.15 and Eq. 3.16 for the dissolution tank.

$$Yield\ \% = \frac{\left(m_{product}\ * Pu_{product}\right) - m_{seeds}}{\left(m_{product}^{theoretical} * 0.5\right) + \left(m_{excess} * 0.5\right)} * 100 \tag{3.13}$$

$$\Pr\left(\frac{g}{h * L}\right) = \frac{\left(m_{product}\ * Pu_{product}\right) - m_{seeds}}{t_{production}\ * V_{crystallizer}} \tag{3.14}$$

$$Yield\ \% = \frac{\left(m_{product}\ * Pu_{product}\right)}{m_{excess} * 0.5} * 100 \tag{3.15}$$

$$\Pr\left(\frac{g}{h * L}\right) = \frac{\left(m_{product}\ * Pu_{product}\right)}{t_{production}\ * V_{crystallizer}} \tag{3.16}$$

Where, $m_{product}$, $Pu_{product}$, m_{seed} and $m_{product}^{theoretical}$ maintain the definition given above, while m_{excess} is the mass of the solid racemate in the dissolution tank. It is worth mentioning that, in the calculation of the yield, m_{excess} is divided by two since the initial solid excess introduced in the dissolution tank is at racemic composition and the maximum amount of enantiomer achievable from the selective dissolution corresponds to its half.

3.3.3 Tubular fluidized bed crystallizer setup

A fluidized bed crystallizer was used for further experimental investigations on the system guaifenesin in isopropanol. PC experiments were carried out exploiting the equipment already developed in ref [112] with a few modifications as shown in Figure 3.6a.

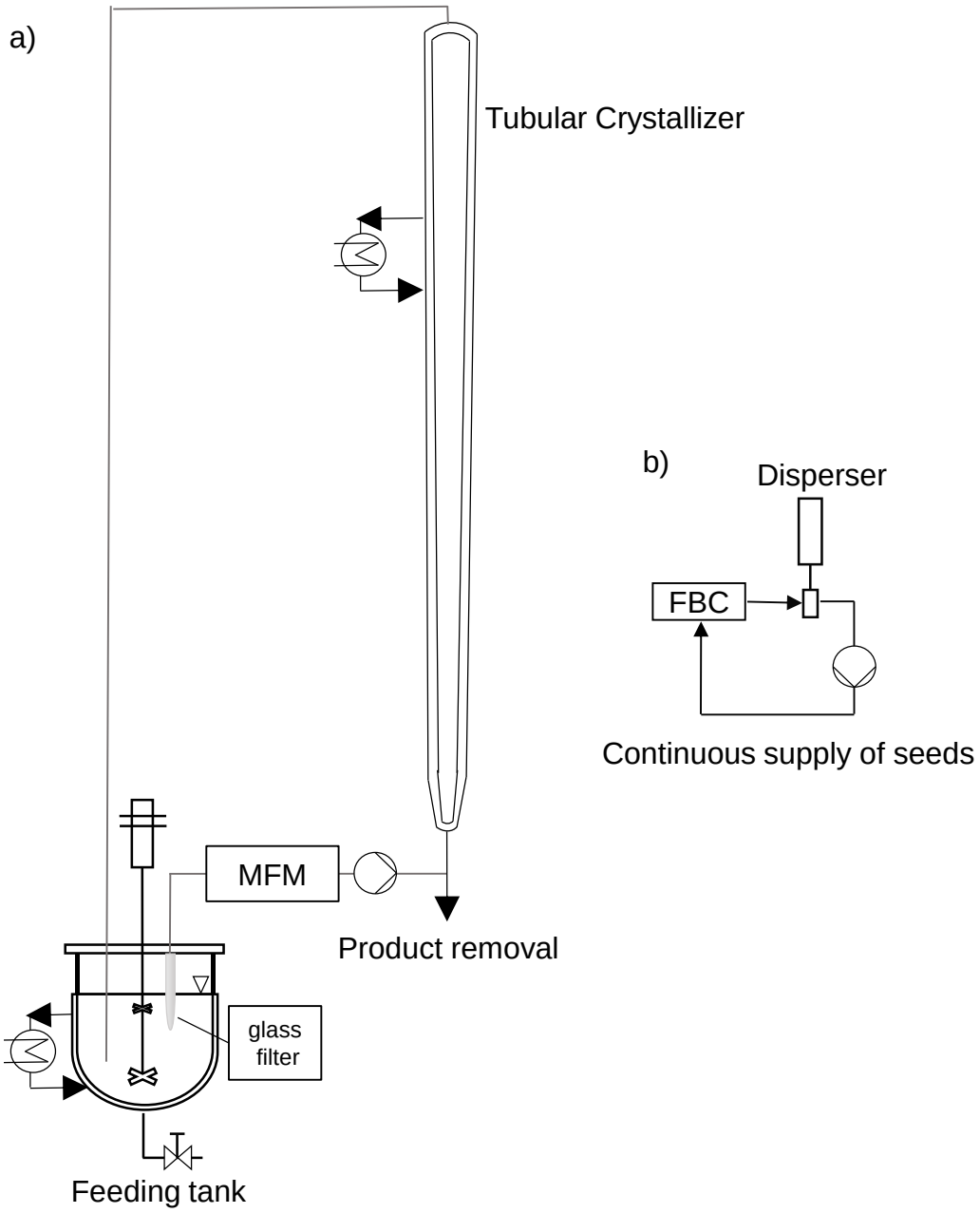

Figure 3. 6 Schematic representation of the fluidized bed setup (a) and of the external bypass for the continuous supply of seed crystals exploiting the disperser as milling device (b).

The setup consists of a tubular crystallizer of 0.478 L and total height of 1.054 m, characterized by a conical shape at the bottom, with an initial internal diameter of 5.63 mm and opening angle of 1.87° and a cylindrical shape in the upper part having internal diameter of 13.05 mm. The tubular crystallizer was connected to a stirred feed tank of 7.5

L volume equipped with a stirrer and a fritted glass filter. The upper part of the tubular crystallizer was connected to an electrically heated pipe, which allowed the solution to be transported back to the stirred feeding tank. All the tanks were double-jacketed and connected to a thermostat. The racemic saturated solution was continuously pumped *via* gear pumps from the feeding tank to the tubular crystallizer and a flow/meter controller was used to monitor the flow rate. The preparation of the experimental runs consisted in preparing a solution within the feeding tank saturated at T_{sat} =35 °C in the presence of *ca.* 200 g of racemic guaifenesin as solid excess. The gear pump was then activated and the crystal free solution was transported to the tubular crystallizer, thermostated at the crystallization temperature. A first preliminary investigation was performed using water as solvent and it has demonstrated the unsuitability of this solvent for the crystallization of enantiopure guaifenesin in a tubular fluidized bed crystallizer. Therefore, further experiments, which are discussed in chapter 4.2, have been performed in a different solvent, *i.e.* isopropanol. A first test run in isopropanol has been carried out using racemic guaifenesin as seed crystals instead of pure enantiomer. The aim was to investigate several experimental conditions such as supersaturation ratio and flow rate of the racemic feed as well as to verify the applicability of the disperser tool as a milling device (Figure 3.6b), for the continuous supply of seed crystals. In such initial investigation, a disperser IKA ultra-turrax T25 digital was used as a milling device for the continuous generation of seed crystals. In general, the mechanism of the disperser device is based on a rotor/stator principle: when the disperser device is activated, the crystals suspended in the saturated solution are dragged between the rotor and the stator due to the high rotation speed of the rotor and then pushed towards the slots of rotor/stator, thus exiting as dispersed suspension (Figure 3.6b). Three different crystallization temperatures between 30 and 25°C and a flow rate between 1.3 and 3.7 L/h were tested during such a preliminary experiment. An amount of 5 g of racemic guaifenesin was introduced as initial seed crystals at each crystallization temperature. After introducing the seed crystals from the top of the crystallizer, the milling device was then activated at the minimum rotation speed of 3000 rpm. The product at each run was collected by emptying the crystallizer and the crystals were washed with ice-cold solvent. In a further investigation, a different seeding strategy was exploited, consisting in the periodical manual introduction of recrystallized homochiral crystals as seed crystals. After saturating the feed tank to saturation concentration (T_{sat}=35 °C), the tubular crystallizer was cooled to T_{cryst}= 25 °C and seed crystals of enantiopure guaifenesin have been manually introduced from the top of the

crystallizer. A constant flow rate of 2 L/h was chosen to ensure a continuous refreshment of the mother liquor up to racemic composition. Five resolution runs have been performed exploiting the periodic manual seeding strategy. The harvesting consisted in the periodic collection of the whole suspension contained within the tubular crystallizer, after 90 min from the seeding with a subsequent vacuum filtration and washing of crystals. The yield of each resolution runs was calculate using Eq. 3.10. Especially, the theoretical mass of the product,$m_{product}^{theoretical}$, was calculated taking into account the total volume of solvent used for each resolution. This is obtained by multiplying the volumetric flow rate of the racemic mother liquor within the tubular crystallizer, 2 L/h, and the time of the run, 1.5 h, thus resulting in 3 L of solvent. The productivity was calculated using Eq. 3.11.

3.3.4 HEL reactor

An autoMate HEL reactor (UK) was used for the resolution runs of methionine enantiomers in aqueous solution. The crystallization setup consisted of a 350 mL vessel, placed in an the automated system equipped with an anchor stirrer and a temperature probe. A reflux condenser with provision to apply vacuum was connected to the vessel. After preparing a solution of methionine enantiomers at the eutectic composition of x_{eu}=0.94 in water, the solution was heated to 60 °C. The temperature of the reactor was maintained constant at 60 °C by means of a programmed thermostat. Water was evaporated at constant temperature of 60 °C by applying a vacuum of 200 mbar. The evaporated water was condensed and collected in a flask placed on a balance. After the evaporation of a targeted amount of water from the saturated solution, the experiment was stopped and the crystallized material was collected by filtration and washed with ice-cold water.

3.3.5 Preparation of seed crystals

For the resolution runs in single stirred tank (single batch PC) as well as for the CPCD runs, the seed crystals of *(R)*-CPG-intermediate and enantiopure guaifenesin were prepared by manually crushing in a mortar homochiral crystals of the desired compound. A chosen amount of the fine powder was then weighted and manually introduced into the crystallizer at the opportune time. The preparation of the seed crystals for the PC in tubular fluidized bed crystallizer consisted in the recrystallization of pure enantiomeric guaifenesin from a solution enriched with respect to the desired enantiomer in isopropanol. Several product amounts collected from the resolution runs in stirred tanks (either single or

coupled tanks) were used. After the determination of the chiral purity (HPLC) of the products collected from each run, the chiral purity of the total amount of solid to be recrystallized was then calculated. At this point, the related amount of impurity defined as racemic mixture has been derived and the amount of solvent needed for its complete dissolution has been calculated from the known solubility data. The final crystallization temperature of the recrystallization run has the been chosen accordingly. The recrystallization run consisted in a first complete dissolution of the solid in isopropanol in the 450 mL volume stirred tank, represented in Figure 3.4. Afterwards, a crash cooling of the solution to T= 5 °C has been performed in order to induce the formation of as many nuclei as possible. The temperature was then increased to a temperature 10 °C higher than the chosen crystallization temperature. It is worth to mention that, at this stage of the recrystallization process, it is necessary that a cloud of crystals remains suspended in solution in the phase of heating and that the solid previously nucleated is not completely dissolved. The idea is that the nuclei present in solution at high temperature act as nuclei of growth during the cooling ramp. The solution has been afterwards cooled to the chosen crystallization temperature with a cooling rate of 1 K/h. The controlled cooling ramp allowed the formation of a uniform population of crystals with respect to the length and width. The suspension was then collected and filtrated and the crystals were washed with ice-cold solvent. In general, the recrystallization procedure described above was used as a further purification step after the resolution processes and it allowed to obtain up to 15 g of pure enantiomeric guaifenesin at high chiral purity (> 99%).

3.4 Process analytics

In this section, the main analytic tools used to monitor the crystallization process as well as to determine the chiral purity of the products collected from the resolution runs are reported.

3.4.1 Turbidity and optical rotation

A turbidity probe (Mettler Toledo, Trb. 8300) located within the stirred tank (Figure 3.4 and Figure 3.5, Dissolution tank), was used to monitor the suspension density during the progress of the resolution runs. In particular, the turbidity signal allowed the observation of the increase of the suspension density during single batch PC experiments while for the CPCD experiments, the probe was inserted into the dissolution tank to observe the

selective dissolution of one enantiomer from the suspended racemic solid phase. The optical rotation of the mother liquor during PC and CPCD experiments was monitored by an on-line polarimeter (POLARmonitor, IBZ, Messetechnik, Germany) equipped with a thermostated polarimeter cell.

3.4.2 Concentration determination using densitometry

Observation of the total concentration profile during the resolution runs *via* single batch PC for the system guaifenesin in isopropanol and water has been possible through an on-line densitometry (DE-40, Mettler Toledo). As the density of the solution was not only dependent by the concentration but also by the temperature of the densitometer cell, a calibration as a function of both concentration and temperature of the cell was necessary. The calibration consisted in the preparation of a solution of the studied system at several concentrations by adding to the solvent subsequent amounts of solid. After each addition, the temperature of the cell was varied and the density was recorded for each temperature. A plot of concentration as a function of temperature of the cell and density was then derived from the obtained data. After fitting the data with an appropriate function, a regression from the experimental density data points, allowed the determination of the total concentration during the experiments.

3.4.3 Enantioselective high performance liquid chromatography (HPLC)

HPLC measurements with a chiral stationary phase have been performed for all of the model compounds in order to determine the purity of the collected products from the resolution runs and the concentration and enantiomeric ratio for the solubility measurements of the studied systems. The determination of the chiral purity of CPG-intermediate samples in acetonitrile was performed using a Chiralpak column IA (5 µm) with a mobile phase of 70:30 (v/v) n-heptan/ethanol, a flow rate of 0.7 mL/min, at 20 °C and with injection volume of 4 µL. For the guaifenesin system a Chiralcel OD-H column (0.46 × 25 cm, Chiral Technologies Europe, Illkirch, France) was used with the following conditions: temperature 23 °C, eluent: 35:65 (v/v), 2-propanol/hexane, flow rate: 1.0 mL/min, and UV wavelength: 265 nm and with injection volume of 4 µL. For the amino acid methionine, a Chirobiotic column T (250 x 4.6 mm, 5 µm) was used, with a mobile

phase 60:40 (v/v) methanol/water, flow rate of 0.5 mL/min, at 25 °C and UV wavelength at 265 nm.

3.5 Liquid and solid-state characterization

3.5.1 Nuclear magnetic resonance (NMR) spectroscopy

Nuclear Magnetic Resonance (NMR) spectroscopy was used to determine possible molecular interactions of racemic guaifenesin in solution. ^{1}H-NMR spectra were recorded on a Brucker BioSpin 600 MHz AV Neo, 400 MHz AVIII or 300 MHz WB, AV I instrument. ^{1}H-NMR samples of racemic guaifenesin were prepared in methanol-d_4 and acetonitrile-d_3 at three different concentrations. The chemical shifts (δ_H) are quoted in part per million (ppm) and referenced to the appropriate residual solvent peak (CD_3OD: δ_H = 3.33 ppm, CD_3CN: δ_H = 1.97 ppm).

3.5.2 X-ray powder diffraction (XRPD) analysis

X-ray powder diffraction (XRPD) measurements were aimed to identify the solid-state form of the solid in equilibrium with the saturated solutions at various temperatures for the systems CPG-intermediate and guaifenesin. An X'Pert Pro diffractometer (PANanalytical GmbH, Germany) was used, with radiation CuKα, 2θ range between 3 and 40°, resolution step 0.017° and 50 s of counting time for each step. Temperature-resolved XRPD of *(R)*-CPG-intermediate has been carried out in order to investigate the stability of the crystal structure of the enantiopure compound as a function of the temperature.

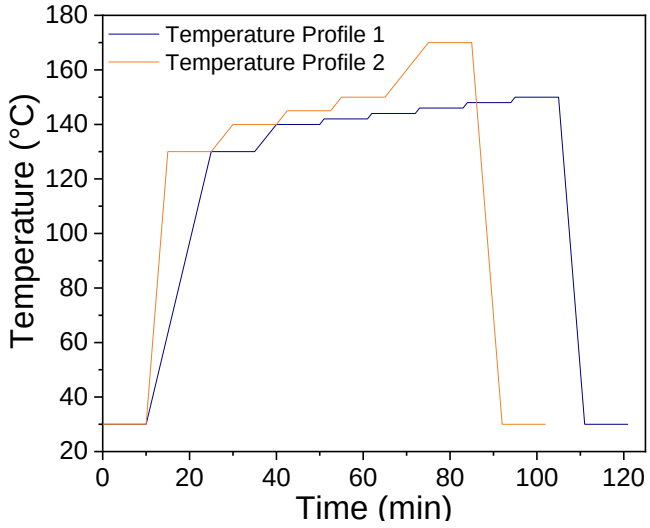

Figure 3. 7 Representation of the two step-wise temperature profiles used for temperature resolved XRPD measurements of *(R)*-CPG-intermediate.

Two step-wise temperature profiles have been used for this purpose: one temperature profile in the range between 130 and 148 °C (Figure 3.7, blue line), and a second temperature profile reaching higher temperatures (Figure 3.7, orange line).

3.5.3 Differential scanning calorimetry (DSC)

Differential scanning calorimetry (DSC) measurements for the system CPG-intermediate were performed with a DSC 131 Setaram (France), calibrated with pure metals (indium, tin, lead), under pure helium atmosphere. Solid samples at various known enantiomeric compositions have been ground with a pestle in a mortar in the presence of few drops of isopropanol, in order to create a homogeneous solution. After evaporation of the solvent, the solid has been ground again and few milligrams of solid mixture have been weighted for DSC measurements. The enantiomeric composition of the prepared mixtures has been verified by HPLC analysis. For the determination of the binary phase diagram heating rates of 2 and 5 K/h were chosen, while for the investigation of thermal behavior of enantiopure and racemic CPG-intermediate several heating rates were explored between 0.1 K/h and 50 K/h. A SETSOFT 2000 software was used to determine the melting points of the substances. The melting point of enantiopure and racemate samples has been determined from the onset temperature of the single endotherm peak. For mixtures at various enantiomeric compositions, the solidus and liquidus line in the phase diagram were determined from the onset temperature of the eutectic endotherm and the temperature at the peak maximum of the component in excess, respectively.

3.5.4 Microscope images and crystal size determination

A Keyence microscope, equipped with a VH-Z100UR magnification lens, has been used in order to determine morphological properties and size of the product crystals collected during the crystallization experiments of guaifenesin in isopropanol in tubular fluidized crystallizer. A sample of crystals of seed or product crystals was located on a glass slide and observed at the microscope. A chosen magnification (between 100 and 200 micron) was selected. Length and width of a population of a minimum of 250 crystals were manually determined for each sample and the related size distribution was then determined.

3.5.5 Liquid and particle density determination

An off-line DM-40 Mettler Toledo densitometer was used to determine the density of various solutions of racemic guaifenesin in five different solvents *i.e.* water, ethanol, acetone, isopropanol, and ethyl acetate. Based on the solubility data previously determined, the solutions saturated at T= 30 °C were prepared and injected into the densitometer cell. The temperature of the densitometer cell was set at 30 °C. Three replicates of the density-measurements were performed.

A pycnometer was used to determine the solid density of one of the studied systems, *i.e.* racemic guaifenesin. After determining the mass of the pycnometer, solid racemic guaifenesin has been introduced into the device up to two third of its volume and the mass of the pycnometer with the solid has been determined. Afterwards, the pycnometer was filled with a solvent in which racemic guaifenesin is completely insoluble, in this case TBME, and covered with its appropriate capillary cap. The total mass with the added solvent was then determined. The solid density of racemic guaifenesin has been hence calculated following Eq. 3.17:

$$\rho_{solid} = \frac{m_2 - m_1}{V_1 - (\frac{m_3}{\rho_3})} \tag{3.17}$$

Where, m_1 is the mass of the empty pycnometer, m_2 is the mass of the pycnometer filled with solid racemic guaifenesin, m_3 is the mass of TBME, ρ_3 is the density of TBME and V_1 is the total volume of the pycnometer.

Chapter 4. Experimental results

In the present chapter, the results of the experimental work done will be presented. The chapter is divided in two sections, one for each model compound investigated. In each section, firstly the attention will be devoted to the fundamental investigations of the solubility of each system as well as its solid-state properties. Then, the operating conditions of the resolution runs and the performances of the crystallization processes will be discussed.

4.1 Clopidogrel (CPG) intermediate system

In the first section of this chapter the attention will be devoted to the substance 2-(benzylideneamino)-2-(2-chlorophenyl) acetamide here named as clopidogrel intermediate (CPG-intermediate). The experimental investigation will comprehend the determination of the solubility of the system as well as the determination of its MSZW. Afterwards the results of the PC runs exploiting two crystallizer configurations will be discussed. An assessment on the applicability of the preferential crystallization technique with respect to the performances of the resolutions as well as the kinetics of the system will be provided. The performances of the resolution runs in single stirred tank will be evaluated over a range of experimental conditions applied, *i.e.* initial supersaturation values, aimed at identifying the best experimental conditions for resolution purposes. The evaluation will be extended to the resolution runs exploiting the coupled configuration for the CPCD approach. Furthermore, the thermal properties of the CPG-intermediate will be described based on the results of the DSC measurements. The attention will be especially

devoted to the experimental determination of the binary melt phase diagram of the system. The peculiar thermal behaviour of the system will be described and considerations on the occurrence of a racemization reaction at the melting temperature will be provided. Based on the molecular structure of the studied system as well as the information on the racemization reaction of similar compounds, a mechanism of racemization will be proposed.

4.1.1 Introduction on Clopidogrel drug and the derivative model compound studied

Clopidogrel, sold as brand name Plavix (Sanofi Pharma Bristol-Myers Squibb), is an antithrombotic agent and inhibitor of platelet aggregation, applied in treatment of arteriosclerosis, myocardial infarction, ischemic stroke and vascular death.[119] The desired biological activity resides in the *(S)*-enantiomer (Figure 4.1a), while the *(R)*-enantiomer is inactive.[120] The drug has developed a formidable presence in the global market over the years, capturing the attention of the scientific community in the field of chemistry, chemical engineering and pharmacological chemistry.[121,122] Although several synthetic methodologies have been developed in order to efficiently produce this molecule at industrial scale, the current industrial synthetic methods of Clopidogrel, suffer from several inconveniences, including low yield, efficiency and high raw material cost.[123] Furthermore, at present, six types of Clopidogrel polymorphs have been reported and among them two forms are selectively used for the manufacturing of its drugs. Hence, the experimental conditions need to be chosen accurately in order to produce only the desired polymorphic form.[121] Not only the production of the right polymorphic form but also the production of the correct enantiomeric form must be taken into account in the manufacturing of Clopidogrel; therefore, much work has been devoted in the field of chiral synthesis, crystallization-based separation processes, and chromatography for the isolation of this compound.[124] Considering the challenging manufacturing of enantiomerically pure product, it has been found advantageous to rather focus on the building blocks of the compound, such as its imine derivatives, which are more accessible and better suited for scale up processes.[125,126]A key intermediate in the synthesis of Clopidogrel is the 2-(benzylideneamino)-2-(2-chlorophenyl) acetamide (Figure 4.1b), which is studied in this first section of chapter 4 and herein reported as CPG-intermediate. Within the field of chiral resolution, CPG-intermediate has been subject of studies in the development of a

promising deracemization technique, namely Attrition Enhanced Deracemization (AED), which is an effective and potential new approach of preparation of pure enantiomers. CPG-intermediate is known as a conglomerate forming system which gives racemization in solution in the presence of DBU.[125,126] In a more recent study, Blackmond *et al.*,[83] have applied the AED approach on the CPG-intermediate system and its isotopic forms and have provided fundamental understanding on the origin and evolution of homochirality as well as information on solubility and melt phase diagram of the chiral system. Although the system appears to be suitable for preferential crystallization, no example of such investigation is reported, to our knowledge.

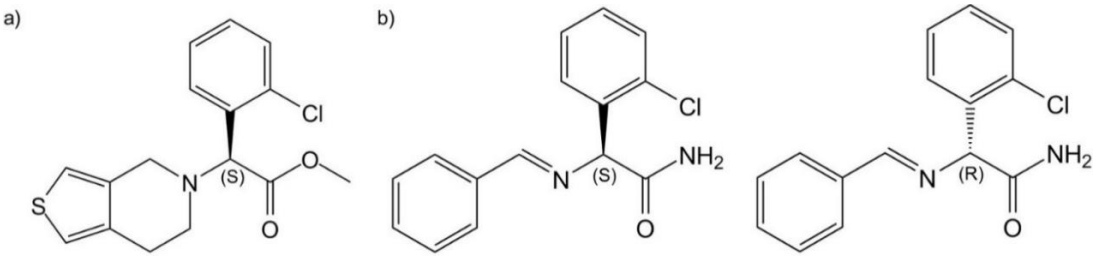

Figure 4. 1 Molecular structure of the active enantiomer of Clopidogrel (Plavix) (a), and enantiomers of CPG-intermediate (b).

4.1.2 Solubility and metastable zone width of CPG-intermediate in acetonitrile

The solubility data of the racemic CPG-intermediate determined in acetonitrile are listed in Table 4.1. The system exhibits low solubility in acetonitrile as well as an upward trend as the temperature increases, from *ca.* C_{sat} =0.01 g $_{solute}$/g $_{solution}$ at 10 °C to 0.036 g $_{solute}$/g $_{solution}$ at 40 °C.

Table 4. 1 Experimental Solubility Data of racemic CPG-intermediate in acetonitrile between 10 and 50°C and related Standard Deviation (SD).

T (ºC)	C_{sat} (g $_{solute}$/g $_{solution}$)	SD%
10	0.0103	0.04
20	0.0134	0.04
25	0.0189	0.09
30	0.023	0.2

40	0.036	0.01
50	0.064	0.8

In order to determine the MSZW of the system, the so-called Nývlt method has been applied. As shown in Figure 4.2a, the ΔT_{max} was calculated at each saturation concentration and plotted as a function of the cooling rate. One can see that, at each cooling rate and saturation concentration, a large variation of the calculated ΔT_{max} occurs, as a result of the typical variation of the cloud points detected at each repetition, due to the stochastic nature of the primary nucleation. The extrapolation of the maximum subcooling at the zero cooling rate, allowed determining the nucleation curve shown, hence the MSZW as shown in Figure 4.2b. As shown, the MSZW increases as the temperature decreases. Specifically, from the width of the metastable region it can be seen that the spontaneous nucleation of the system in acetonitrile can be avoided when the solution is subcooled up to 4 °C at a saturation concentration of 0.03 g $_{solute}$/g $_{solution}$ and to 1 °C at a saturated concentration of 0.02 g $_{solute}$/g $_{solution}$.

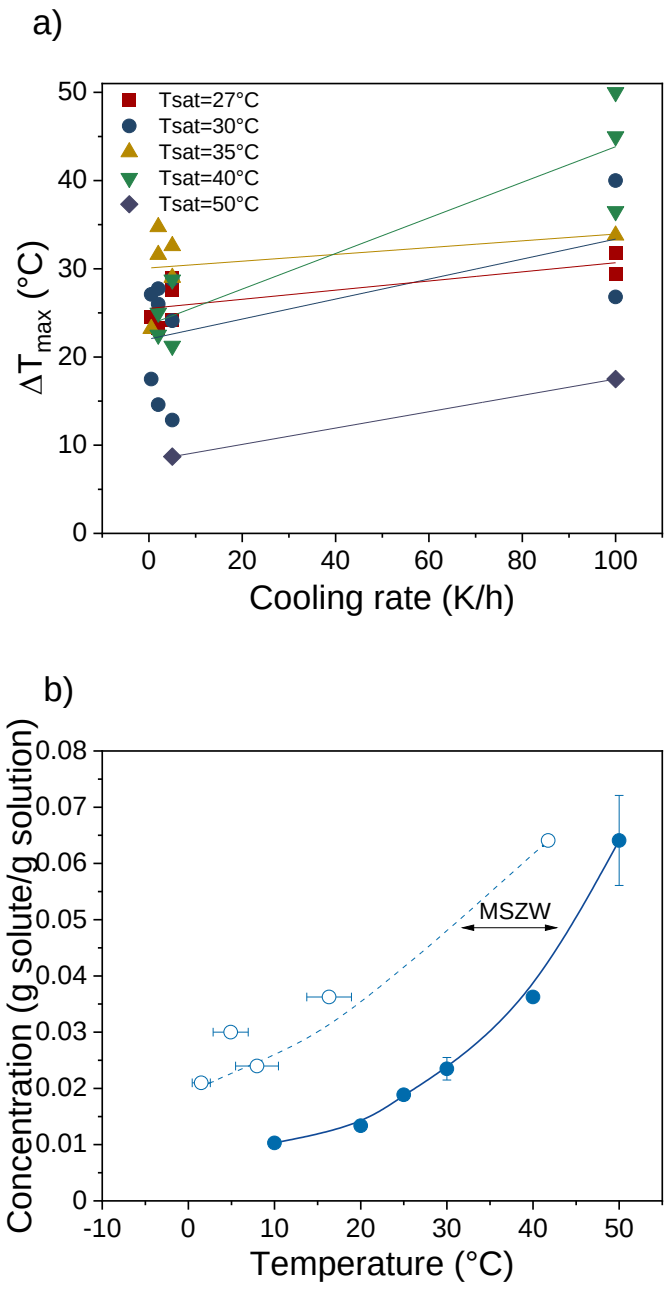

Figure 4. 2 Representation of the experimental ΔT_{max} (°C) as a function of the cooling rate determined for solutions of racemic CPG-intermediate in acetonitrile (a). Experimentally determined solubility data (full blue dots) and nucleation points for a fictitious zero cooling rate (empty blue dots) of racemic CPG-intermediate in acetonitrile (b). Solid and dashed lines are a guide for the eyes.

The solubility ternary phase diagram of the system between 10 and 40 °C is illustrated in Figure 4.3a. The system behaves as a conglomerate forming system under the studied conditions, with the highest solubility at racemic composition. The experimental solubility data refer to mixtures with *(R)*-CPG-intermediate in excess; therefore, they are located in the left side of the ternary phase diagram in Figure 4.3. The right side is constructed symmetrically to the racemate-solvent line (black, dashed line in Figure 4.3).

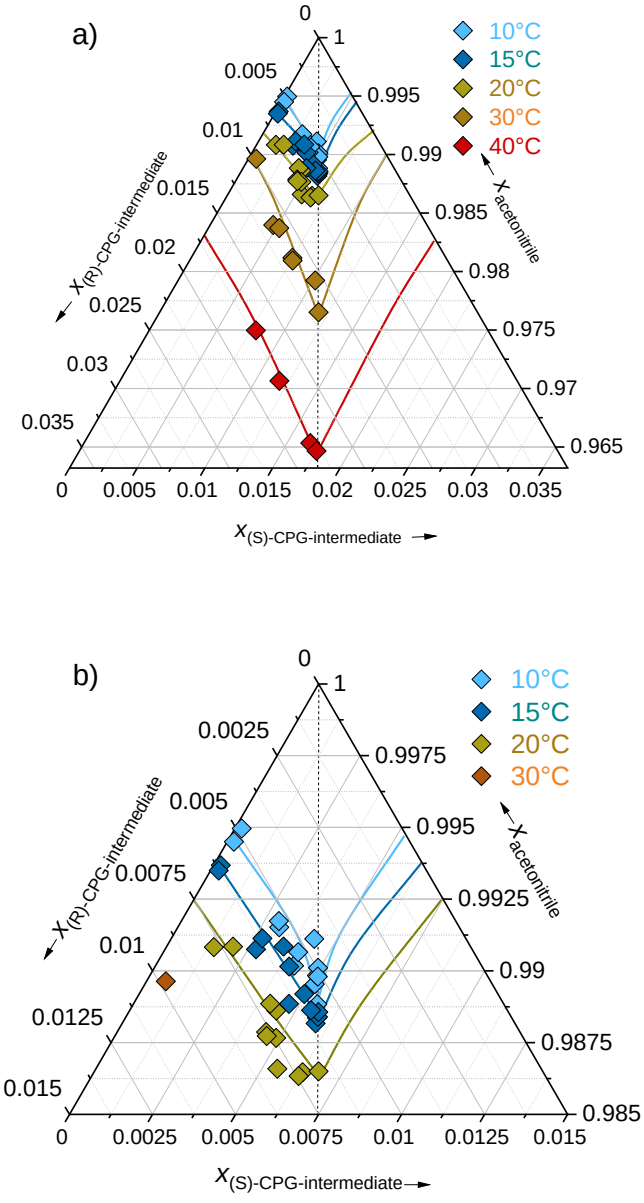

Figure 4. 3 Experimentally determined solubility data of *(R)-/(S)*-CPG-intermediate in acetonitrile between 10 and 40 °C. Magnification of the upper 3.5 % (a) and magnification of the upper 1.5 % (b) of the complete phase diagram are represented.

The values of the Meyerhoffer coefficient, α, at different temperature can be derived from the ratio of solubility between the racemic mixture and the enantiopure system. The coefficient value is 2.01 at 10 °C, 1.73 at 20 °C (from the extrapolated value of solubility at enantiopure composition) and 2.11 at 30 °C, hence suggesting that the double solubility rule is closely observed under the studied conditions. After equilibration of the saturated solutions, the solid in excess has been filtrated, dried and analyzed by XRPD in order to verify the presence of only one solid-state form of racemic CPG-intermediate. Figure 4.4 shows the X-ray diffractograms of the solid phase in equilibrium with saturated solutions of racemic CPG-intermediate in acetonitrile at different temperatures. As the XRPD patterns are identical with the reference one, it can be assumed that the system does not exhibit polymorphism or solvates formation under the studied conditions.

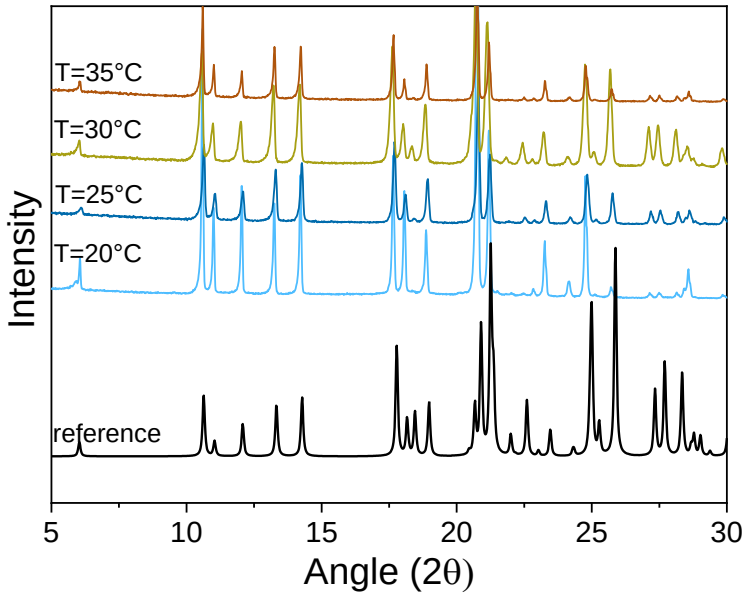

Figure 4. 4 Experimental XRPD patterns of solid racemic CPG-intermediate in equilibrium with its saturated solution in acetonitrile, between 20 °C and 35 °C . Reference pattern from ref [83] is illustrated at the bottom of the figure.

4.1.3 Single batch PC of *(R)*-CPG-intermediate in acetonitrile

The preferential crystallization of *(R)*-CPG-intermediate from its racemate solution has been carried out in acetonitrile as solvent. After filling the stirred tank with 355 g of solvent, the analytics of the setup have been activated and the stirred tank was thermostated to a temperature 5 to 10 °C above the desired saturation temperature. Afterwards, a chosen amount of the solute racemic CPG-intermediate was added to the solvent and completely dissolved. After equilibrating the system for *ca.*15 min at high temperature, the solution was cooled to the chosen crystallization temperature, which for each experiment was 20 °C. After equilibrating the system at such temperature, 0.2 g of manually ground seed crystals have been introduced into the stirred tank in order to initiate the preferential crystallization of the seeded enantiomer. The experimental conditions of the runs are listed in Table 4.2.

Table 4. 2 Experimental conditions of single batch PC runs of *(R)*-CPG-intermediate in acetonitrile.

experiment	1	2	3	4
supersaturation (S)	1.78	1.96	2.40	2.75
T_{cryst} (°C)	20	20	20	20
T_{sat} (°C)	30	32	35	37
m_{solute} (g)	8.6	9.6	11.1	12.5
$m_{solvent}$ (g)	355	355	355	355
m_{seed} (g)	0.2	0.2	0.2	0.2
C_{sat} ($g_{solute}/g_{solution}$)	0.024	0.026	0.030	0.034

Four experiments at different supersaturation ratios between 1.78 and 2.75 were conducted. Such values were achieved by keeping constant the crystallization temperature and varying the starting point of the separation process, *i.e.* the initial saturation concentration of the racemic solution (Figure 4.5).

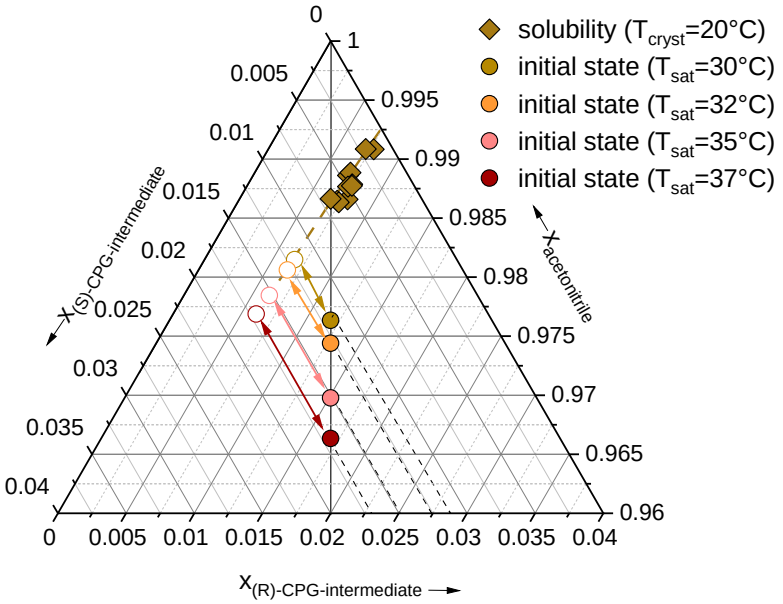

Figure 4. 5 Representation of the supersaturation degree for single batch PC runs of (R)-CPG-intermediate in acetonitrile. Full brown rhombuses in the upper part of the ternary phase diagram represent the solubility points at T_{cryst}, *i.e.* 20 °C. The full coloured dots at racemic composition represent the initial state of the system for each experiment, *i.e.* the initial saturated conditions. The empty coloured dots represent the reference state of the system for each saturation concentration. The arrows between the two states represent the initial driving force of each process.

A strategy control of the resolution runs was mainly given by the optical rotation signal of the mother liquor during the crystallization experiments. Although it is not possible to detect the exact moment of the nucleation of the counter-enantiomer using the optical rotation signal, a rough orientation of the depletion of the mother liquor with respect to the seeded enantiomer can be provided by observing the trend of the signal in time. The optical rotation signals of the four single batch PC runs are represented in Figure 4.6. As crystals of pure *(R)-(+)*-CPG-intermediate were used as seed crystals, the optical rotation of the mother liquor exhibits negative values as the crystallization of the seeded enantiomer proceeds. As illustrated by the curves, towards the end of each process the optical rotation signals decrease with lower speed compared to the initial trend. This behavior is primarily caused by the fact that as the crystallization of the seeded enantiomer

proceeds, its crystallization driving force decreases and therefore its crystallization kinetic is slower.

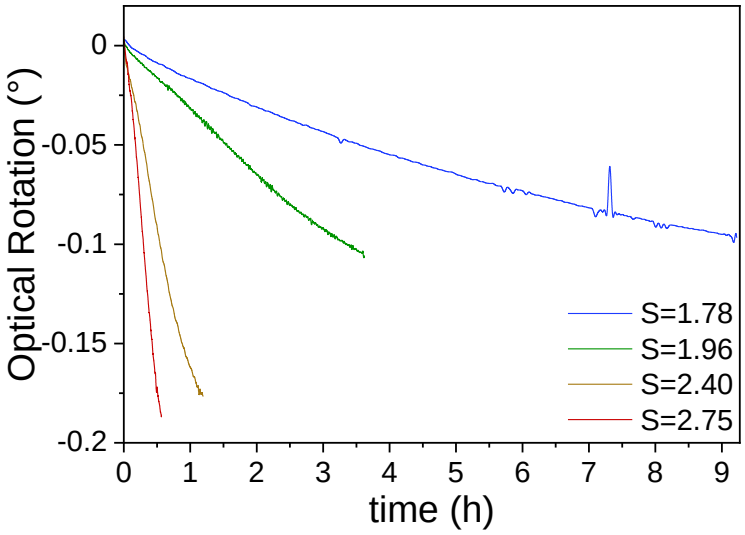

Figure 4. 6 Representation of optical rotation signals of the mother liquor in single batch PC runs of *(R)*-CPG-intermediate in acetonitrile at different supersaturation ratio. Seeding time corresponds to zero.

In general, the contamination of the counter-enantiomer is detected by the optical rotation signal only when the growth rate of the seeded enantiomer has reached levels such that the solution concentration difference between preferred and counter-enantiomer has been decreasing, hence causing a change of the sign of the optical rotation signal.[104,127] In the present investigation the crystallization processes has been interrupted before the occurrence of the change of sign of the optical rotation signal, specifically in correspondence of a change in the decay rate of the signal.

Table 4. 3 Experimental results of single batch PC runs of *(R)*-CPG-intermediate in acetonitrile.

experiment	1	2	3	4
$m_{product}$ (g)	0.8	0.9	1.5	1.8
$t_{production}$ (h)	9.3	3.7	1.2	0.58
Pu %	95.8	97.5	98.7	95.4
Pr (g/h/L)	0.1	0.4	2.4	5.8
Y %	30	30	41	40

The experimental results of the four runs are listed in Table 4.3. As the supersaturation ratio increases, the production time decreases from 9.3 hours to roughly half an hour. The chiral purity of the product is low in two cases, at lower initial supersaturation, *i.e.* experiment 1, due to the long production time (over 9 hours) and at higher initial supersaturation, *i.e.* experiment 4, probably due to the fast nucleation kinetics of the counter-enantiomer. Experiment 2 and 3 provided chiral purity of 97.5 and 98.7 %. An upgrade of the purity up to >99 % can be achieved either by further washing of the collected products or by a recrystallization run, exploiting the solubility ternary phase diagram data.

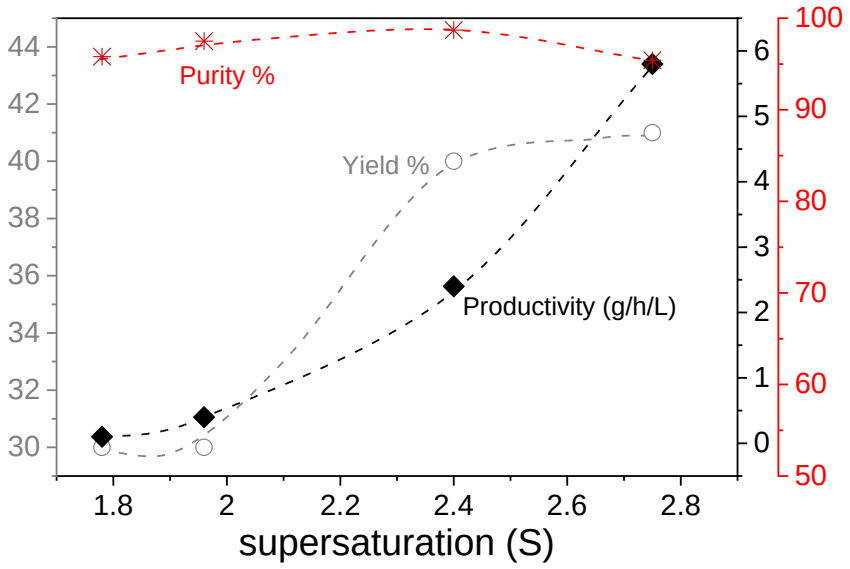

Figure 4. 7 Representation of obtained KPIs for single batch PC runs of (*R)*-CPG-intermediate in acetonitrile as a function of the initial supersaturation ratio.

As shown in Figure 4.7, based on the performance parameters calculated for each experiments, the best operation conditions for the production of pure CPG-intermediate in acetonitrile *via* single batch PC can be chosen at a supersaturation degree between 2.4 and 2.75.

4.1.4 Coupled batch PC and dissolution of *(R)*-CPG-intermediate in acetonitrile

CPCD experiments have been carried out using the coupled configuration described in chapter 3. Two runs have been performed, referred as experiment 1 and experiment 2 in Table 4.4. After the preparation of the racemic solution in both the crystallization and dissolution tank, saturated at 32 °C for experiment 1 and at 35 °C for experiment 2, the crystallization tank has been cooled to T_{cryst}=20 °C in both of the experiments. Hence, a supersaturation degree of 1.96 for experiment 1 and 2.40 for experiment 2 was achieved in the crystallization tank. An amount of 15 g of racemate in excess was introduced into the dissolution tank for both of the experiments. The process has been started by seeding the supersaturated solution into the crystallization tank with 0.2 g of pure *(R)*-CPG-intermediate and by activating the solid liquid exchange to a rate up to 30 mL/min.

Table 4. 4 Experimental conditions of CPCD runs of *(R)*-CPG-intermediate in acetonitrile.

experiment 1		
	crystallization tank	dissolution tank
supersaturation (S)	1.96	
T_{cryst} (°C)	20	
T_{sat} (°C)	32	32
m_{solute} (g)	9.6	9.6
$m_{solvent}$ (g)	355	355
m_{seed} (g) | m_{excess}(g)	0.2	15
C_{sat} ($g_{solute}/g_{solution}$)	0.026	0.026
experiment 2		
	crystallization tank	dissolution tank
supersaturation (S)	2.40	
T_{cryst} (°C)	20	
T_{sat} (°C)	35	35
m_{solute} (g)	11.1	11.1
$m_{solvent}$ (g)	355	355
m_{seed} (g) | m_{excess}(g)	0.2	15

C_{sat} ($g_{solute}/g_{solution}$)	0.030	0.030

Figure 4.8 illustrates the optical rotation signals of the mother liquor within the crystallization tank and dissolution tank for the two experiments. For the first experiment (Figure 4.8a), it can be observed that the optical rotation signal of the mother liquor in the crystallization tank increases in absolute value from the seeding, *i.e.* as soon as the crystallization of the seeded enantiomer is triggered (Figure 4.8a, red line). Ideally, the composition of the mother liquor in the crystallization tank is expected to be close to racemic values, as a result of the exchange of the mother liquor between the two tanks. Therefore, an optical rotation signal close to zero should be observed (Figure 4.8, dashed black line). As the optical rotation signal of the mother liquor in the crystallization tank deviates from zero, it can be deduced that the activation of the liquid exchange is not able to balance the depletion of the preferred enantiomer in the mother liquor within the crystallization tank. A similar trend is observed for the optical rotation signal of mother liquor in the dissolution tank (Figure 4.8, blue line). Such behavior indicates that the mother liquor within the dissolution tank is enriched with respect to the counter-enantiomer. Although this should trigger the selective dissolution from the solid racemate in excess, it appears that the dissolution process occurs slowly. As a result, both of the mother liquors are enriched with respect to the counter-enantiomer. Such behavior might be due to the low difference of concentration between the mother liquor within the crystallization tank and the saturated solution within the dissolution tank.

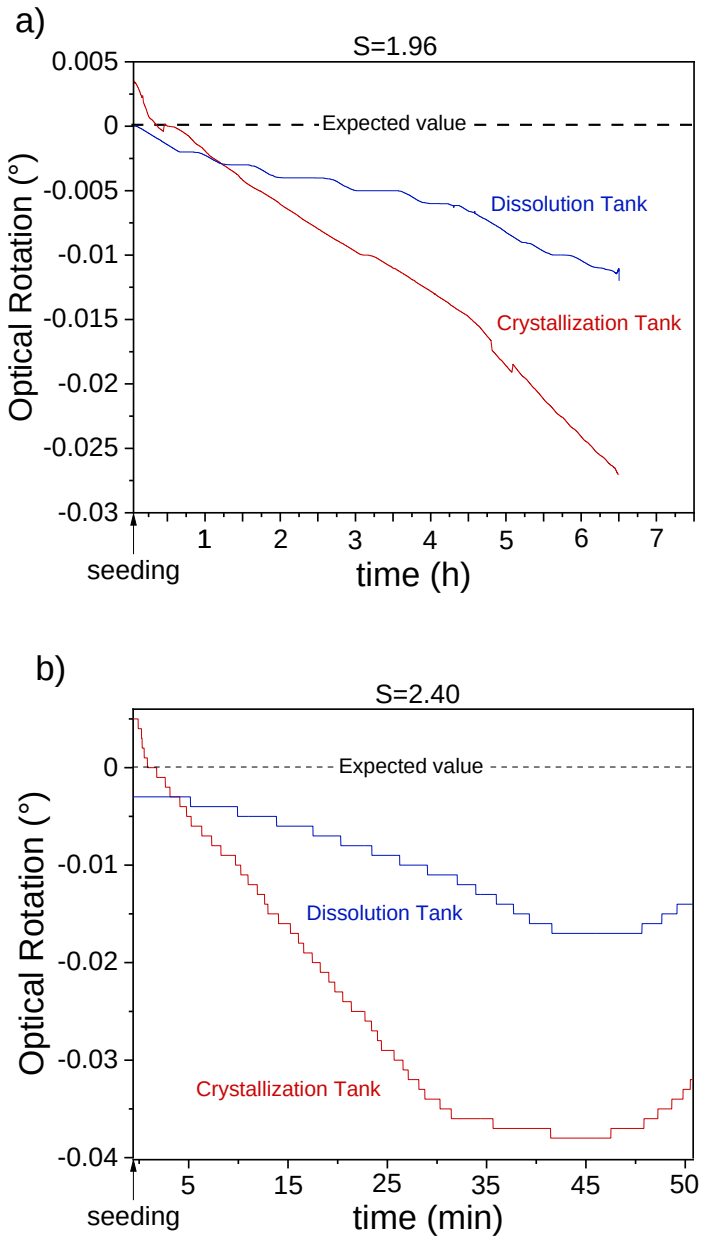

Figure 4. 8 Representation of optical rotation signals of the mother liquor within the crystallization tank (red line) and dissolution tank (blue line) in CPCD runs of (R)-CPG-intermediate in acetonitrile at initial supersaturation S=1.96 (a) and S=2.40 (b).

In order to overcome this limitation, an increase of the difference of temperature between the two tanks has been investigated. The optical rotation signals of the mother liquor from crystallization and dissolution tank of the second experiment are illustrated in Figure 4.8b. A higher concentration difference between the mother liquors should lead to a faster

selective dissolution within the dissolution tank. However, from Figure 4.8b, it can be seen that also for experiment 2 (Table 4.4), *i.e.* by keeping the crystallization temperature constant at 20 °C and increasing the saturation temperature of both of the tanks to 35 °C, the optical rotation signal of both solutions increases in absolute value. This suggests that the difference of saturation conditions explored in experiment 2 was not able to trigger the partial dissolution from the solid excess in the dissolution tank and to refresh the mother liquor up to racemic values. Moreover, due to the high supersaturation conditions, the production time is reduced to less than an hour, due to the nucleation of the counter-enantiomer within the crystallization tank.

Table 4. 5 Experimental results of CPCD runs of *(R)*-CPG-intermediate in acetonitrile.

experiment 1		
	crystallization tank	dissolution tank
$m_{product}$ (g)	1.6	13.5
$t_{production}$ (h)	6.75	6.75
Pu %	99.6	51.8
Pr (g/h/L)	0.47	2.31
Y %	0.14	0.93
experiment 2		
	crystallization tank	dissolution tank
$m_{product}$ (g)	1.55	14.88
$t_{production}$ (h)	0.93	0.93
Pu %	89.6	51.4
Pr (g/h/L)	2.85	18.27
Y %	0.11	1.01

The experimental results of the two CPCD resolution runs are summarized in Table 4.5. It can be seen that the limitations discussed above strongly affect the performances of the two runs. A small amount of product, *i.e.* 1.6 g and 1.55 g respectively for experiment 1 and 2 (Table 4.5), could be collected from the crystallization tank. Additionally, due to the contamination from the counter-enantiomer, the purity of the product collected from experiment 2 is reduced to 89.6 %. It is worth clarifying the high productivity value of 18.27

g/h/L reported for the dissolution tank in experiment 2. This value derives from the fact that the experiment 2 presents a lower production time compared with the production time of experiment 1 (Table 4.5), rather than a higher performance of the process. In fact, as expressed in Eq. 3.14 in chapter 3, the productivity of the CPCD process expressed for the dissolution tank, is defined as a function of $1/t_{production}$. Therefore, although the racemate solid excess in the dissolution tank remains at racemic composition and in high quantity during the experiment, at low production time, high productivity value can be expected.

4.1.5 Binary melt phase diagram and thermal behavior

The experimental DSC thermograms of racemic and enantiopure CPG-intermediate acquired at 2 K/min are depicted in Figure 4.9. One sharp endothermic peak related to the melting phase transition is observed at 143 °C and 148 °C respectively for the system at racemic and enantiopure composition. Under these conditions, no particular deviation of the heat flow due to decomposition of the system after melting is observed until 160 °C.

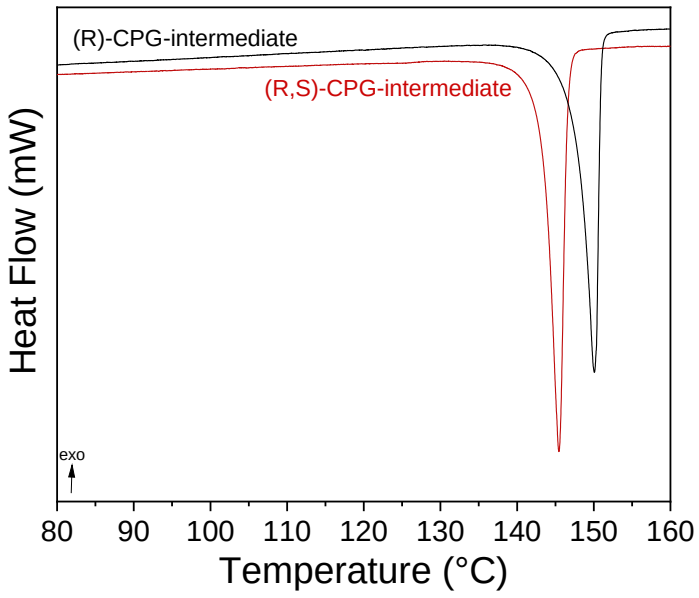

Figure 4. 9 DSC thermograms of CPG-intermediate at racemic and enantiopure composition between 80 and 160°C, at heating rate of 2K/min.

DSC measurements of the system at various enantiomeric compositions have been acquired at two different heating rates, *i.e.* at 2 and 5 K/min. The experimental melt binary phase diagram of the system at the two heating rates investigated is represented in Figure 4.10. As shown, while the melting temperature of the eutectic remains unvaried at 145 °C in both of the investigations, the points on the liquidus line are shifted towards higher temperatures for the investigation at higher heating rate, 5K/min (Figure 4.10, red triangles). Moreover the points on the liquidus line tend to flatten for enantiomeric composition x>0.75, hence showing a lack of dependency of the melting temperature from the enantiomeric excess.

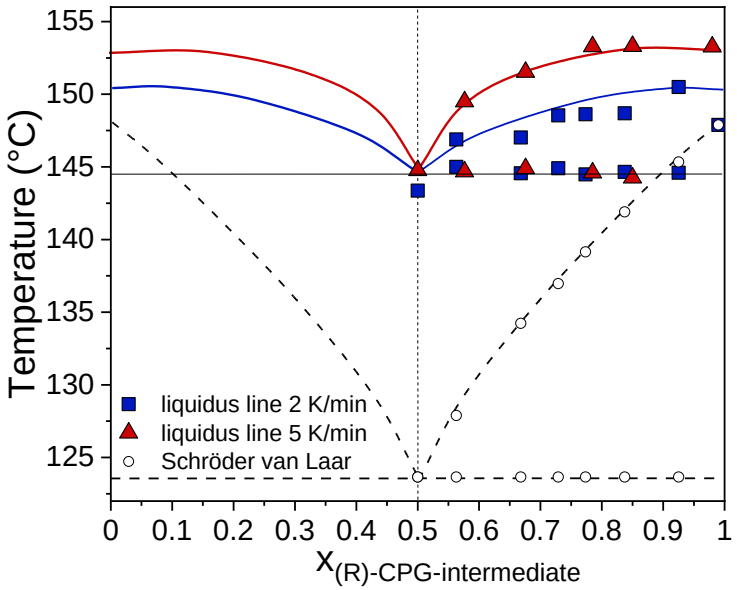

Figure 4. 10 Experimental melting point phase diagram of CPG-intermediate acquired at constant heating rate of 2 K/min (blue squares) and 5 K/min (red triangles). Eutectic line (black line), liquidus line at 2 K/min (blue line) and at 5 K/min (red line), are guides for the eye. The empty dots represent the predicted data from the simplified Schröder van Laar equation, using the experimental melting temperature and melting enthalpy of pure *(R)*-CPG-intermediate obtained at 2 K/min.

Using the data obtained for enantiopure component, the theoretical ideal liquidus curve has been calculated by means of the simplified Schröder van Laar equation (section 2.3.3). By comparing the theoretical data obtained with the experimental phase diagram,

it can be seen that the experimental points displayed in Figure 4.10 are not in agreement with the theoretical data (Figure 4.10, empty dots), suggesting that certain intermolecular interactions occur during heating, leading to a strong non-ideal behavior. Additional investigations on the molten material at enantiopure composition, by means of chiral HPLC, have shown the presence of two peaks on the chromatogram corresponding to the two enantiomeric forms of CPG-intermediate. Such investigation suggests that when the system is heated up to its melting temperature a change of its initial configuration occurs. As a consequence, it can be deduced that racemization occurs when the enantiopure compound is heated to its melting temperature as also reported by a very recent study on the same system.[83] Most likely, racemization and melting occur simultaneously during the heating with different kinetics. As a consequence of the racemization process, the enantiomeric composition of the enantiopure sample, as well as of the enantioenriched samples, decreases towards the racemic value, leading to a decrement of their melting temperatures. Moreover, from the experimental melting points at 2 and 5 K/min in Figure 4.10, it can be observed that the liquidus line tends to flatten at enantiomeric compositions close to pure enantiomer, indicating a faster racemization rate at higher enantiomeric excess. This can be attribute to the higher driving force for the racemization at higher enantiomeric excess, as observed already for other racemizable conglomerates.[128]

It can be expected that at lower heating rates, the melting event occurs with kinetics comparable to the racemization process, hence leading to the conversion of the enantiopure compound to its racemate form and therefore, causing a variation of the melting point of the studied mixture. On the other hand, at higher heating rates, the racemization process would occur with a certain delay with respect to the melting event, as the equilibrium conditions are no longer guaranteed. Under such conditions, the composition of the analyzed sample should not vary during the calorimetric analysis. Therefore, in order to find experimental conditions in which the racemization process was kinetically prevented, further investigations on the determination of the real melting temperature of the enantiopure compound have been done by performing DSC measurements at various heating rates between 0.1 and 50 K/min. From the DSC thermograms reported Figure 4.11, it can be seen that the melting of the enantiopure compound undergoes a shift from 143 °C to 154 °C as the heating rate increases from 2 to 20 K/min (Figure 4.11a).

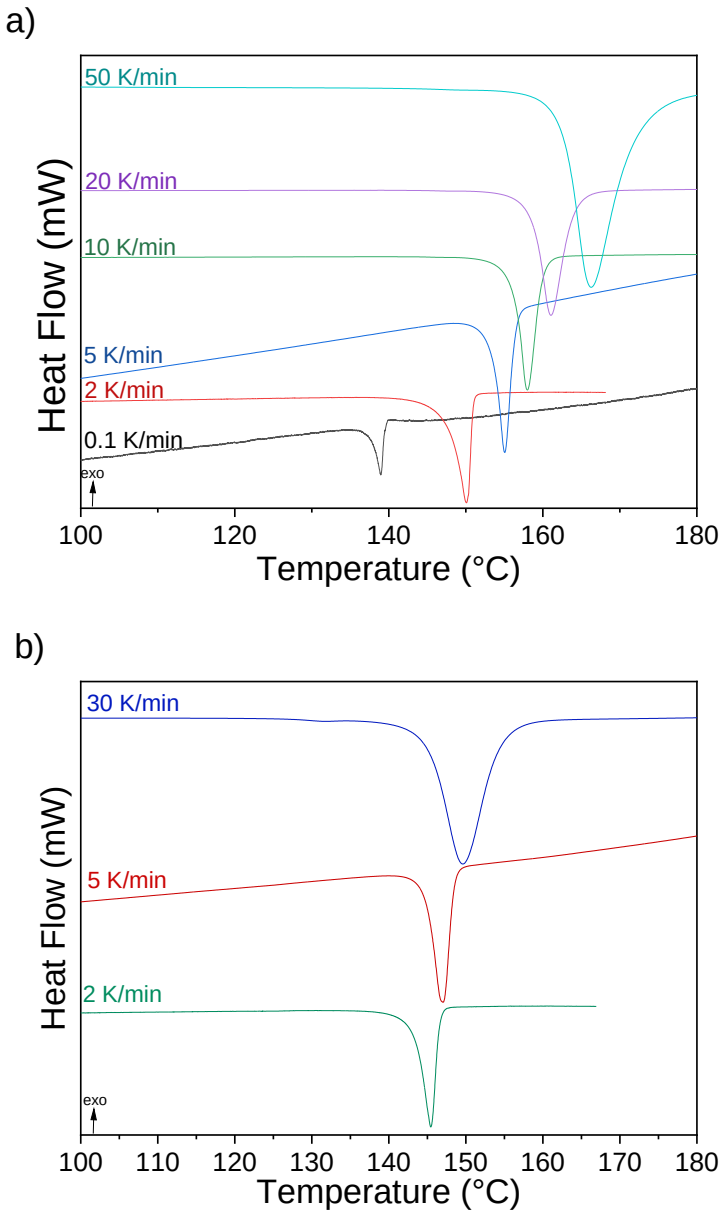

Figure 4. 11 DSC thermograms of CPG-intermediate at enantiopure composition between 100 and 180 °C, at heating rate between 0.1 and 50 K/min (a) and racemic composition at heating rates between 2 and 30 K/min (b).

On the other hand, the melting endothermic peak of the racemic mixture moves slightly from 145 to 146 °C from 2 to 30 K/min (Figure 4.11b). This difference of behavior suggests that the variation of the heating rate strongly effects the melting of the enantiopure compound but only slightly that of the peak of the eutectic (racemic) mixture. By calculating the theoretical melting temperature of the eutectic composition *via* Schröder van Laar

equation for different heating rates, a better agreement with the experimental results has been observed for heating rates higher than 20 K/min (Figure 4.12).

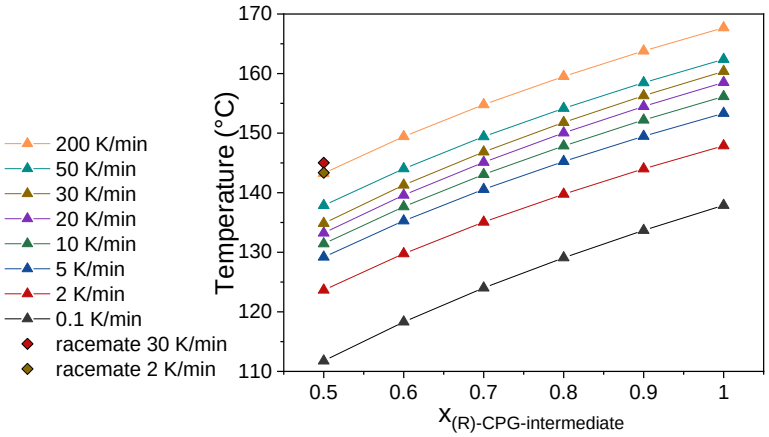

Figure 4. 12 Theoretical liquidus lines for different heating rates calculated through the Schröder van Laar equation. Enantiopure melting points for heating rates between 0.1 K/min and 50 K/min were experimentally determined, as well as the racemate points for heating rates at 2 and 30 K/min. The melting point of enantiopure at fictitious heating rate of 200 K/min has been extrapolated from the available experimental data.

Only a fictitious heating rate of 200 K/min provides a melting temperature at eutectic composition close to 143°C, while the melting point for the enantiopure results at 167 °C. Knowing the melting enthalpy of the enantiopure at heating rate of 200 K/min ($\Delta H^f = 43253$ J/mol), its melting temperature ($T^f = 440.86$ K), and the measured melting temperatures of the samples at enantioenriched compositions in K, the real composition of the enantioenriched samples present during the melting at 2 K/min and 5 K/min can be easily re-calculated through Schröder van Laar equation. A comparison between such calculated theoretical compositions with the experimental data, is shown in Figure 4.13. The corresponding data are compared in Table 4.6.

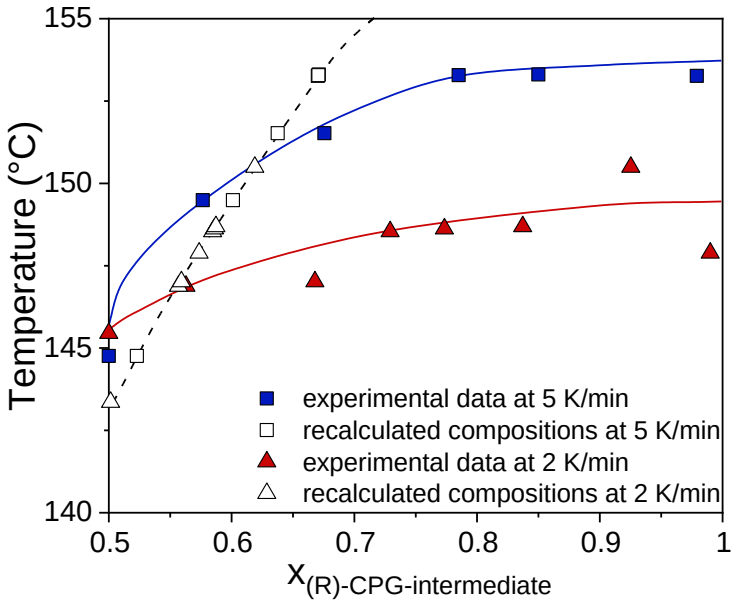

Figure 4. 13 Comparison between the theoretical composition calculated *via* Schröder van Laar at heating rate of 200 K/min and experimental liquidus lines measured at 2 and 5 K/min.

Table 4. 6 Experimental melting temperature of samples of CPG-intermediate at various enantiomeric compositions determined at 2 and 5 K/min and calculated values of theoretical enantiomeric compositions.

enantiomeric composition (HPLC)	experimental data (°C)	enantiomeric composition recalculated *via* SvL
Heating rate 5K/min		
0.98	153.3	0.67
0.85	153.3	0.67
0.79	153.3	0.67
0.68	151.6	0.64
0.58	149.5	0.60
0.5	144.8	0.52
Heating rate 2K/min		
0.99	147.9	0.57
0.93	150.5	0.62
0.84	148.7	0.59
0.77	148.6	0.59
0.73	148.5	0.58

0.67	147.0	0.56
0.56	146.9	0.56
0.5	143.4	0.50

The results indicate that the racemization process strongly affect the composition of the samples during the melting. As illustrated in Figure 4.13, the calculated theoretical compositions deviate towards racemic compositions for both of the experimental conditions (*i.e.* at the two heating rates) studied. The values of the experimental melting temperatures determined at the two heating rates, as well as the theoretically calculated melting temperatures, are summarized in Table 4.6. It can be observed that, for a heating rate of 2 K/min, the theoretical calculated compositions result closer to racemic values respect to the values calculated at 5 K/min, suggesting that the racemization rate is temperature dependent. In particular, at lower heating rates, the racemization process tends to completeness while at higher heating rates the racemization is only partial. On-line measurements of the composition of the samples during the heating phase of the experiment would be necessary in order to accurately assess the racemization kinetics of the system. Nevertheless, our investigation provides preliminary information on the racemization kinetics of the CPG-intermediate under the studied conditions.

4.1.6 Proposed mechanism of temperature-induced racemization of CPG-intermediate.

Previous studies on the racemization of amino acids have shown that the rate-determining step of the racemization of the derivatives of the amino acid glycine, involves the removal of the proton attached to the α-carbon, leaving behind a planar carbanion.[129,130] It has been demonstrated that the racemization rate depends on the electronegativity of the substituents on the α-carbon. Especially, electronegative substituents would facilitate the elimination of the proton as they stabilize the carbanion generated at the rate-determining step.[130] In fact, it has been found that the amino acid phenylglycine exhibits faster racemization kinetics than the amino acid alanine. Furthermore, any substitution on the oxygen of the carboxylic group having electro-withdrawing inductive effect would facilitate the elimination of the proton thus enhancing the racemization rate. The studied system CPG-intermediate can be seen as a glycine-derivative, as shown in Table 4.7, having a benzyl group as R_1, a chloro-phenyl group as R_2 and a carboxamide group instead of the

carboxylic group. Especially, in the presence of a strong base such as the DBU in solution, the electro-withdrawing inductive effect of R_1 and R_2 in the CPG-intermediate would stabilize the carbanion generated after the removal of the proton on the α-carbon in the rate-determining step, hence promoting the racemization reaction.

Table 4. 7 Functional groups of the amino acid glycine and selected derivatives.

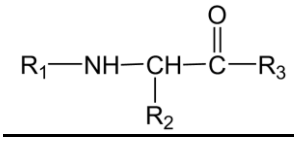	R_1	R_2	R_3
Glycine	-H	-H	-OH
Alanine	-H	-Me	-OH
Arylglycine	-H	-Ar	-OH
CPG-intermediate	-CHPh	-PhCl	-NH2

In the present work, it is assumed that a racemization reaction occurs during the melting, thus in the absence of solvent or catalyst. Therefore, the formation of the planar carbanion cannot be taken into account for the mechanism of racemization reaction. Nonetheless, from the molecular structure of CPG-intermediate one can see that a keto-enol tautomerism could occur, involving the displacement of the proton on the α-carbon. A possible mechanism of racemization reaction of CPG-intermediate in absence of catalyst or solvent is given is given in Scheme 4.1. The migration of the proton from the chiral carbon to the oxygen of the carboxamide, leads to the formation of a planar intermediate (Scheme 4.1, middle position), specifically a conjugated enol. At this point, the subsequent reattachment of the hydrogen can occur with equal probability on the two faces of the planar double bond, hence yielding both *(R)*- and *(S)*- configuration products and therefore leading to the formation of the racemate.

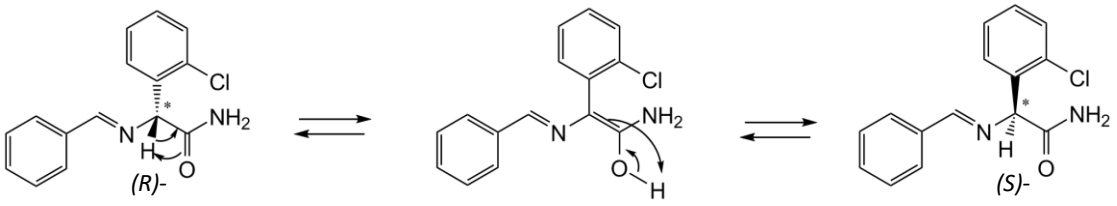

Scheme 4. 1 Proposed mechanism of CPG-intermediate racemization reaction through formation of the planar intermediate. The chiral carbon is marked by an * and the arrows indicate the movement of the electrons.

Since the proposed racemization reaction does not need the presence of any solvent and it appears to occur spontaneously when the solid sample is heated up to its melting point, a study aimed to investigate the stability of the crystal structure of the *(R)*-CPG-intermediate as a function of the temperature has been done, by acquiring temperature resolved XRPD of a sample of enantiopure compound. Two different stepwise temperature profiles have been used as described in the experimental section.

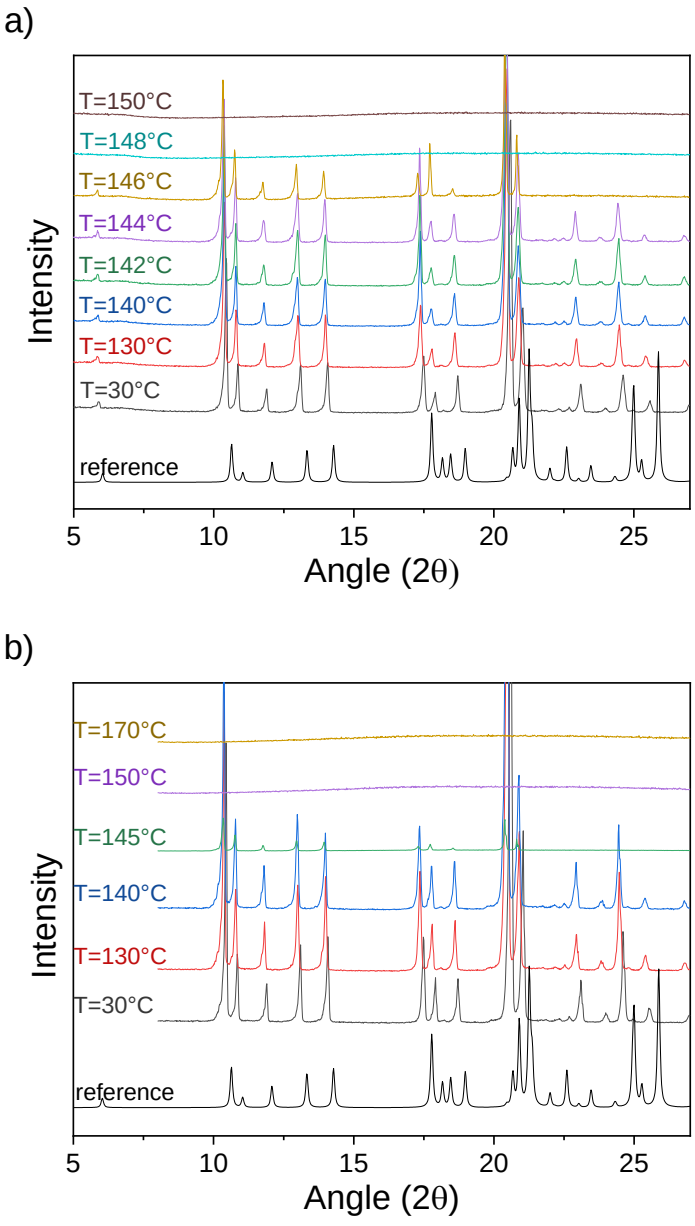

Figure 4. 14 Temperature-resolved XRPD patterns of enantiopure *(R)*-CPG-intermediate between 30 °C and 150 °C (a) and between 30 °C and 170 °C (b). Reference pattern from ref [83] is illustrated at the bottom of the figures.

The coloured diffractograms depicted in Figure 4.14 are identical with each other and superimposable with the reference pattern[83] until T= 145 °C. At this temperature, the XRPD patterns start to flatten as consequence of the melting of the solid enantiopure sample. It can be assumed that, if the racemization reaction occurred at the solid state, a change of the crystal structure of the enantiopure compound would have been observed as a result of the transient formation of the planar intermediate and hence of the change of H-bonding network that links the molecules within the lattice. The fact that no change of the crystal structure of the *(R)*-CPG-intermediate has been observed with the temperature, suggests that the CPG-intermediate racemization reaction is more likely to occur at the molten state rather than at the solid state.

4.2 Guaifenesin system

The model compound presented in section 4.2 is the API guaifenesin. A comprehensive overview on the experimental conditions which can be used for an efficient resolution of this system *via* preferential crystallization processes will be provided. Firstly, the solubility of the system in several organic solvents will be described and compared with the already available solubility data in water. Given the peculiar solubility-temperature dependency of the system in aqueous solution, few considerations on the molecular interactions in solution will be proposed based on the ^{1}H-NMR spectra of racemic guaifenesin in a polar-protic and a polar-aprotic solvent. Afterwards, the results related to the enantioseparation *via* preferential crystallization will be presented. The first crystallizer configuration discussed will consist of a single stirred tank, used for the enantioseparation of the guaifenesin in isopropanol and water. Based on the results of the single batch PC runs, the role of the solvent on the crystallization kinetics of the system, thus on the performances of the resolution will be examined. Further resolution runs exploiting a second configuration for the CPCD approach will be described. A range of experimental conditions has been used in order to assess the applicability of this technique to the studied system. In the final part of section 4.2, the results related to the resolution in a tubular fluidized crystallizer will be presented. The study will deal with the practical issues related to the resolution of the guaifenesin enantiomers using the tubular fluidized bed crystallizer (FBC) in a continuous operation mode. Based on the fundamental information of the thermodynamics of the system, the choice of an appropriate solvent will be discussed. Afterwards, the implementation of a continuous supply of seed crystals will be tackled, considering the morphological and crystallization properties of guaifenesin. Essential insights on the resolution of the studied system which could be of relevance in the exploitation of a tubular FBC in continuous operation will be provided.

Part of the results presented in this section has been subject of publication, especially the results related to the enantioseparation of guaifenesin in a single stirred tank as well as part of the results of the CPCD study.[100,107] Furthermore, the findings on the resolution in tubular fluidized bed crystallizer have been used for further experimental investigations, which are not presented in the thesis and have been integrated in a manuscript to be submitted.

It is worth mentioning that the values of the supersaturation ratio for the preferential crystallization in single stirred tank in isopropanol and water differ from the values reported in ref [100]. The reason lies on the fact that, from the time of the published work to present additional investigations on the solubility of the guaifenesin in the two solvents at the studied crystallization temperature have been carried out. As the solubility data are essential in the calculation of the supersaturation ratio, the additional solubility data measured for the two systems have produced a variation of the function used for the fitting of the solubility isotherm. Interestingly the additional investigations have modified the supersaturation values to the same extent for the two studied systems.

4.2.1 Introduction on the API guaifenesin system

Guaifenesin is an antitussive agent widely used as expectorant in many cough suppressive formulations as well as for respiratory tract infections and bronchitis. It is an ether of guaiacol, a constituent of guaiac resin from the wood of Guajacum officinale Linne,[131] and it is chemically designed as (*R,S*)-3-(2-methoxyphenoxy)-propane-1,2-diol (Figure 4.15).

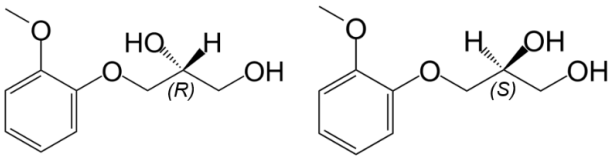

Figure 4. 15 Molecular structure of the enantiomers of 3- (2-methoxyphenoxy) -propane-1, 2-diol.

Guaifenesin has gained much attention in the scientific community, not only as cough medication but also due to its enhanced therapeutic effect when combined with nonsteroidal anti-inflammatory drugs (NSAINDs) in the treatment of the common cold. The co-administration of medication for cough and pain relievers is a common procedure to alleviate the symptoms of the common cold and in this scenario the API guaifenesin has been found to influence the adsorption of paracetamol and NSAIDs such as ibuprofen and nimesulide.[132] The lack of reported research on the pharmacodynamics and pharmacokinetics of the single enantiomers of the system suggests that still much effort must be made in order to clarify the role of the guaifenesin enantiomers in the treatments

of lung diseases and related issues.[133] As consequence, the API guaifenesin is marketed in racemic form. However, recent studies have speculated that one enantiomer may exhibit better physiological activity or fewer side effects.[134] As it is considered a desirable practice to administer chiral compounds as single enantiomers, developing methods to obtain high pure enantiomers has becoming crucial for the pharmaceutical industry. For the resolution of enantiomers of guaifenesin, much work has been done using chromatographic techniques such as simulated moving bed chromatography[135] and supercritical chromatograpy.[136] Normal phase HPLC has been also used using polysaccharide-base stationary phase,[137] however the major drawbacks of these methods are that they require expensive and complicated operating systems and that they can be used only for qualitative analysis.

4.2.2 Solubility behavior of guaifenesin in organic solvents

The solubility of racemic guaifenesin in several organic solvents was determined exploiting the isothermal method described in the experimental description (section 3.2.1). The solubility data are listed in Table 4.8 and graphically represented Figure 4.16a. For comparison, the solubility data of the racemic guaifenesin in water are reported as well, although they have been determined in previous (partly our own) studies.[107,138]

Table 4. 8 Experimental solubility data of racemic guaifenesin in several organic solvents between 10 and 60 °C and related Standard Deviation (SD).

T (ºC)	C_{sat} ($g_{solute}/g_{solution}$)	SD%
ethanol		
10	0.070	0.5
20	0.104	0.2
30	0.194	0.9
40	0.337	0.6
50	0.58	1.2
60	0.75	6.4
acetone		
10	0.066	0.1
20	0.094	0.2
30	0.166	0.4
40	0.295	0.4
50	0.501	0.2
60	0.70	5.6

isopropanol		
10	0.039	0.7
15	0.050	0.4
20	0.065	0.4
25	0.087	0.5
30	0.109	0.1
35	0.154	0.4
40	0.205	0.3
50	0.39	1.0
60	0.67	1.8
ethyl acetate		
10	0.018	0.1
20	0.023	0.3
30	0.047	0.2
40	0.087	0.5
50	0.194	0.5
60	0.451	1.8

The data show that racemic guaifenesin is highly soluble in polar solvents, exhibiting an increase of solubility of *ca.* 1.7 times from T_{sat}=25 °C to T_{sat}=35 °C in all solvents investigated. A higher temperature dependency is given for guaifenesin in water,[107] specifically in the temperature range between 30 and 40 °C (Figure 4.16a, empty dots). As shown in Figure 4.16b, the XRPD patterns of the solid phases in equilibrium with the saturated solutions in organic solvents are superimposable with the reference pattern and therefore no polymorphs or solvates can be identified under the studied conditions. The same behaviour has been observed for the solid excess in equilibrium with the saturated solutions in water, as reported by Fayzullin *et al*..[138]

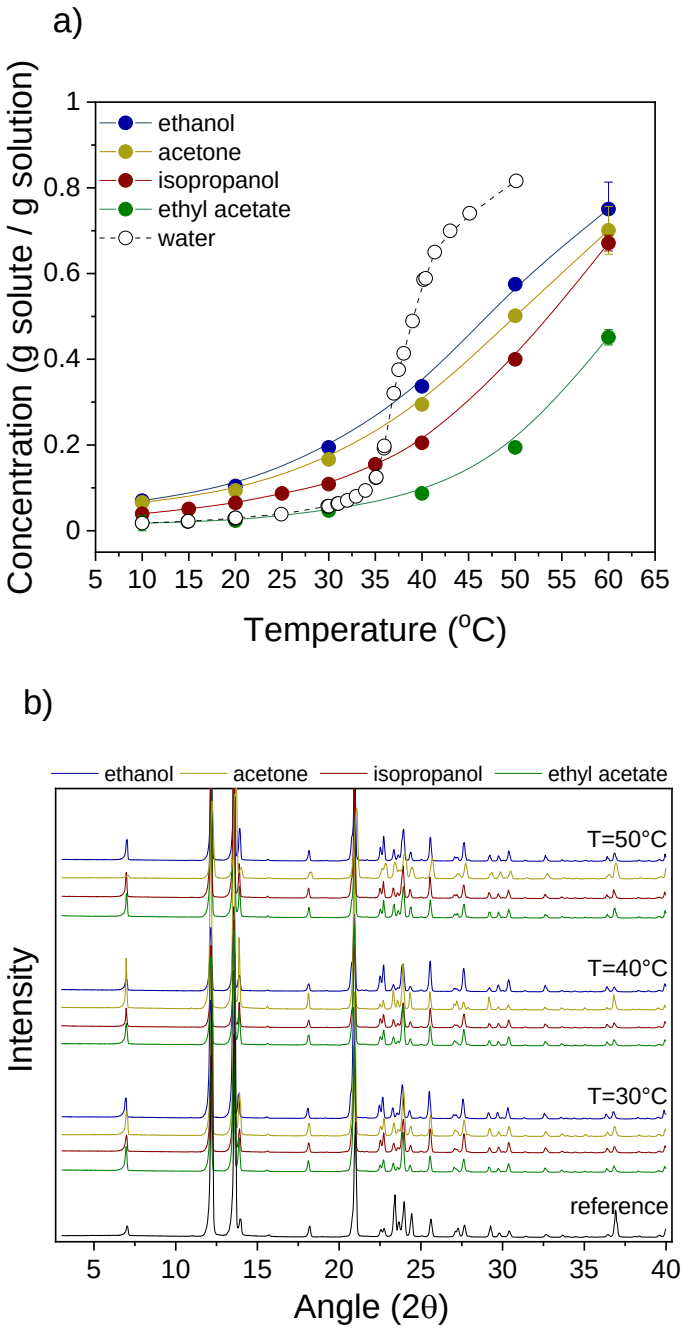

Figure 4. 16 Experimental solubility data of racemic guaifenesin in several organic solvents (colored full dots) and in water from ref [107] (black empty dots) (a). Experimental XRPD patterns of solid racemic guaifenesin in equilibrium with its saturated solution in different solvents, between 30 °C and 50 °C (b). Racemic guaifenesin purchased from TCI (Deutschland GmbH) was used as a reference.

In previous studies, the high solubility of guaifenesin in water has been attributed mainly to the H-bonding formation of the solute with the water molecules.[139] However, the

presence of donor and acceptor functional groups may lead to the formation of solute-solute H-bonding.[140] Some investigations to clarify the tendency of guaifenesin to form solute-solute H-bonds in the presence of protic solvents have been done in the present work. Using the thermodynamic parameters available in literature,[141] the activity values of the dissolved solid racemic guaifenesin as a function of temperature have been calculated using Eq. 4.1.

$$\ln(a) = -\frac{\Delta H^f}{RT}\left(1 - \frac{T}{T^f}\right) \qquad \text{(Eq. 4.1)}$$

Where, *a* is the activity of racemic guaifenesin, ΔH^f is the melting enthalpy of racemic guaifenesin in *J mol*$^{-1}$, *R* is the gas constant in *J mol*$^{-1}$ *K*$^{-1}$, *T* is the temperature at which the solubility has been determined in *K*, and T^f is the fusion temperature of racemic guaifenesin in *K*. In particular, a melting enthalpy ΔH^f = 37.6 *KJ mol*$^{-1}$ and a melting temperature T^f =353.35 *K* were considered for the calculation of the activity values at each saturation temperature. Given the activity values, *i.e.* the ideal solubility setting *γ=1*, the activity coefficients of racemic guaifenesin in each solvent have been determined at different saturation concentrations, by dividing the activity, *a*, with the real concentration values in mole fraction, thus comparing the ideal solubility and the experimental solubility data (Eq. 4.2).

$$\gamma = \frac{a}{x} \qquad \text{(Eq. 4.2)}$$

Figure 4.17 illustrates the solubility of racemic guaifenesin in the studied solvents, expressed in mole fraction (Figure 4.17a) as well as the variation of the activity coefficient, *γ*, as a function of the saturation temperature (Figure 4.17b). A qualitative evaluation of the solute-solute and solute-solvent interactions is given by the values of the activity coefficient, *γ*. It can be observed that. for all the solvents investigated, a positive deviation from the ideal behaviour occurs. In fact, values of *γ*>1 are reported over the whole range of temperature studied (Figure 4.17b).

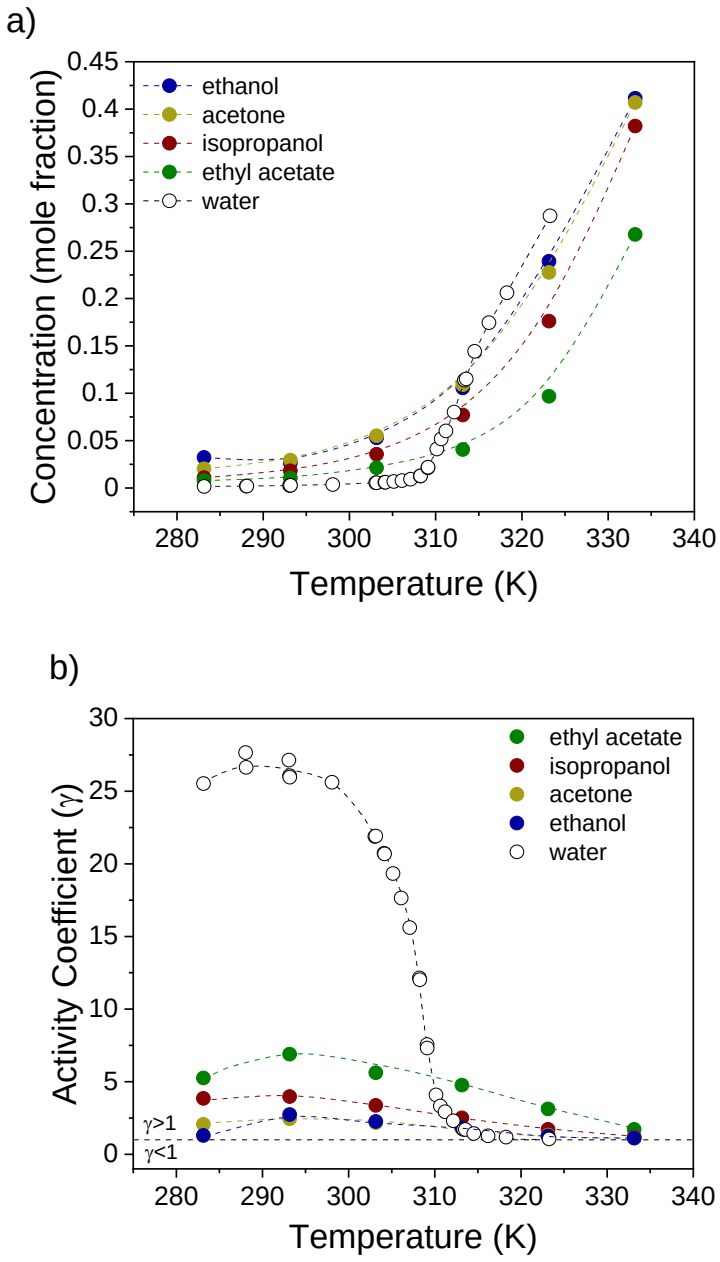

Figure 4. 17 Solubility data of racemic guaifenesin in organic solvents and in water expressed in mole fraction (a) and representation of the related activity coefficients as a function of the temperature (b).

As the saturation concentration, *i.e.* the saturation temperature, increases, *γ* tends to 1 (Figure 4.17b), meaning that at higher concentration the solute-solute interactions prevail over the solute-solvent interactions. Such behaviour is observed for all the solvents investigated, however it is particularly enhanced for the water system in the temperature

range between 300 and 315 K, which corresponds to the temperature range where the steep increase of solubility occurs, as show in Figure 4.17a.

Since ^{1}H-NMR spectra can provide information regarding the interaction of the molecules in solutions,[142–144] investigations have been done in order to identify the possible association of the solute molecules in solution using NMR spectroscopy. Samples of racemic guaifenesin in two deuterated solvents, one polar protic (methanol-d_4) and one polar aprotic (acetonitrile-d_6), were prepared at different concentrations and the related ^{1}H-NMR spectra were recorded. The concentration values of the samples are listed in Table 4.9.

Table 4. 9 Concentration values of ^{1}H-NMR samples of racemic guaifenesin in methanol-d_4 and acetonitrile-d_6.

sample	$m_{racemic\ guaifenesin}$ (mg)	$V_{solvent}$ (µL)	C (mg/mL)
methanol-d_4			
1	25.3	750	33.7
2	50.26	750	67.0
3	64	750	88.6
acetonitrile-d_6			
1	53.0	750	70.6
2	64.2	750	85.6
3	80.2	750	106.9

Figure 4.18 and 4.19 show the ^{1}H-NMR spectra of racemic guaifenesin in methanol-d_4 and acetonitrile-d_3, respectively, at different concentrations. The ^{1}H-NMR signals can be unambiguously assigned to the protons of the molecule as reported by the numbers on the guaifenesin structures within Figures 4.18 and 4.19. At first glance, one can see from Figure 4.18 that the signals generated by the hydroxyl protons of the molecule are not visible in the spectrum, as a result of the proton exchange with the deuterium of methanol-d_4. Furthermore, the increase of the concentration of guaifenesin in the sample has no influence on the appearance of the spectrum over the whole range of assignment.

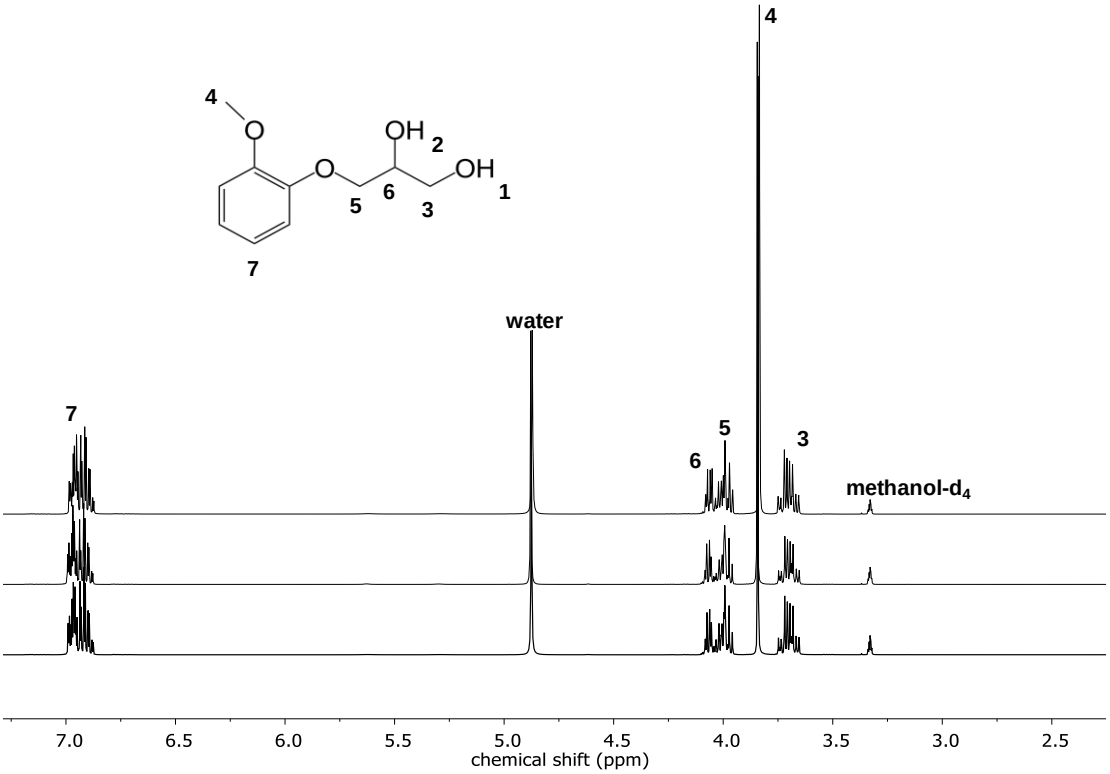

Figure 4. 18 ^{1}H-NMR spectra of racemic guaifenesin in CD_3OD at different concentrations increasing from bottom up.

The analysis in an aprotic deuterated solvent like acetonitrile-d_3 allows the signals attributed to the hydroxyl protons to be visible, as expected, in the range of chemical shift between 2.7 and 3.5 ppm (Figure 4.19). Moreover, the chemical shift of signal 1 and 2 varies with the concentration. As the concentration of racemic guaifenesin in acetonitrile-d_3 increases, the signals of -OH(1) and -OH(2) move towards higher ppm: from 2.93 ppm to 3.04 ppm and from 3.27 to 3.41 ppm, respectively for signal 1 and 2. Considering the molecular structure of guaifenesin, it can be assumed that the hydroxyl protons act as donors and acceptors of H-bonds. As the H-bonding reduces the electron density around the hydroxyl protons, these result de-shielded and their signals are shifted to higher ppm (lower field). Therefore, the observed de-shielding of hydroxyl protons 1 and 2 can be attributed to the intermolecular H-bond formation between solute molecules, which is favored as the concentration of solute increases.

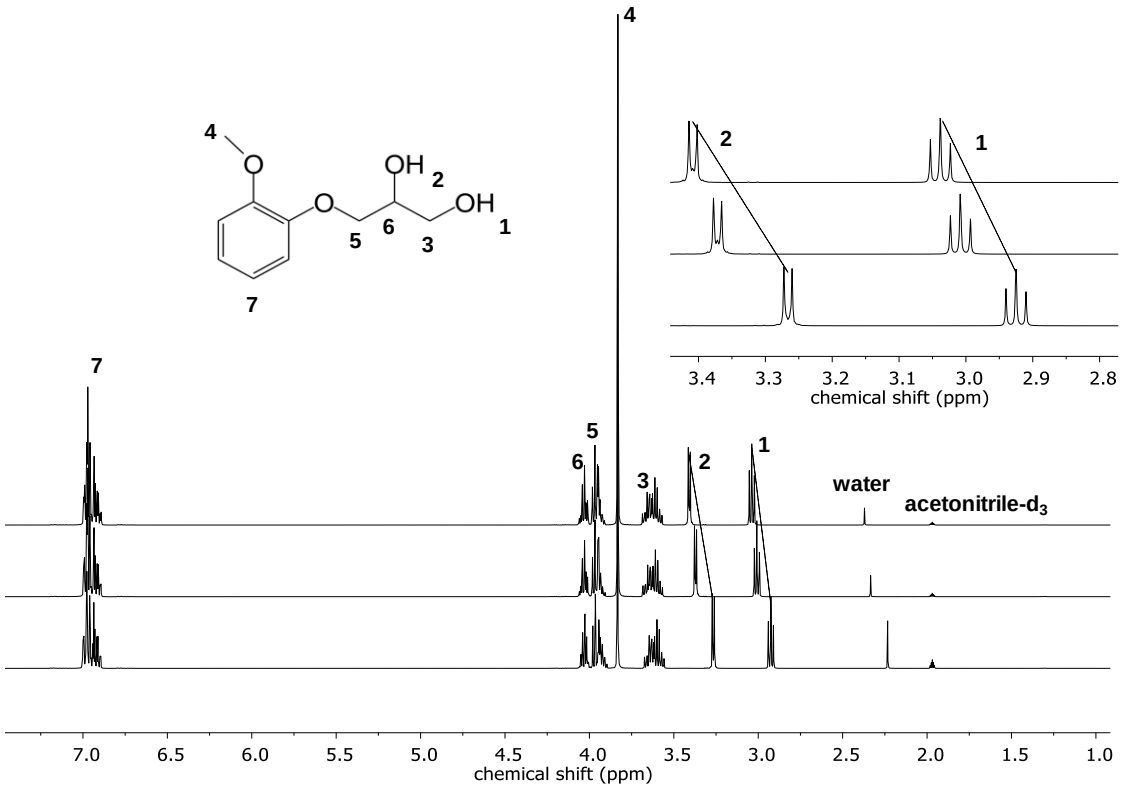

Figure 4. 19 ^{1}H-NMR spectra of racemic guaifenesin in CD_3CN at different concentrations increasing from bottom up.

Based on the observation of the ^{1}H-NMR spectra, it can be assumed that molecules of guaifenesin in solution form self-association structures, such as dimers, through H-bonding. An example of the association mechanism, where the hydroxyl protons act as donors and acceptors of H-bonds leading to the formation of a dimer of guaifenesin molecules, is proposed in Scheme 4.2.

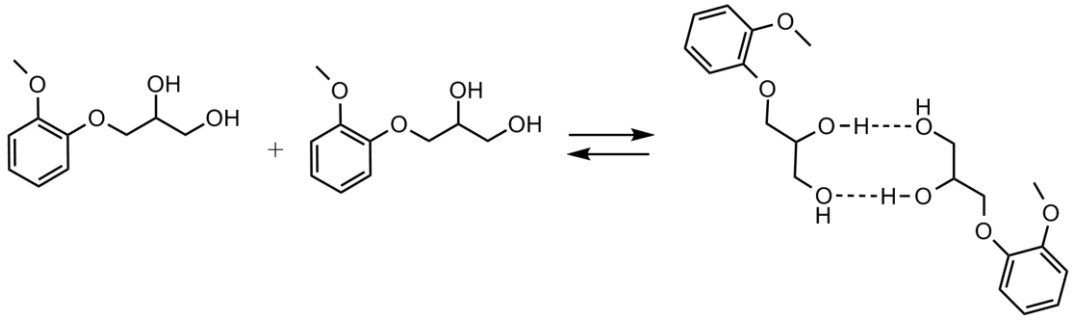

Scheme 4. 2 Proposed mechanism of formation of a self-association structure of guaifenesin molecules in solution.

Further experimental and computational investigations would deliver a deeper understanding of the molecular organization in solution, hence enabling the determination of possible supramolecular structures of guaifenesin as well as providing insights about the early organization of the molecules during the crystallization event.

The investigation on the thermodynamics of guaifenesin has been extended to the determination of the solubility ternary phase diagram. Figure 4.20 illustrates the experimental solubility data of guaifenesin at various enantiomeric composition and different temperatures in isopropanol. This solvent was used for the resolution runs *via* preferential crystallization.

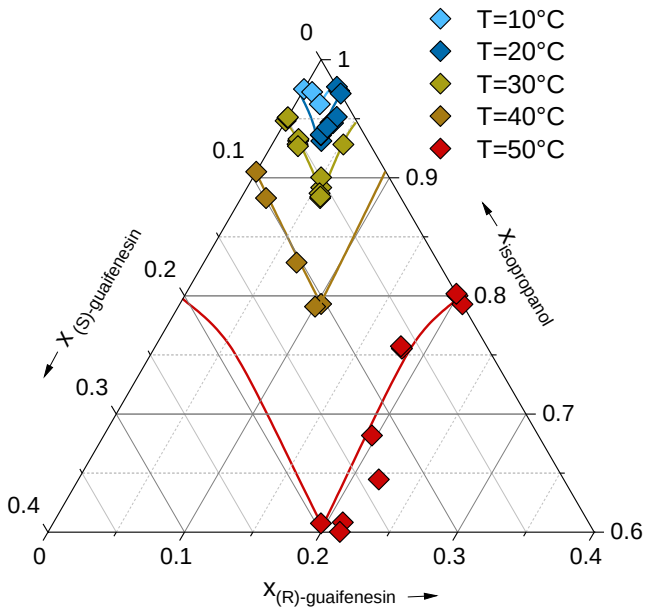

Figure 4. 20 Experimentally determined solubility ternary phase diagram of *(R)-/(S)*-guaifenesin in isopropanol between 10 and 50°C. Magnification of the upper 40% of the complete phase diagram is represented.

It can be seen that at a fixed temperature, the maximum solubility is at racemic composition, while the minimum solubility is at enantiopure composition, as expected for a typical conglomerate forming system. The ratio between the solubility at racemic and

enantiopure composition, so-called Meyerhoffer coefficient, α, varies between 1.77 at 10 °C and 2.18 at 30 °C (Table 4.10).

Table 4. 10 Values of the Meyerhoffer coefficient, α, of guaifenesin in isopropanol at various saturation temperatures.

T(°C)	α
10	1.77
20	2.18
30	2.18
40	1.96
50	1.99

As the temperature increases, the system tends to ideality, as also previously observed in the description of the activity coefficients (Figure 4.17).

4.2.3 Metastable zone width of racemic guaifenesin in isopropanol

In order to perform controlled crystallization-based resolution experiments, the MSZW of racemic guaifenesin has been determined in isopropanol at different saturation concentrations. Figure 4.21a, shows the temperature differences, T_{sat}-T_{nucl}, as a function of the cooling rate, for the various concentrations investigated. As shown, at a certain saturation temperature, hence saturation concentration, the experimental ΔT_{max} are scattered in a broad range of temperatures. As the Nývlt method relies on the determination of the generation of first crystals from a supersaturated solution *via* primary nucleation, such wide variation of the ΔT_{max} is given on account of the stochastic nature of the primary nucleation event.

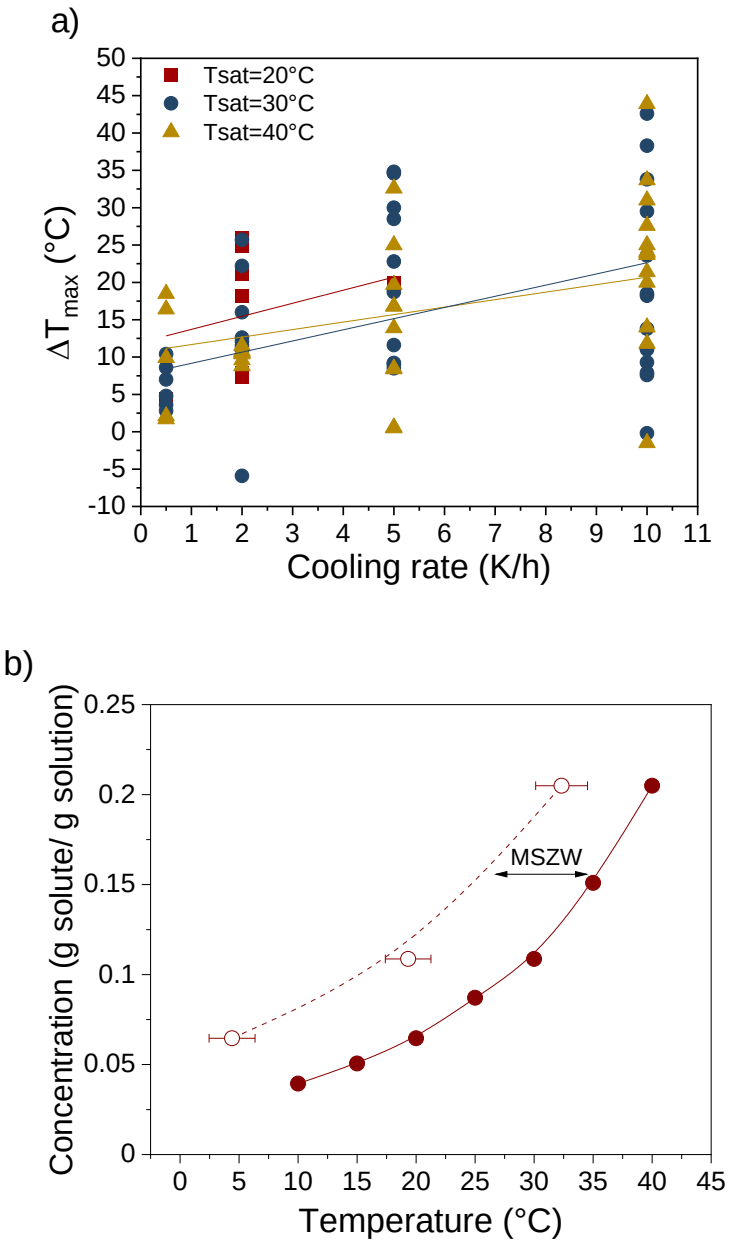

Figure 4. 21 Representation of the experimental ΔT_{max} (°C) as a function of the cooling rate determined for solutions of racemic guaifenesin in isopropanol (a). Experimentally determined solubility data (full red dots) and nucleation points for a fictitious zero cooling rate (empty red dots) of racemic guaifenesin in isopropanol (b). Solid and dashed lines are a guide for the eyes.

From the extrapolation of the ΔT_{max} to a ´´zero´´ cooling rate for the three saturation concentrations investigated, the nucleation points, thus the the metastable region can be

represented as shown in Figure 4.21b. One can see that the maximum subcooling reachable without spontaneous nucleation is of 8 °C when the racemic solution is saturated at 40 °C and of 15 °C when the solution is saturated at 20 °C. Given the experimentally determined solubility of racemic guaifenesin in isopropanol at various temperatures (Figure 4.21b, full red dots), the unknown solubility points at intermediate temperatures were obtained using the polynomial function C_{sat} = 1.122E-05T^4 -6.9778E-04T^3 + 0.02445T^2 - 0.1561T + 3.65164.

4.2.4 Single batch PC of *(R)*-guaifenesin in isopropanol and water

The experimental conditions of the two resolution runs of guaifenesin in water and isopropanol are listed in Table 4.11. The runs were performed at the same initial supersaturation, S=2. As reported in the experimental description (section 3.2.4), the calculation of the supersaturation ratio has been done considering the mass fraction of the pure enantiomer at initial state of the process and the mass fraction of the pure enantiomer at the reference state.

Table 4. 11 Experimental conditions of single batch PC runs of *(R)*-guaifenesin in isopropanol and water.

solvent	isopropanol	water
supersaturation (S)	2	2
T_{cryst} (°C)	25	25
T_{sat} (°C)	36.5	33
m_{solute} (g)	69.5	39.1
$m_{solvent}$ (g)	355	400
m_{seed} (g)	1.5	1.5
C_{sat} ($g_{solute}/g_{solution}$)	0.16	0.09

Figure 4.22 illustrates the driving force of the two crystallization runs within the ternary phase diagram for the system in isopropanol (Figure 4.22a) and in water (Figure 4.22b). As shown, the initial state for both of the cases is represented by the mass fraction of the single enantiomer at racemic composition at the initial saturation concentration, while the reference state is represented by the mass fraction of the pure enantiomer at the intersection between the tie line from pure enantiomer corner through the initial state and the extension of the solubility isotherm at crystallization temperature, *i.e*. 25 °C.

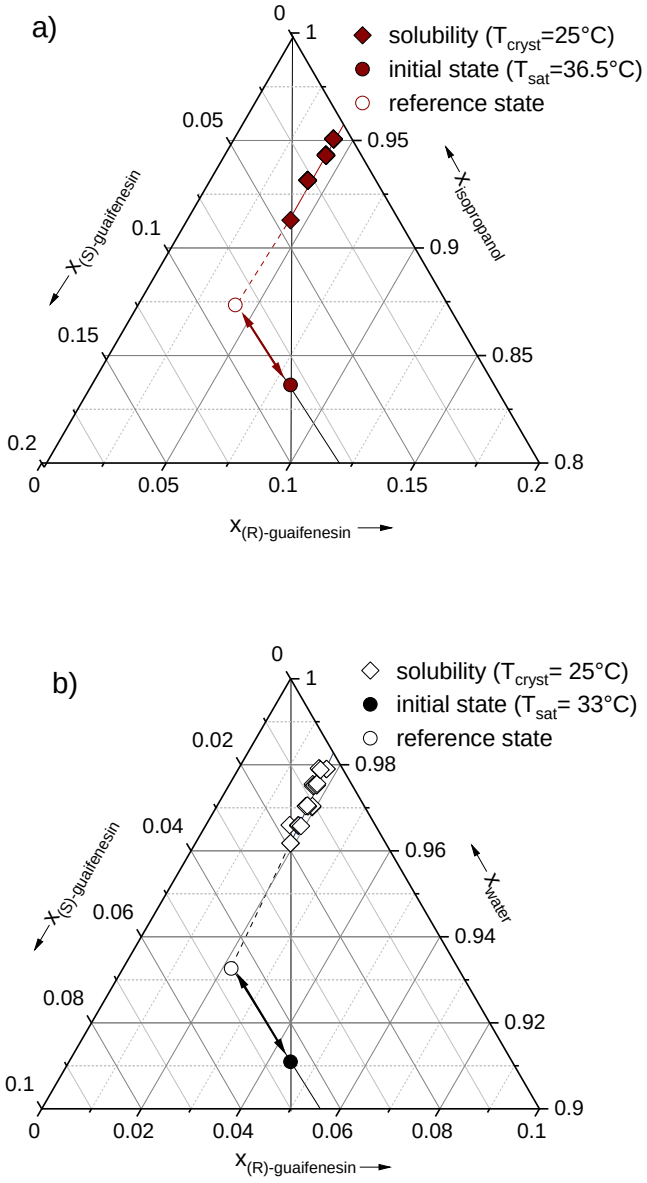

Figure 4. 22 Representation of the supersaturation degree for single batch PC runs of (R)-guaifenesin in two different solvents. Full red (a) and empty black (b) rhombuses in the upper part of the ternary phase diagram represent the solubility points at T_{cryst}, *i.e.* 25 °C. The full red (a) and black (b) dots at racemic composition represent the initial state of the system, *i.e.* initial saturation conditions, in isopropanol and water respectively. The empty red dot (a) and black dot (b) represent the reference state of the system for each saturation concentration. The arrows between the two states represent the initial driving force of each process.

After the complete dissolution of the racemic solid phase, and equilibration of the clear solution, the tank was cooled to T_{cryst}=25 °C. Afterwards, 1.5 g of manually ground crystals of pure *(R)*-guaifenesin were introduced in the supersaturated solutions, hence triggering the preferential crystallization of the seeded enantiomer. The process was monitored with an on-line polarimeter and densitometer as well as an in-line turbidity meter. A rough estimation of the depletion of the preferred enantiomer from the mother liquor, was given by the optical rotation signal, while the increase of the suspension density was indicated by the turbidity signal.

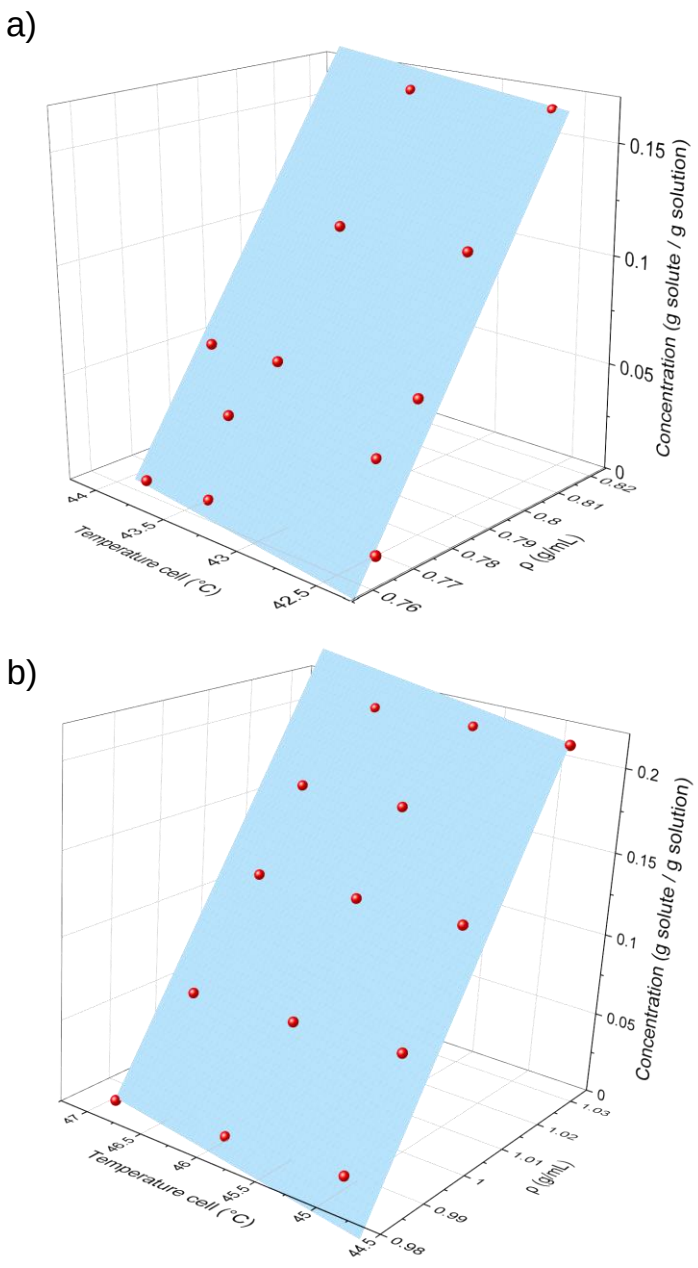

Figure 4. 23 Representation of experimental density values acquired for the calibration of the density signal as a function of the temperature of the cell and the concentration of the solution in isopropanol (a) and in water (b).

In order to determine the variation of the concentration of the mother liquor during the process from the density values, a calibration of the densitometer as a function of the concentration and as a function of the temperature of the densitometer cell was necessary. The experimental points illustrated in Figure 4.23 have been fitted with a plane function

$z=z_0+ax+by$, where x is the density, ρ, expressed in g/mL, y is the temperature of the densitometer cell in °C and z is the concentration in g_{solute} / $g_{solution}$. The parameters of the equation, z_0, a, b for the two systems are summarized in Table 4.12.

Table 4. 12 Equation parameters for the calibration of the density signal as a function of the temperature of the densitometer cell and the concentration in isopropanol and water solutions.

	isopropanol	water
z_0	-2.797	-5.739
a	3.154	5.288
b	0.009	0.011

The trajectories of the analytic signals recorded during the two resolution runs are represented in Figure 4.24. Before the seeding time, the signals refer to the preparation and equilibration of the saturated solution as well as the cooling phase, while after seeding the signals refer to the production of the preferred enantiomer. The optical rotation signal increases in absolute value in both of the experiments after seeding. In particular, for the resolution in isopropanol it can be observed that the optical rotation increases with lower rate already after 1 h from the seeding, while for the water system such variation is observed after more than 2 h from the seeding. In fact, the process in isopropanol has been interrupted after 1.5 h from the seeding (Figure 4.24a) while the resolution in water was interrupted after more than 4 h (Figure 4.24b).

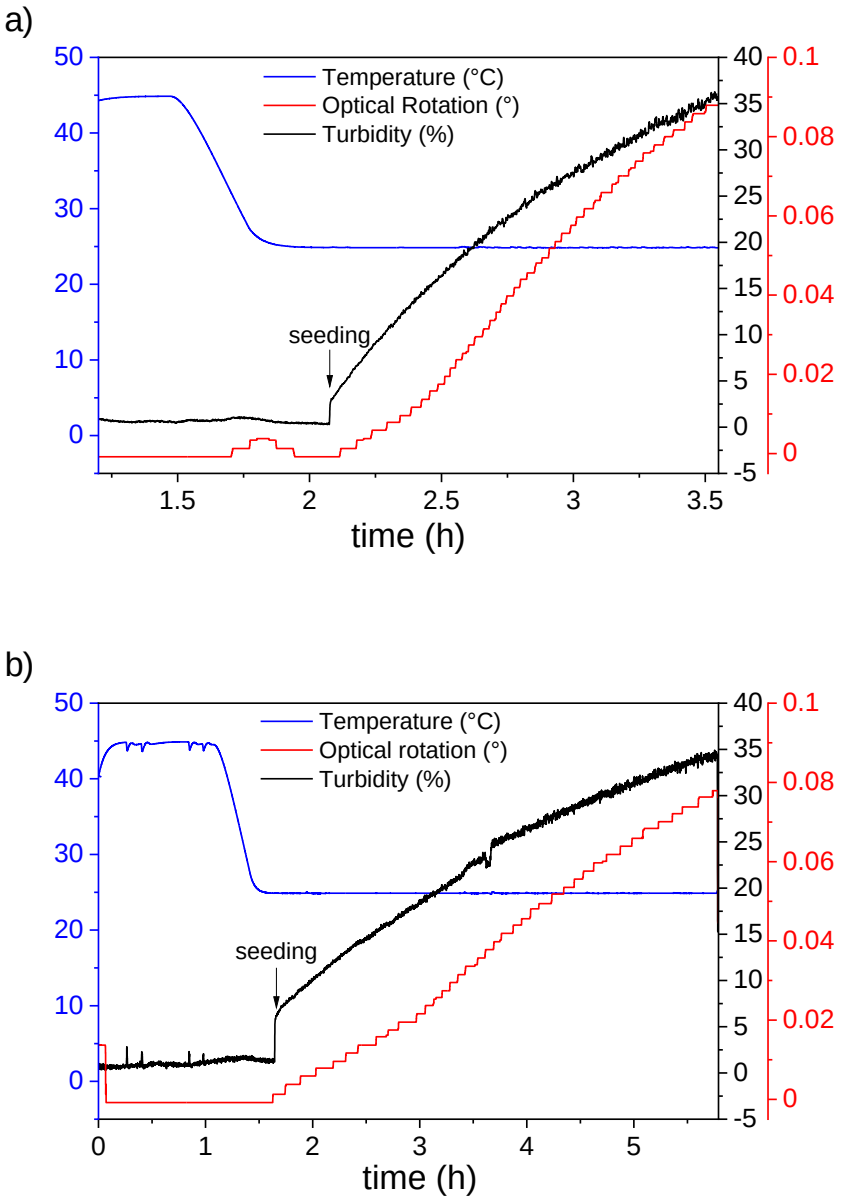

Figure 4. 24 Trajectories of temperature profile (blue line), optical rotation (red line) and turbidity signal (black line) of the single batch PC runs of guaifenesin in isopropanol (a) and in water (b).

The two different trends of the optical rotation signals demonstrate that the depletion of the seeded enantiomer from the mother liquor in isopropanol occurs faster than the depletion in water. A clear representation of this event is given by the depletion of the

mother liquor concentration with respect to the seeded enantiomer, as shown in Figure 4.25.

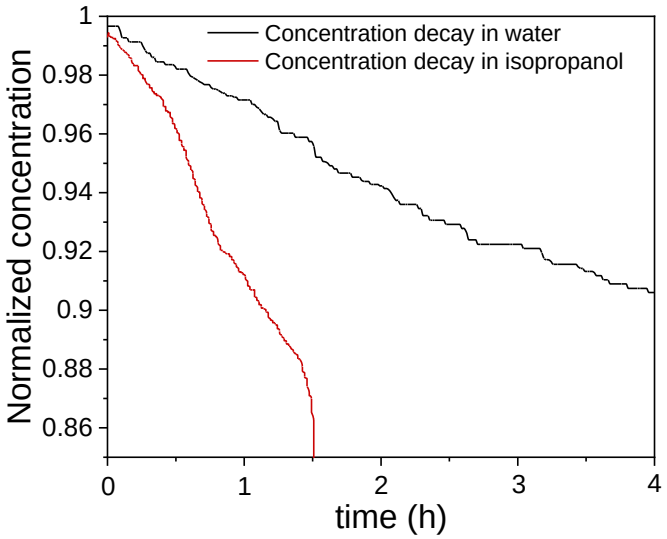

Figure 4. 25 Representation of the depletion of the seeded enantiomer from the mother liquor during the single batch PC runs of guaifenesin in water (black) and isopropanol (red). Seeding time was chosen as zero.

Such representation has been derived from the density values of the mother liquor in isopropanol and water, which have been converted in concentration values and normalized with respect to the maximum concentrations in solution, *i.e.* the initial saturation concentrations. It can be noted that the depletion of the seeded enantiomer in isopropanol occurs faster than the one from aqueous solution, thus suggesting different crystallization kinetics between the two systems.

Furthermore, a higher negative slope is shown for the isopropanol system towards the end of the process, probably due to the nucleation of the counter-enantiomer as also indicated by the values of the chiral purity of the collected product from the isopropanol solution (96 %). Such variation of the slope is not observed for the water system, meaning that the nucleation of the counter-enantiomer did not occurred in aqueous solution as also shown by the chiral purity of the product collected from the aqueous system (98 %).

Table 4. 13 Experimental results of single batch PC runs of *(R)*-guaifenesin in isopropanol and water.

solvent	isopropanol	water
$m_{product}$ (g)	7.55	3.01
$t_{production}$ (h)	1.5	4.1
Pu %	96	98
Pr (g/h/L)	8.5	0.8
Y %	32.1	13.1

The experimental results in Table 4.13 show that a higher amount of product in a shorter range of time has been collected for the isopropanol system compared to the water system. Therefore, the performances of the resolution in isopropanol, especially productivity, and yield, are higher compared to the performances of the resolution run in water. Nonetheless, a slight contamination of the product collected from the single batch PC in isopropanol has been observed. This can be attributed to the phase of washing of the collected product as well as to the faster crystallization kinetics of the *(R)*-guaifenesin in isopropanol as mentioned above. The reason of the differences in resolution performances lies in the different crystallization kinetics of the guaifenesin system in the two solvents, which could be related to the difference of molecular interactions of the solute molecules at the solvated state. As shown in section 4.2.1, the thermodynamic investigation of the solubility of the racemic guaifenesin in different solvents has suggested that the intermolecular H-bonding between the molecules of guaifenesin in solution may lead to the formation of dimers surrounded by molecules of solvent. It can be assumed that, when this association occurs in water, there is an additional energetic contribution favoring the formation of dimers due to the hydrophobic interaction between the water molecules and the solute molecules. The formation of self-association structures in solution prevents the desolvation of the solute molecules, which is necessary for the molecules to be transported to the solid phase. Therefore, slower crystallization kinetics are observed for the aqueous system as the solute molecules in solvated state in water are energetically more favored than the solute molecules in solvated state in isopropanol. Slow crystallization kinetics of guaifenesin in water have been observed also in a previous work done in our laboratories, *i.e.* the resolution of guaifenesin enantiomers exploiting the CPCD process,[100] as well as a tubular fluidized bed crystallizer as reported in the final part of this section. In the following part of the chapter the results related to the resolution of racemic guaifenesin in isopropanol using the CPCD approach are presented.

4.2.5 Coupled batch PC and dissolution of enantiopure guaifenesin in isopropanol

For the system guaifenesin in isopropanol several runs of CPCD were performed, exploiting the coupled setup described in the experimental section. The experimental conditions were chosen by varying the crystallization temperature between 24°C and 27°C and keeping the other conditions *i.e.* saturation concentration and seed mass unvaried. The experimental conditions of the CPCD runs are listed in Table 4.14. For all the experiments a solution at saturation concentration C_{sat}=0.15 $g_{solute}/g_{solution}$ was created by adding 65.1 g of racemic guaifenesin to 355 g of isopropanol in both crystallization and dissolution tank.

Table 4. 14 Experimental conditions of CPCD runs of enantiopure guaifenesin in isopropanol.

	crystallization tank			dissolution tank	
experiment	T_{cryst}(°C)	T_{sat}(°C)	m_{seed} (g)	T_{sat}(°C)	$m_{solid\ excess}$(g)
1	24	35	1.1 *(R)*-	35	20
2	24	35	1.1 *(R)*-	35	40
3	24.5	35	1.1 *(R)*-	35	40
4	25	35	1.1 (S)-	35	40
5	25.5	35	1.1 *(R)*-	35	40
6	25.5	35	1.1 *(R)*-	35	40
7	25.5	35	1.1 *(R)*-	35	40
8	27	35	1.1 *(R)*-	35	40

After the complete dissolution and equilibration of the solutions, 40 g of racemic solid guaifenesin were added into the dissolution tank, thus creating a suspension. For the experiment 1, 20 g of solid excess were used instead of 40 g. After equilibration of the two saturated solutions *via* activation of the liquid exchange, the crystallization tank was cooled to T_{cryst} and 1.1 g of seed crystals of *(R)*-guaifenesin was added to the supersaturated solution, hence starting the preferential crystallization of the seeded

enantiomer. Only for experiment 4, crystals of *(S)*-guaifenesin were used. The variation of the crystallization temperature (Table 4.14) allowed the implementation of small increasing steps of crystallization temperature (0.5 °C), hence investigating multiple experimental conditions in a small range of temperature. Such investigation would have not been possible by varying the saturation temperature, as the available solubility data refer to a variation of temperature between 5 and 10 °C. Furthermore, it is worth mentioning that the knowledge of the temperature at which the solution is saturated is crucial for the CPCD process as the dissolution tank remains at saturation temperature for the whole duration of the experiment. Any gap from the saturated conditions would yield an undersaturated or oversaturated solution within the dissolution tank, hence causing the partial dissolution or the crystallization of the added solid excess.

The on-line and in-line analytic tools allowed the monitoring of the process over the time as well as to identify the stop time of the resolution. In particular, the observation of both the optical rotation signal of mother liquor within the crystallization tank and the turbidity signal of suspension within the dissolution tank allowed the interruption of the process before having contamination of the product in the crystallization tank. In fact, as shown in Table 4.8, the chiral purity of the collected products is >88 %. On the other hand, the nucleation of the counter-enantiomer was unavoidable in the studied experimental conditions.

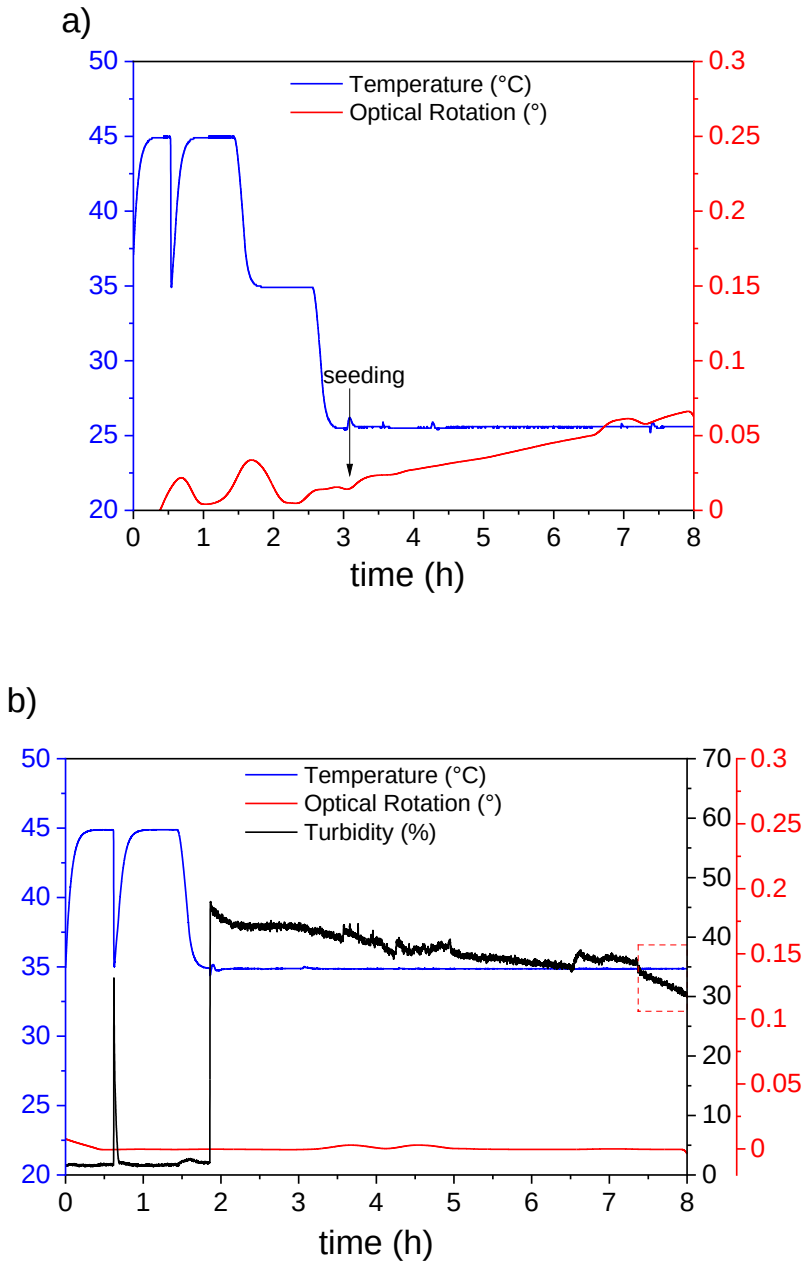

Figure 4. 26 Trajectories of temperature profile (blue line), optical rotation (red line) and turbidity signal (black line) referring to the crystallization tank (a) and dissolution tank (b) of a CPCD run of guaifenesin in isopropanol (experiment 6).

Figure 4.26 illustrates the trajectories of the optical rotation, as well as the temperature profile of the two tanks and turbidity signal in the dissolution tank for an exemplary CPCD run of guaifenesin enantiomers in isopropanol (experiment 6). The optical rotation signal of the mother liquor in the crystallization tank starts to increase in absolute value after the

seeding. According to the description of the CPCD process given in the experimental part, the optical rotation of the mother liquor in both the dissolution and the crystallization tank should be close to zero over the time, meaning that the two mother liquors remain at racemic composition. In order to keep the mother liquors close to racemic composition, the exchange rate has to be high enough to counterbalance the depletion of the preferred enantiomer within the crystallization tank. In the investigation herein reported, an exchange rate of 30 mL/min was implemented. It can be assumed that such exchange rate, under the studied conditions, was not able to ensure the counter-balancing effect leading to the refreshment of the mother liquor up to racemic composition. Furthermore, from the results of the resolution runs in single stirred tank, it has been found that the system exhibits faster crystallization kinetics when the crystallization is performed in isopropanol. Therefore, the increase of the optical rotation (Figure 4.26a) can be rationalized taking into account the exchange rate used in the investigation and the fast crystallization kinetics under the studied conditions. Concerning the turbidity signal in Figure 4.26b it can be seen that, after seeding, the turbidity values decrease according to the decrease of the suspension density, due to the dissolution of the racemate solid excess into the dissolution tank. A faster decrease of the signal is observed in the final part of the trajectory (Figure 4.26b, red dashed square), suggesting that a faster dissolution of the solid racemate in suspension into the dissolution tank is occurring. A faster decrease of the suspension density into the dissolution tank can be related to the fact that, at this stage of the experiment, the dissolution of the solid excess is not selective to the seeded enantiomer but it involves also the counter-enantiomer. Therefore, it can be assumed that the mother liquor transported from the crystallization tank in the final stage of the experiment is depleted with respect to the counter-enantiomer, meaning that its nucleation in the crystallization tank is occurred. For this reason, the process has been interrupted. The purity of the product collected from the crystallization tank (Table 4.15, experiment 6) shows a contamination from the counter-enantiomer, hence confirming the validity of strategy control using the turbidity signal described above.

Table 4. 15 Experimental results of CPCD runs of guaifenesin in isopropanol (crystallization tank).

experiment	T_{cryst} (°C)	Pu %	Pr (g/h/L)	*Pr (g/h/L)	Y %
1	24	95.8	13.68		28.30
2	24	88.5	11.36		30.46

3	24.5	94.2	9.09		21.84
4	25	89.0	12.51		28.77
5	25.5	96.8	5.71	8.36	24.37
6	25.5	96.0	5.86	9.30	23.53
7	25.5	95.5	5.47	7.16	34.81
8	27	96.2	-0.03	1.92	-0.12

* calculated considering the solid product remained on the filters

Table 4. 16 Experimental results of CPCD runs of guaifenesin in isopropanol (dissolution tank).

experiment	Pu %	Pr (g/h/L)	*Pr (g/h/L)	Y %	*Y %
1	76.9	18.48		71.52	
2	71.26	12.46		62.53	
3	63.87	17.45		76.55	
4	66.0	20.24		82.87	
5	68.8	10.34	10.34	78.4	78.43
6	80.0	11.55	12.51	82.36	89.2
7	80.0	6.83	8.39	77.16	94.8
8	54.44	7.17		52.10	

* calculated considering the solid product remained on the filters

The performance indicators of the CPCD runs are listed in Table 4.15 for the crystallization tank and Table 4.16 for the dissolution tank. A representation of the performances of the each CPCD run as a function of the crystallization temperature is given in Figure 4.27. It can be observed that as the crystallization temperature increases, the productivity for both crystallization and dissolution tanks decreases, probably due to the fact that, at higher crystallization temperature, the difference of concentration between the solutions into the crystallization and dissolution tank decreases, hence the supersaturation in the crystallization tank decreases and the production time of the process increases.

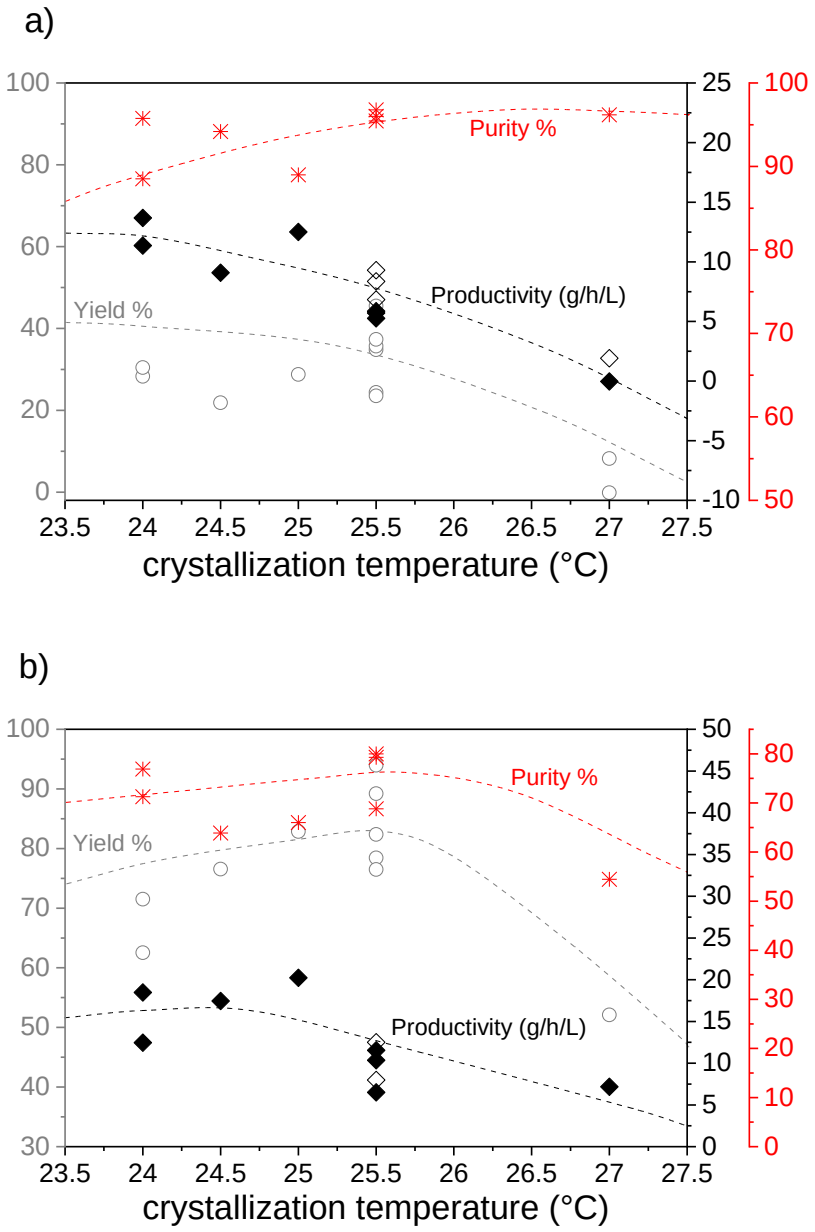

Figure 4. 27 Representation of the obtained KPIs for CPCD runs of enantiopure guaifenesin in isopropanol for the crystallization tank (a) and for the dissolution tank (b), as a function of the crystallization temperature.

As the crystallization temperature increases, the yield for the crystallization tank decreases, due to the fact that less amount of enantiomer is produced at lower supersaturation conditions. On the other hand, the purity of the product collected from the crystallization tank remains at high values, a consequence of the fact that at lower

supersaturation conditions, the nucleation of the counter-enantiomer is less likely to occur. Concerning the performances calculated for the dissolution tank, results show that lower crystallization temperatures, thus higher supersaturation values in the crystallization tank, allow a larger undersaturation of the mother liquor with respect of the preferred enantiomer in the dissolution tank, hence favoring the selective dissolution under the studied experimental conditions.

4.2.6 PC of enantiopure guaifenesin in tubular fluidized bed crystallizer

In the present section, the results of the resolution of the guaifenesin enantiomers using a tubular fluidized bed crystallizer are presented.

A first investigation has been done in determining the density, ρ, of the solid guaifenesin as well as the density of the saturated solution using different solvents. A solid density, ρ_{solid}, of 1.28 g/cm^3 and a solution density, $\rho_{solution}$, ranging between 1.0078 g/cm^3 for the aqueous solution and 0.8094 g/cm^3 in isopropanol were observed, as summarized in Table 4.17.

Table 4. 17 Experimentally determined density values of solutions of racemic guaifenesin in various solvents, saturated at T=30 °C.

	C_{sat} (g_{solute}/ $g_{solution}$)	T_{cell} (°C)	$\rho_{solution}$ (g/cm^3)
water	0.06	30	1.0078
ethanol	0.19	30	0.8438
acetone	0.17	30	0.8302
isopropanol	0.11	30	0.8094
ethyl acetate	0.05	30	0.9004

In a first preliminary experiment of resolution of guaifenesin in a tubular fluidized bed crystallizer water has been used as solvent. In such investigation, a wide range of experimental conditions was applied, by varying supersaturation conditions and the volumetric flow rate within the tubular crystallizer. It was found that the water is an unsuitable solvent for the resolution of guaifenesin enantiomer exploiting the tubular crystallizer under the applied conditions. In particular low purity of the product and low product masses have been observed. As the sedimentation rate of the solid particles in

an upward flowing fluid depends *i.a.* on the difference between density of the particles in the fluid and the density of the fluid,[145,146] the reason of the low performances can be related to the small difference $\rho_{solid} - \rho_{solution}$ for the water system. When the density of the solid particles is comparable to the density of the saturated solution, the particles within the tubular crystallizer tend to be transported with the upstream flow rather than settling at the bottom of the crystallizer. Furthermore, as also seen for the preferential crystallization of guaifenesin in single stirred tank from aqueous solution, the system exhibits slow crystallization kinetics when the resolution is performed in water. Therefore, it can be assumed that those two properties of the system*, i.e.* slow crystallization kinetics and small difference in density values, have caused a loss of the seed crystals and of the crystallizing material during the experiments, leading to the observed low performances.
Based on those observations, isopropanol was chosen as solvent for the subsequent investigations presented here, as it provides the larger density difference with respect to all the solvents investigated. A preliminary test run was performed using racemic guaifenesin as seed material and a disperser as milling device for the continuous supply of seed crystals. The experimental conditions of the preliminary test run are summarized in Table 4.18.

Table 4. 18 Experimental conditions of the preliminary test crystallization run of racemic guaifenesin in isopropanol in the tubular fluidized bed crystallizer.

T_{cryst} (°C)	30-27-25
T_{sat} (°C)	35
m_{seed} (g)	5-5-5 racemic
$m_{solid\ in\ excess}$ (g)	200
C_{sat} ($g_{\ solute}$ / $g_{\ solution}$)	0.15
$\dot{V}$ (L /h)	1.3 – 3.7
Rotation speed disperser (rpm)	3000

Initially, a crystallization temperature T_{cryst}=30 °C and a flow rate $\dot{V}$=1.3 (L /h) were investigated and no settling of the crystals was observed after 45min from the seeding. Therefore, the crystallization temperature was decreased to T_{cryst}=27 °C and an additional amount of seed crystals, 5 g, was introduced. After 1 h 40 min from the second seeding,

the suspension contained into the crystallizer was collected and filtrated and 6.03 g of crystals were obtained. In this range of time, the flow rate was initially increased to 3.7 L/h and then lowered to 2.3 L/h. The third condition investigated, was T_{cryst}=25 °C and a flow rate of 2.5 L/h. After 70 min from the seeding, 1.07 g of product was collected (Table 4.19).

Table 4. 19 Experimental results of the preliminary test crystallization run of racemic guaifenesin in isopropanol in the tubular fluidized bed crystallizer: mass and particle size.

	m (g)	length±SD (μm)	width±SD (μm)
initial seed crystals	15	159±88	45±22
product 1	6.03	398±88	105±38
product 2	1.07	282±83	159±22

Overall, a partial loss of the seeded and crystallised material has been observed in the initial test run. As the dissolution of the generated seed crystals can be neglected at the studied experimental conditions, it can be assumed that once the seed crystals have been crushed and dispersed by the milling device, a large portion of the generated fines was unable to exhibit fluidization and afterwards sedimentation and therefore it was dragged out of the crystallizer. The lack of sedimentation may be due to the low growth kinetics of the seed crystals within the tubular crystallizer at the studied conditions. By decreasing the crystallization temperature to 25 °C, still a loss of particles was observed, meaning that also at high supersaturation conditions the particles were not able to grow to the critical size needed to remain within the crystallizer.

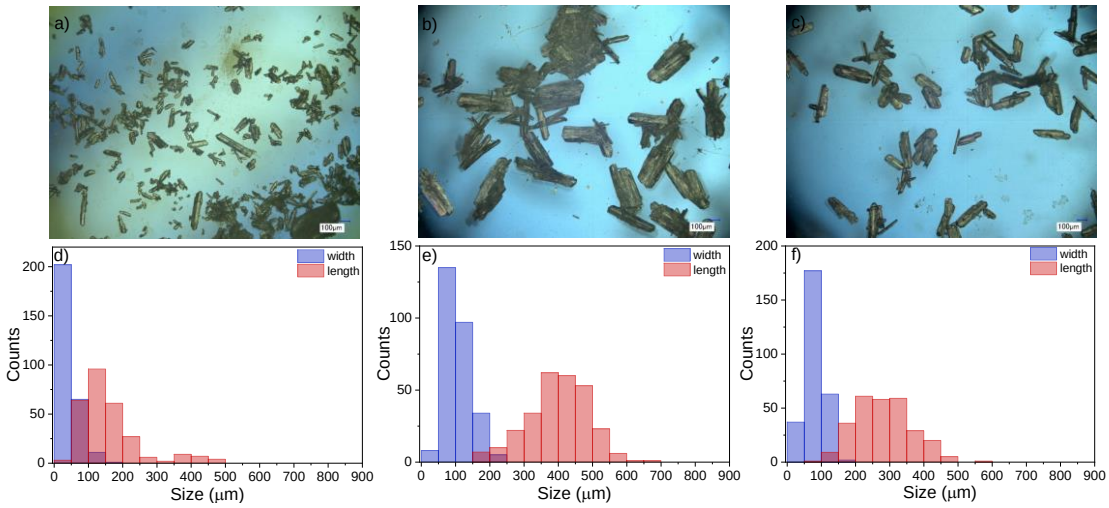

Figure 4. 28 Micrographs and experimentally determined width and length distributions of the initial seed crystals (a,d), product 1 (b,e) and product 2 (c,f).

In Figure 4.28, the experimentally determined length and width of the initial seed crystals and the two collected products as well as their micrographs are shown. The manually introduced seed crystals present a needle-like morphology with a mean length of 159±88 µm and a mean width of 45±22 µm. From Table 4.19, one can see that the portion of seed crystals remaining within the tubular crystallizer could grow in both length and width directions, up to 398±88 µm and 105±38 µm for the product 1 and up to 282±83 µm and 159±22 µm for the product 2. This suggests that only the crystals having a certain size in length and width are able to settle within the crystallizer, while the remaining population of crystals crushed by the milling device, follows the upstream flow and is dragged out of the crystallizer. With this in mind, the subsequent experiment has been designed without the exploitation of the milling device and using seed crystals of pure *(R)*- and *(S)*- guaifenesin, produced *via* recrystallization as described in section 3.3.4 and manually introduced from the top of the tubular crystallizer. The experimental conditions of the resolution experiment of the guaifenesin enantiomers in isopropanol exploiting the tubular fluidized bed crystallizer are reported in Table 4.20.

Table 4. 20 Experimental conditions of the resolution of guaifenesin enantiomers in isopropanol in the tubular fluidized bed crystallizer.

T_{cryst} (°C)	25
T_{sat} (°C)	35
total m_{seed} (g)	6.5 (S)- / 5 (R)-
$m_{solid\ in\ excess}$ (g)	200
C_{sat} ($g_{\ solute}$ / $g_{\ solution}$)	0.15
$\dot{V}$ (L /h)	2

The experiment consisted in five resolution runs of 90 min. In each run seed crystals of pure guaifenesin enantiomer were manually introduced at the top of the crystallizer and the product was harvested after 90 min from the seeding. The product removal consisted in the collection of the whole suspension contained into the tubular crystallizer. The mass and handedness of the seed crystals were varied as reported in Table 4.21. In the first three runs, seed crystals of *(S)*-guaifenesin were used while in the last two run *(R)*-guaifenesin was used.

Table 4. 21 Properties of the seed crystals used in PC runs of enantiopure guaifenesin in isopropanol in tubular fluidized bed crystallizer.

	m_{seed} (g)	length±SD (µm)	width±SD (µm)
run 1	2.0 *(S)*-	150±69	11±4
run 2	2.0 *(S)*-	150±69	11±4
run 3	2.5 *(S)*-	150±69	11±4
run 4	2.5 *(R)*-	118±42	14±5
run 5	2.5 *(R)*-	118±42	14±5

It can be observed that the recrystallized material used as seed crystals have a narrow size distribution in length and width, which guarantees the absence of fines, as also shown in Figure 4.29, thus avoiding an eventual loss of the seed crystals.

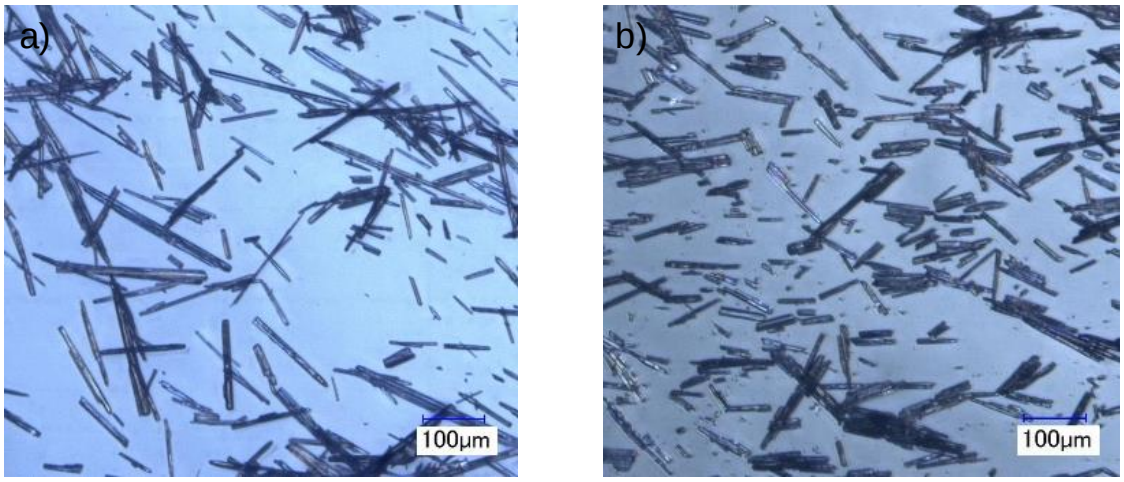

Figure 4. 29 Microscopic photographs of recrystallized *(S)*-guaifenesin (a) and *(R)*-guaifenesin (b) used as seed crystals in PC runs of enantiopure guaifenesin in isopropanol in tubular fluidized bed crystallizer.

The performances of the resolution runs in terms of purity of the collected product, productivity and yield are listed in Table 4.22 and graphically represented in Figure 4.30 The first three runs refer to the production of the *(S)*-guaifenesin enantiomer and show an increase of productivity from 2.6 g/h/L to 6.7 g/h/L and yield from 2 % to 5.3 % respectively.

Table 4. 22 Experimental results of PC runs of enantiopure guaifenesin in isopropanol in tubular fluidized bed crystallizer.

	$m_{product}$ (g)	Pu %	length±SD (µm)	width±SD (µm)	Pr (g/h/L)	Y %
run 1	4.0	95.7 *(S)*-	243±103	32±12	2.6	2.0
run 2	5.9	95.9 *(S)*-	252±106	32±11	5.0	3.9
run 3	7.8	94.7 *(S)*-	270±109	30±10	6.7	5.3
run 4	8.6	96.5 *(R)*-	239±84	39±14	8.0	6.3
run 5	9.2	96.3 *(R)*-	269±93	44±26	8.9	7.0

The increase of productivity and yield between run 2 and run 3 can be attributed to the increase of the mass of seed crystals at run 3, (Table 4.22). While for the last two runs, which refer to the production of *(R)*-guaifenesin, the productivity increases from 8 g/h/L to

8.9 g/h/L and the yield increases from 6.3 % to 7 %. It is worth mentioning that a dissolution step was performed between the runs, consisting in increasing the temperature of the tubular crystallizer as well as the flow rate of the mother liquor transported from the feeding tank, in order to remove the uncollected particles after each harvesting. Nonetheless, a certain accumulation of undissolved particles within the connection pipes of the setup as well as on the walls of the crystallizer could not be completely avoided. Therefore, the overall increase of the mass of the product for the first three runs can be, to some extent, attributed to the accumulation of the product from the previous run. It is worth noting that also between run 3 and run 4, an increase of productivity and yield is observed, (Figure 4.30).

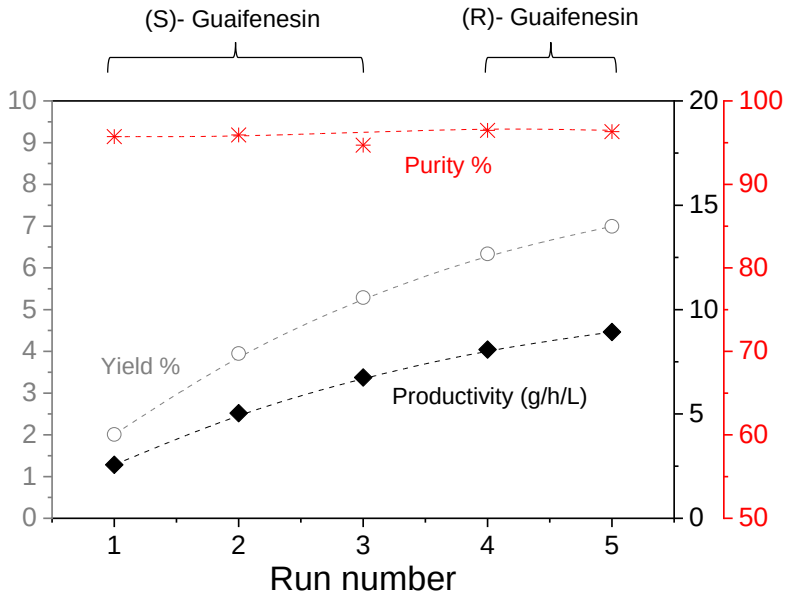

Figure 4. 30 Representation of the obtained KPIs for PC runs of enantiopure guaifenesin in isopropanol in tubular fluidized bed crystallizer.

In this case, the accumulation effect cannot be taken into account since the high purity of the collected product suggests that no contamination of the product occurred. Therefore, the reason may lie in the different properties of the seed crystals. In fact, the seed crystals of *(S)*-guaifenesin grow from 150±69 µm to 270±109 µm in length and from 11±4 µm to 30±10 µm in width (Table 4.15). On the other hand, the seed crystals of *(R)*-guaifenesin seem to grow more in both length and width, *i.e.* up to 269±93 µm and 44±26 µm from 118±42 µm and 14±5 µm.

Chapter 5. Discussion

The present chapter will summarize the key findings of the experimental work done. The first two sections will provide a qualitative discussion of the experimental results presented in the previous chapter for the model compounds CPG-intermediate and guaifenesin. The last section will present a novel methodology of crystallization-based resolution processes, which has been applied to a racemic compound forming system, hence broadening the applicability of crystallization processes to a wider range chiral substances.

5.1 CPG-intermediate system

The first model compound studied was a novel conglomerate forming system, which, to our knowledge, has not been previously investigated in terms of its solubility and direct resolution techniques. The substance, here named CPG-intermediate, is a chiral building block in the production of a largely marketed pharmaceutical molecule and it was studied in parallel projects within the mentioned EU project “CORE”.

The solid-liquid equilibria of the system in acetonitrile were determined, demonstrating that the compound exhibits low solubility in acetonitrile and is a conglomerate forming system under the studied conditions. The resolution runs *via* preferential crystallization have been designed based on the experimentally determined solubility ternary phase diagram in acetonitrile and the MSZW of the system. Firstly, the results of the single batch PC runs over a range of experimental conditions have been presented. It has been found that pure enantiomer of the studied system can be successfully isolated in single batch mode, in a window of operating conditions, *i.e.* by choosing a supersaturation ratio

between 2.5 and 2.75 and a crystallization temperature of 20 °C. The performances of the resolution in single tank have demonstrated that at lower supersaturation conditions, the production time of the process increases and low product masses are collected, hence reducing the productivity of the process. On the other hand, at higher supersaturation conditions, higher productivity can be achieved, although a certain contamination of the product occurs. A second crystallizer configuration has been applied to resolve enantiomers of the system, using the so-called CPCD approach. The results have demonstrated a certain limit of the applicability of the technique for this system. In particular, although pure enantiomer could be collected from the crystallization tank, the selective dissolution of the racemate solid excess in the dissolution tank was to some extent impaired. The reason could be related to the small difference of concentration between the saturated solution in the dissolution tank and the supersaturated solution in the crystallization tank. However, an increase of the concentration difference between the mother liquors into the two tanks, and therefore an increase in the saturation temperature, has been investigated. It has been observed that also with a higher difference of concentration between the two solutions, the depletion of the preferred enantiomer from the mother liquor in the crystallization tank was not high enough to trigger the selective dissolution of the solid racemate in excess in the dissolution tank. Furthermore, an early nucleation of the counter-enantiomer has been observed due to the high supersaturation conditions in the crystallization tank.

The experimental studies on the CPG-intermediate have covered its melting behavior and its solid-state properties. Both its theoretical and experimental melting solid-liquid equilibria have been determined. The experimental data of the DSC measurements combined with an HPLC investigation of the molten enantiopure compound have shown the tendency of the system to give racemization when heated up to its melting point. Based on the information given in literature about the racemization mechanism of amino acid derivatives, as for the case of CPG-intermediate, a mechanism of racemization has been proposed. Usually the racemization mechanism in solution involves the removal of the proton on the α-carbon in the presence of a base, which for the case of CPG-intermediate is DBU.[126,147] In the present work, a racemization reaction has been proposed in absence of solvent or catalyst. It can be assumed that the functional groups around the α-carbon exhibit a stabilizing effect on the planar intermediate generated at the rate-determining step and therefore, the racemization reaction becomes a spontaneous reaction at high temperatures. The investigation has provided instructive insights on the experimental

conditions that lead to the racemization of the molecule, addressing an essential aspect related to pharmaceuticals*, i.e.* the configuration stability. The phenomenon of the inversion of configuration is of particular interest for pharmaceutical molecules in the context of drug development, since the pharmaceutical ingredient must remain in the desired enantiomeric form in the bulk as well as in the final dosage form. Moreover, the observation of the racemization at the molten state has implications on the determination of the chiral purity during the melting point determination, since the racemization event leads to the decrease of the melting temperature due to the change of the enantiomeric composition, especially at high enantiomeric purity. The present study highlights the importance of understanding the mechanism of racemization in case of pharmaceutically relevant molecules, as it could occur under various and unexpected experimental conditions, hence enabling novel deracemization processes.

5.2 Guaifenesin system

As a second chiral substance, the API guaifenesin was studied. This compound was selected as it represents a case of pharmaceutical molecule marketed as racemate. As to our knowledge, there is a lack of reported experimental investigations on the pharmacological and pharmacokinetic effects of the single enantiomers of such API, the aim was to provide experimental data on its fundamental properties, as well as to deliver examples of successful enantiomeric resolution using crystallization processes.

Initially, a systematic investigation on the solubility and its MSZW in the solvent chosen for the crystallization runs was carried out. Due to an observed peculiar solubility behavior of this API in water, the investigations have been extended to a broader range of organic solvents. The thermodynamic investigations have shown that the system exhibits high solubility in a range of solvents specifically in polar protic solvents such as water and ethanol. Few considerations on the molecular interactions in solution have been proposed based on the calculation of activity coefficients of the system in various solvents as well as by interpreting ^{1}H-NMR spectra of the racemic guaifenesin in methanol-d_4 and acetonitrile-d_6. It has been suggested that the guaifenesin molecules tend to create, through the formation of H-bonds, intermolecular self-associations structures, such as dimers, which favor the solvation of the molecules. Based on the shift of the signal related to the hydroxyl protons of the molecule observed in the ^{1}H-NMR spectra in acetonitrile-d_6, an example of self-association structure has been proposed. It can be assumed that such intermolecular interactions are particularly favored in water in the range of temperature

between 30 and 40 °C, where the steep increase of solubility occurs, due to an additional energetic contribution, *i.e.* the hydrophobic interactions between the water molecules and the dimers of guaifenesin. As the molecular interactions of APIs in solution are of importance in life science disciplines as well as in process development, the present thermodynamic study on the API guaifenesin has provided useful insights on a possible scenario of the molecular interactions in solution. This could be applied to a number of pharmaceutical molecules exhibiting peculiar solubility behavior and crystallization properties.[148,149] Furthermore, since the solution-phase assembly of the molecules is a key link for the organization of the molecules at the solid-state, the understanding of assembly characteristics in solution could pave the way towards the identification of mechanism of formations of conglomerates, racemic compound forming systems and solid solutions.[150,151]

The second part of section 4.2 has been devoted to the application of the preferential crystallization for enantioseparation purposes. It can be seen that the results obtained in the thermodynamic investigations, can be related to the resolution experiments in single stirred tank. The guaifenesin enantiomers in water exhibits slower crystallization kinetics compared to the kinetics of the system in isopropanol, as given by the results of the preferential crystallization investigation in single stirred tank. The comparison of the performances of the resolution runs in isopropanol and the resolution in aqueous solution has demonstrated that, at the same driving force conditions, lower productivity and yield resulted from the resolution in water. The reasons have been attributed to the slower crystallization kinetics of guaifenesin in aqueous solution compared to the isopropanol system. Overall, the evaluation of the performances of the resolution processes has shown that it is possible to produce pure enantiomeric guaifenesin *via* preferential crystallization, *i.e.* from a solution in isopropanol, with high yield and productivity.

By exploiting the coupled crystallizer configuration, it has been concluded that the fast crystallization kinetics in isopropanol limit the applicability of the CPCD process. In fact, the results of the resolution runs of guaifenesin in isopropanol over a range of experimental conditions have shown that, at the experimental exchange rate applied, it is not possible to counterbalance the depletion of the preferred enantiomer from the mother liquor into the crystallization tank over a long range of time. In fact, the chiral purity of the product collected from the dissolution tank was below 80 %. Previous investigations done in our laboratories on the CPCD process applied to the guaifenesin system have

demonstrated the possibility to upgrade the chiral purity of the product from the dissolution tank and achieve higher productivity values, by performing the CPCD process in water. The present investigation on the CPCD technique applied to the guaifenesin in isopropanol has demonstrated that the crystallization properties of the system are crucial in the choice of an appropriate resolution method. Specifically, for the guaifenesin system, when exploiting a single tank configuration, the resolution in isopropanol is characterized by high crystallization kinetics, which lead to high resolution performances. On the other hands, when using the coupled configuration for the CPCD approach, it has been found that lower crystallization kinetics favor the counter-balancing effect between the depletion of the preferred enantiomer form the mother liquor into the crystallization tank and its selective dissolution from the solid racemate in excess into the dissolution tank, at the studied exchange rate. In this case, the choice of a different solvent enabling slower crystallization kinetics, such as water, would lead to higher resolution performances.

The final part of the section 4.2 focuses on the technical concerns related to the exploitation of a tubular fluidized bed crystallizer for continuous operation. Firstly, it has been discussed how a certain density difference between the solid and the saturated solution, ρ_{solid}- $\rho_{solution}$, is needed in order to enable the sedimentation of the solid particles in solution within the tubular crystallizer. Secondly, a fundamental aspect for the continuous operation mode has been addressed, *i.e.* the seeding strategy. It has been found that a continuous supply of seed crystals using the disperser as milling device is not appropriate for the studied system. In particular, it causes the formation of fine particles, which are not able to grow and settle at the bottom of the crystallizer, primarily due to the slow crystallization kinetics of guaifenesin. A different seeding strategy has been therefore exploited, consisting in the periodic manual seeding of pure homochiral crystals having a chosen crystal size distribution. In this case, enantiomers of guaifenesin have been produced with high purity and a productivity up to 8.9 g/h/L. Although the experimental investigation with periodic manual seeding and periodic removal of the product cannot be considered as a proof of principle of continuous resolution, it provides essential insights on the seeding strategy, especially on the quality of the seed crystals to be continuously supplied in a possible continuous process for the studied system. Especially, it has been found that it is necessary to introduce seed crystals of guaifenesin of a certain size in length and width, in order to observe their sedimentation and growth within the fluidized bed crystallizer.

5.3 Enabling resolution for a racemic compound forming system

The experimental studies discussed so far have involved pharmaceutical molecules belonging to the category of conglomerate forming systems. These are commonly estimated to make up to 10 % of the known chiral systems. The most abundant category is represented by the racemic compound forming system, which comprises up to 90 % of the chiral molecules. Solid solutions are rarely encountered. As mentioned in the theoretical background, a prerequisite to apply preferential crystallization starting from a racemic solution is the immiscibility of the enantiomers in the solid state, thus that the system crystallizes as a conglomerate. This limits the applicability of such a direct and simple technique to a minor portion of chiral systems. Given the importance and the need for chiral resolution, it is the subject of the present section to provide additional considerations related to isolation of pure enantiomers, using an alternative crystallization technique. Since this methodology eludes the methods and the main technologies described for the two studied conglomerate systems, the rational approach as well as the experimental procedures applied and the results obtained will be found in the annex of this thesis. The separation strategies rely on the interpretation of the ternary phase diagram and exploit a peculiar fundamental characteristic of the chiral system. The studied substance is a racemic compound forming system, namely the amino acid methionine and exhibits a shift of the eutectic composition in solution at different temperatures. Two specific separation strategies are described in the annex. These two strategies are capable to resolve, under specific conditions, the enantiomers of compound forming systems. One strategy exploits the evaporation of a selected amount of solvent from the initial solution at eutectic composition, while the second consists in the addition of solvent to an enantiomerically enriched solid mixture. The aim is to demonstrate that a correct interpretation of the solubility ternary phase diagram and a rational exploitation of the shift of the eutectic composition with the temperature can enable the application of new resolution techniques in addition to the known preferential crystallization at the eutectic composition.

Chapter 6. Conclusions

6.1 Concluding remarks

Chirality is an important concept in life science. Small chiral molecules such as amino acids and sugars are the building blocks of biomolecules of living systems and therefore, many properties related to the interaction of drugs, agrochemicals as well as natural chiral compounds with the biological environment exhibit a marked enantioselectivity. Due to the potential different pharmacokinetics, side effects, toxicology, pharmacodynamics of enantiomers of medicinal chiral molecules, chiral drugs are almost exclusively marketed and applied as single enantiomers. The methods used for the provision of pure enantiomers of chiral molecules are mostly based on exploiting a chemical modification of the starting material, *i.e.* by using chiral precursors of the target molecule, as well as by transforming the desired enantiomer in a pair of diastereomeric salts. A direct method, which does not need the presence of chemical auxiliaries to produce a pure enantiomer of a chiral molecule is preferential crystallization, which allows to isolate with high chiral purity the preferred enantiomer from a supersaturated eutectically composed solution.

In the context of enantiomeric resolution, the present thesis has evaluated several aspects crucial for the applicability of preferential crystallization for pharmaceutically relevant molecules. Firstly, through systematic preliminary experimental investigations, the solid-liquid equilibria of pharmaceutical molecules have been identified. This information was subsequently exploited to design the crystallization experiments. The resolution runs have

been performed over a range of experimental conditions exploiting various crystallizer configurations. The experimental investigation of the fundamental properties have been performed in a small laboratory scale, while the crystallization runs were carried out in larger scale, up to 500 mL volume, hence providing a proof of concept of process development for the provision of pure enantiomers of the studied chiral pharmaceutical systems. The results have demonstrated how the thermodynamic and kinetic properties of the substances have profound implications on the performances of the resolution runs. Together with the feasibility study of crystallization-based resolution techniques the thesis has addressed one of the decisive aspects for the process development, *i.e.* the performance assessment of the crystallization processes, by determining chosen key performance indicators of the resolution runs such as purity, productivity and yield. The purity of the collected product was determined using enantioselective HPLC, while the productivity and yield of the processes have been defined separately for each crystallizer configuration exploited, allowing to analyze certain tradeoffs between KPIs.

By exploiting a single tank configuration, it has been found for both of the conglomerates studied, that fast crystallization kinetics allow to achieve high productivity values. This could be enabled either by increasing the supersaturation degree, as shown for CPG-intermediate, or by changing the medium of crystallization, *i.e.* by changing solvent as observed for the guaifenesin system. It has been proved that an appropriate monitoring strategy of the crystallization process is fundamental in order to identify the operation window at major risk of contamination. The monitoring strategy used in the present experimental studies consisted in a qualitative observation of the optical rotation signal combined with the turbidity signal. As those signals are related to the depletion of the preferred enantiomer from the mother liquor, they have allowed to interrupt the process before or in correspondence of the nucleation of the counter-enantiomer. Although the nucleation of the counter-enantiomer could not be prevented in some cases, the chiral purity of the product collected in single batch mode was above 95 % for both of the studied systems. Such value of chiral purity confirm to some extent the robustness of the strategy control used. Moreover, it has been proved that a purification step based on the recrystallization of the multiple fractions of product collected can be easily operated to upgrade the chiral purity up to enantiopure values. As third performance indicator, the yield of the processes has been determined for both of the studied systems. While the productivity indicator depends on the technical parameters of the process, such as the

volume of crystallizer and the production time, the yield depends on the theoretical mass achievable by crystallization, which is the difference between the concentration at the initial saturation condition and the final equilibrium concentration. Therefore, a lower solubility difference between the saturation and the crystallization temperature, allowed to achieve higher yield, according to the definition of yield for a single batch PC process given in the experimental section. In fact, the maximum values achieved where of *ca.* 40 % for CPG-intermediate in acetonitrile and 32 % for the guaifenesin system.

Concerning the coupled configuration exploited for CPCD runs, defining the performance of the resolution process is a challenging task as the performance indicators have been related to each crystallizer exploited for this approach, rather than to the overall process. Ideally, a high performing process would yield the production of the pair of enantiomers with high chiral purity. In order to achieve this result, the depletion of the preferred enantiomer into the crystallization tank and the selective dissolution into the dissolution tank should proceed in such a way that the mother liquor remains at racemic composition in both of the tanks. Furthermore, an appropriate exchange rate must be chosen in order to counterbalance the two events. The results of the CPCD runs for the studied systems have shown how the fundamental characteristics of a substance, such as fast crystallization or slow dissolution kinetics can limit the applicability of this technique. While for CPG-intermediate it has been conducted a feasibility study of the CPCD technique for resolution purposes, for the guaifenesin system a range of operative conditions, leading to a chiral purity of 95.5 % and 80%, respectively for the seeded and unseeded enantiomer, has been identified.

A further study on the guaifenesin system has been directed towards a continuous resolution operation mode, by exploiting a third crystallizer configuration, namely the tubular fluidized bed crystallizer. The attention has been devoted on the technical aspects such as the choice of an appropriate solvent and the seeding strategy. It has been found that a higher density difference between the solid guaifenesin and the saturated solution in isopropanol is preferred to enable sedimentation of the particles in the crystallizer. Concerning the seeding strategy, it has been found that for the guaifenesin system, the exploitation of the milling device is not optimal, as it cause the formation of fines, which are dragged out of the crystallizer, also at low flow rates. With a different seeding strategy, consisting in periodical manual seeding of seed crystals with narrow size distribution in

length and width, it has been possible to achieve productivity values comparable with the two configurations previously exploited, as well as high chiral purity of the product.

Overall, this thesis has provided important tools to efficiently apply resolution techniques based on the preferential crystallization principle on two substances that are relevant for the pharmaceutical industry. Advantages and limits of the single batch and the coupled crystallizer configuration have been demonstrated for the two studied systems, through evaluation of chosen KPIs of the processes. The applicability of the fluidized bed crystallizer in continuous operation mode has been studied for the API guaifenesin, hence paving the way to a further development of this promising method for the resolution of the enantiomers of other chiral systems. The investigations were based on the experimentally determined solubility ternary phase diagrams of the systems, which have played a crucial role in designing the crystallization runs. Such representation of the solubility of the systems have enabled the identification of the so-called Meyerhoffer coefficient and the calculation of the supersaturation degree of the crystallization processes. Further aspects on the relevance of the ternary phase diagrams for resolution purposes are explained in a supplementary section of the thesis, namely annex, dedicated to the system methionine in water.

6.2 Future perspectives

Based on the results provided in the present thesis a number possible research directions can be engaged. The results obtained for the CPG-intermediate system suggest that additional investigations would allow to identify other experimental conditions that enable the racemization event. Further steps could be directed towards the investigation of the kinetics of racemization at the molten state as well as an investigation on the extent of the racemization as a function of the temperature and the time. In general, understanding the incidence of thermally-induced racemization events among conglomerate forming systems as well as racemic compound forming systems and solid solutions could be of relevance for pharmaceutical chiral molecules.

Improvements of the configuration used for the CPCD approach are required in order to guarantee the counterbalance effect between the selective dissolution and the depletion of the preferred enantiomer from the mother liquor in the crystallization tank, specifically for systems exhibiting fast crystallization kinetics.

Also for the guaifenesin system, further investigations are needed in order to better understand the molecular interactions in solution, which could be used to elucidate the solubility behavior of many other APIs. Based on the studies related to the applicability of the fluidized bed crystallizer for the guaifenesin system, future studies will be devoted to the implementation of a seeding unit able to transport continuously the seed crystals of a desired crystal size distribution to the tubular crystallizer. A possible way could consist in suspending the homochiral crystals in a saturated solution in a stirred tank, connected to the fluidized bed crystallizer *via* peristaltic pump. The investigation on the experimental conditions such as, supersaturation conditions, volumetric flow rate of the seeding as well as the total volumetric flow rate within the tubular crystallizer will be subject of further investigations. Finally, as the majority of the chiral systems crystallizes as racemic compound forming systems, future investigations could be aimed to a further development and application of efficient resolution methods which are based on the fundamental properties of the chiral substances, as the strategies discussed in the annex.

Annex

This annex is intended to provide additional considerations related to isolation of pure enantiomers using an alternative crystallization technique. The attention will be devoted to a rational crystallization approach which differs from the one exploited for the previous chiral systems. The approach discussed is in fact applicable for racemic compound forming systems, hence extending the experimental investigation to a wider category of crystalline enantiomeric systems. In particular, the studied chiral system is the amino acid methionine, which exhibits a peculiar characteristic of the eutectic composition in solution at different temperatures. Based on the interpretation of the ternary solubility phase diagram of the chiral molecule, the separation of its enantiomers, exploiting the characteristic shift of the eutectic composition with the temperature will be described. Two separation strategies will be examined, one consisting in the evaporation of a selected amount of solvent from the initial solution at eutectic composition, while the second consists in the addition of solvent to an enantiomerically enriched solid mixture. The rational approach in designing the separation process will be discussed as well as the experimental procedures applied and the results obtained. The following chapter will provide an essential guide in exploiting ternary solubility phase diagrams of chiral systems, with a focus on the interpretation of the phase equilibria for resolution purposes. The qualitative investigation here presented contributes to the understanding of several alternative case studies already present in literature.[102,152] The separation strategies and the results described have been used for a publication.[103]

A.1 Methionine system

Methionine is a proteogenic sulfur-containing amino acid that is essential for life. In organisms it can serve as precursor of cysteine.[153] The racemate is used as additive in animal feed, while L- and D- enantiomers find pharmaceutical application as liver protection agent and as otoprotective agent respectively (Figure A.1).[154]

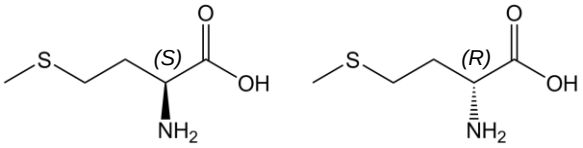

Figure A. 1 Molecular structure of methionine enantiomers.

Methionine is known to be a racemic compound forming system[155] and its solubility in water has been experimentally determined in a previous work by Polenske *et al*.[156] The system exhibits a peculiar feature, that the eutectic composition, x_{eu}, for a specific temperature moves to lower enantiomeric excesses as the temperature increases, specifically from x_{eu}=0.94 at T=1 °C to x_{eu}=0.86 at T=60 °C (Figure A.2).

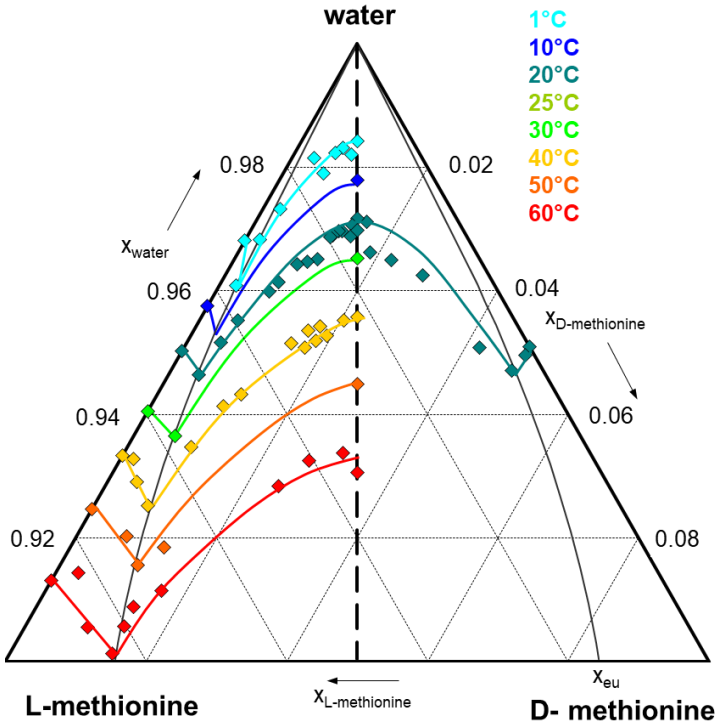

Figure A. 2 Ternary solubility phase diagram of the methionine enantiomers in water between 1°C and 60°C adapted from ref [156]. The upper 10% of the full phase diagram is shown. The thin black line represents the change in the eutectic composition x_{eu} with the temperature. Isotherm lines are given as guides to the eye.

A.2 Selective crystallization of L-methionine: strategy 1

In the present section, the first strategy used for the resolution of methionine enantiomers in aqueous solution is described. The strategy consists in the exploitation of the shift of the eutectic composition of the system as the temperature increases and it is schematically represented in Figure A.3. Two solubility isotherms have been considered for this strategy, *i.e.* the solubility at 1°C and at 60 °C, respectively T_{low} and T_{high} in Figure A.3. The strategy starts with the preparation of an aqueous solution of the system at the eutectic composition at lower temperature and its equilibration at high temperature. At this point, the removal of the solvent *via* vacuum evaporation, leads to the variation of the composition of the system as shown by the red arrows moving along the solvent line in Figure A.3. The initial point of the separation process corresponds to a solution of methionine enantiomers in water at eutectic composition corresponding to x_{eu}=0.94 (blue points in Figure A.3), heated and equilibrated at 60°C. The removal of a selected amount of solvent allows to locate the system either into the 2-phase domain or into the 3-phase domain (red points 1 and 2, in Figure A.3a and b, respectively), yielding a different chiral purity of the solid phase.

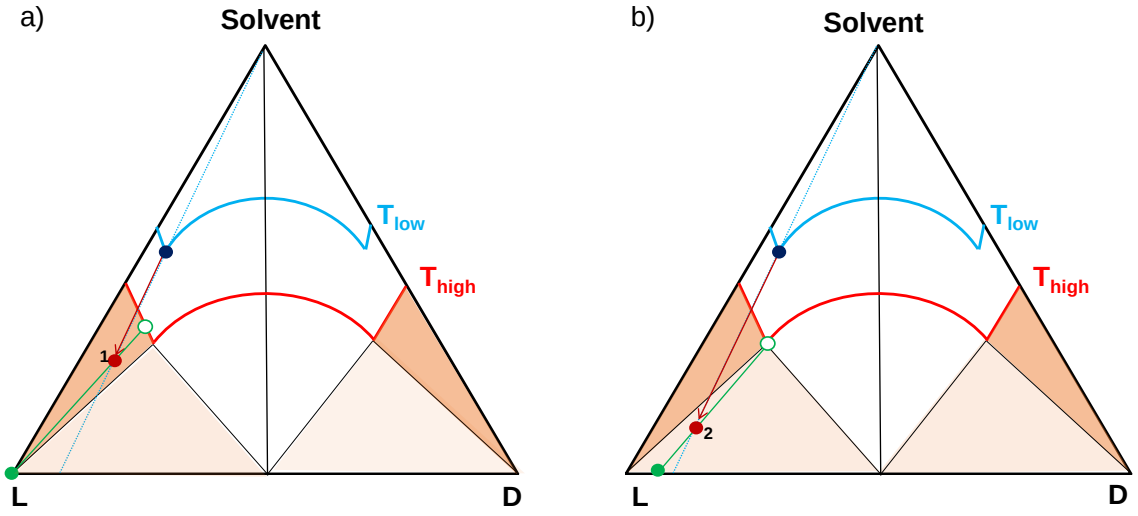

Figure A. 3 Representation of the composition evolution during the separation experiment by evaporation of the solvent. Two different temperatures (T_{low} and T_{high}, *i.e.* 1°C and 60°C) are considered. Starting from an enantiomerically enriched solution (blue dot on the eutectic composition at T_{low} in both figures) the system is placed in the 2-phase region at T_{high} (red dot labelled 1) (a) or into the 3-phase region (red dot labelled 2) (b).

The red arrows show the trajectory of the composition during the evaporation process. The green tie lines specify the equilibrium compositions of coexisting solid and liquid phases of the resulting system at the given temperature (T_{high} here).

Two experimental runs have been performed in a 350 mL crystallizer, as described in the experimental description (section 3.3.4), consisting in the variation of the amount of water to evaporate during the process. The experimental conditions of the two experiments exploiting the evaporation of a selected amount of water are summarized in Table A.1

Table A. 1 Experimental conditions of the selective crystallization experiments of L-methionine exploiting the strategy 1.

experiment	1	2
$m_{DL\text{-methionine}}$ (g)	1.32	1.32
$m_{D\text{-methionine}}$ (g)	10.39	10.38
$m_{solvent}$ (g)	300	300
$m_{solvent\ evaporated}$ (g)	170	260

The first experiment consisted in crystallizing solely the target enantiomer L-methionine from the solution. Starting from a solution at composition x_{eu}=0.94, 170 g water have been evaporated at 60°C under vacuum, leading the system into the outer left biphasic domain (red dot labelled 1 in the outer red region, Figure A.3a). As the solution is supersaturated, crystallization in the system can be expected. Considering that the system is located in the 2-phase region, pure L-methionine can be observed at the solid state in equilibrium with a saturated solution. The composition of the latter is defined by the isotherm at high temperature. In particular, the composition of the solid is represented by the green dot at the pure L-methionine corner, while the composition of the mother liquor is given by the green empty dot in Figure A.3a. Following this procedure, a further experiment was performed with the intention to locate the system into the 3-phase region thus demonstrating the potential of the knowledge of the ternary phase diagram in designing the separation process. Starting from a solution of methionine enantiomers in water at the same composition as for the previous experiment (blue dot in Figure A.3b), an amount of 260 g of water was evaporated. The resulting system corresponds to the red dot labelled 2 in Figure A.3b. As the system is located into the 3-phase domain, an enriched solid with respect to the most abundant enantiomer can be collected, while the remaining liquid

phase results at the eutectic composition at the final operative temperature, T_{high}, 60°C here.

The results of both experiments are illustrated in Figure A.4. As shown, the starting point of both experiments is represented by the blue dot on the eutectic composition of the solubility isotherm at 1°C. Then, the evaporation of a targeted amount of water in experiment 1, led the system into the 2-phase region (red dot labelled 1, Figure A.4). The HPLC analysis of the solid phase showed a chiral purity of >99.9 % L-methionine. The evaporation of a higher amount of water in experiment 2 allowed to locate the system on the boundary of the 3-phase region (red dot labelled 2, Figure A.4) and HPLC analysis defined the chiral purity of the separated solid phase to 96 % L-methionine.

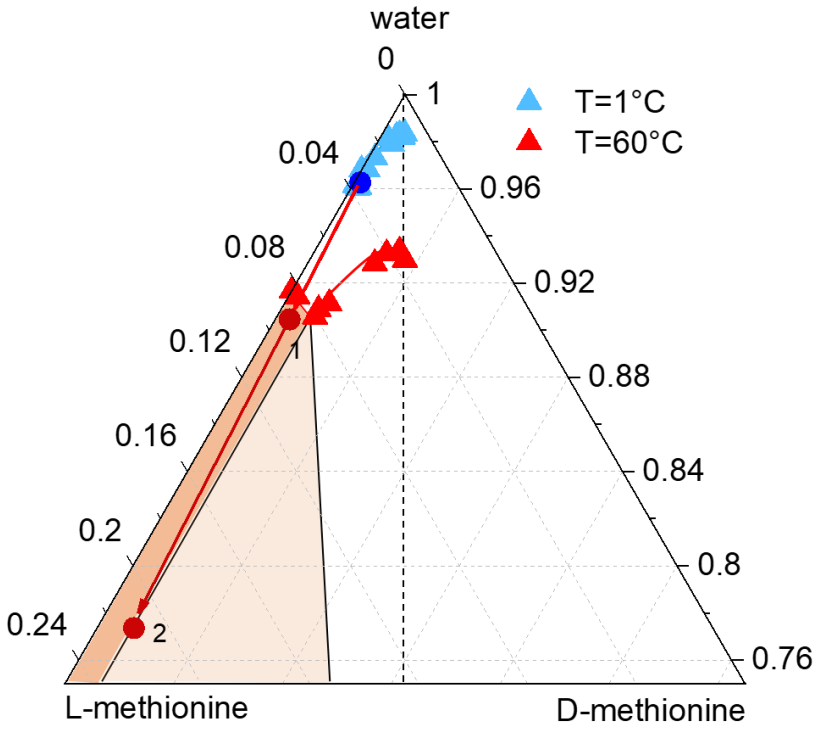

Figure A. 4 Representation of the results of the evaporation experiments within the ternary phase diagram of methionine enantiomers in water. Only the upper 25% and solubility isotherms at 1°C and 60°C are shown. Isotherm lines are guides to the eyes. The red arrows show the trajectories of the composition during the separation processes (compare with Figure A.3a and b).

The experimental results clearly demonstrate how the understanding of the ternary phase diagrams for the studied system allows a rational design of the separation process. The evaporation of a predetermined amount of water permits to predict not only the phase-

domain in which the system is eventually placed, but also the chiral purity of the solid state as well as the solution composition.

A.3 Selective dissolution of DL-methionine: strategy 2

The second strategy consists in the addition of a selected amount of water to a solid mixture of methionine enantiomers. The initial solid mixture is at the eutectic composition at low temperature (blue dot, Figure A.5). By adding a targeted amount of water at constant temperature (T_{high}=60°C) to the initial solid mixture, it is possible to place the system either in the 3-phase region (Figure A.5a) or in the 2-phase region (Figure A.5b) of the corresponding solubility isotherm. The points labelled 1 and 1` in Figure A.5a correspond to two replicates carried out by adding different amounts of water and remaining in the 3-phase region. It can be observed that when the system is placed in the 3-phase region, the mother liquor composition is fixed at the eutectic composition on the solubility isotherm, while the enantiomeric composition of the solid phase can vary. On the other hand, when the system is placed in the 2-phase region (Figure A.5b), the separation yields pure solid enantiomer, while the composition of the saturated liquid phase given on the related solubility isotherm can vary.

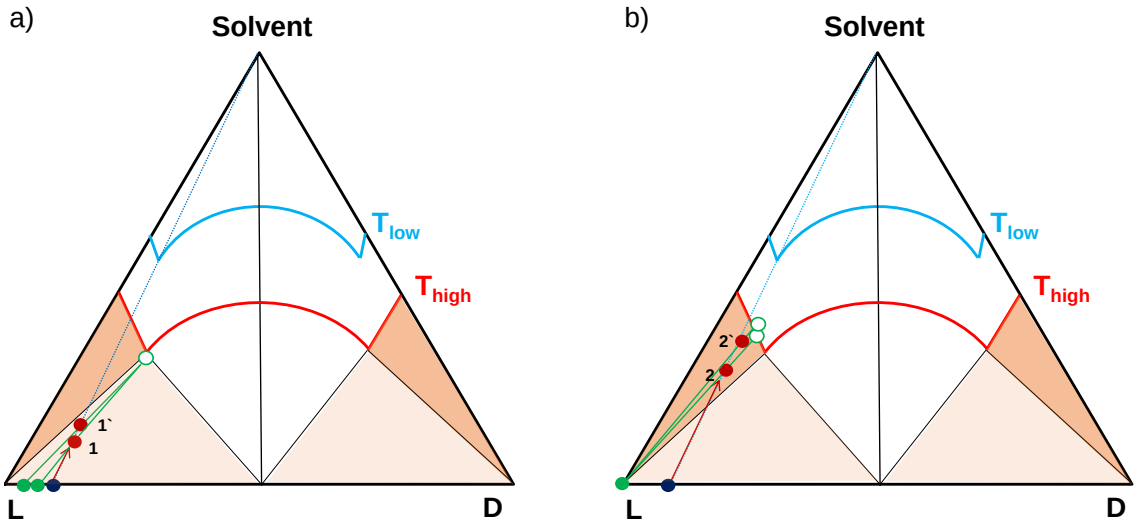

Figure A. 5 Representation of the composition evolution during a separation experiment by addition of solvent. Two different temperatures (T_{low} and T_{high}, *i.e.* 1°C and 60°C) are considered. Starting from an enriched solid mixture of L- and D- enantiomers (blue dots at the bottom coordinate in both figures), the system is placed in the 3-phase region (red dots labelled 1 and 1`) (a) or in the 2-phase region (red dots labelled 2 and 2`) (b). The red arrows show the trajectory of the composition during the solvent addition process. The

green tie lines specify the equilibrium composition of coexisting solid and liquid phases of the resulting system at the given temperature (T_{high} here).

The experiments were carried out in 20 mL vials equipped with a magnetic stirrer bar and located in a 200 mL double wall vessel connected to a thermostat for temperature control. The starting point of the experiments was a solid mixture of the methionine enantiomers of composition x_{eu}=0.94. After addition of the desired amount of water and equilibration at 60°C under stirring, the solution was filtrated under vacuum and both, solid and liquid phase, were analyzed by HPLC for composition. Table A.2 summarizes the experimental conditions of the two sets of experiments and Figure A.6 shows the results obtained.

Table A. 2 Experimental conditions of the selective dissolution experiments of DL-methionine exploiting the strategy 2.

Experiment	1	1´	2	2´
$m_{DL\text{-}methionine}$ (g)	0.25	0.20	0.01	0.08
$m_{D\text{-}methionine}$ (g)	1.88	1.46	0.71	0.54
C_{final} (g_{solute} /$g_{solution}$)	0.3	0.25	0.14	0.11

Starting from a solid mixture of methionine enantiomers at composition x_{eu}=0.94, a calculated amount of water is added at constant temperature (T=60°C) until a total final concentration, C_{final}, of 0.3 g_{solute} /$g_{solution}$ for the experiment 1 and 0.25 g_{solute} /$g_{solution}$ for the experiment 1` is reached. The overall composition of the system is represented by the red dots 1 and 1` in the 3-phase region of the ternary phase diagram in Figure A.6. The green dots at the bottom line of the diagram in Figure A.6a represent the composition of the solid phases of the two experiments 1 and 1´ after the solid-liquid phase separation, while the corresponding liquid phase compositions refer to the green empty dot on the solubility isotherm at 60°C. HPLC analysis of the solid phases and the mother liquor provided purities of 96.3 % L-methionine and 99.1 % L-methionine for the solid phase and 85.7% L-methionine for the mother liquor, respectively for experiment 1 and 1`. The results indicate that by placing the system in the 3-phase domain, the maximum enantiomeric enrichment expected for the liquid phase corresponds to the eutectic composition at the operating temperature, (x_{eu}=0.86 at T=60°C) while a higher enantiomeric enrichment in the solid phase can be achieved according to the corresponding tie line reached at this temperature.

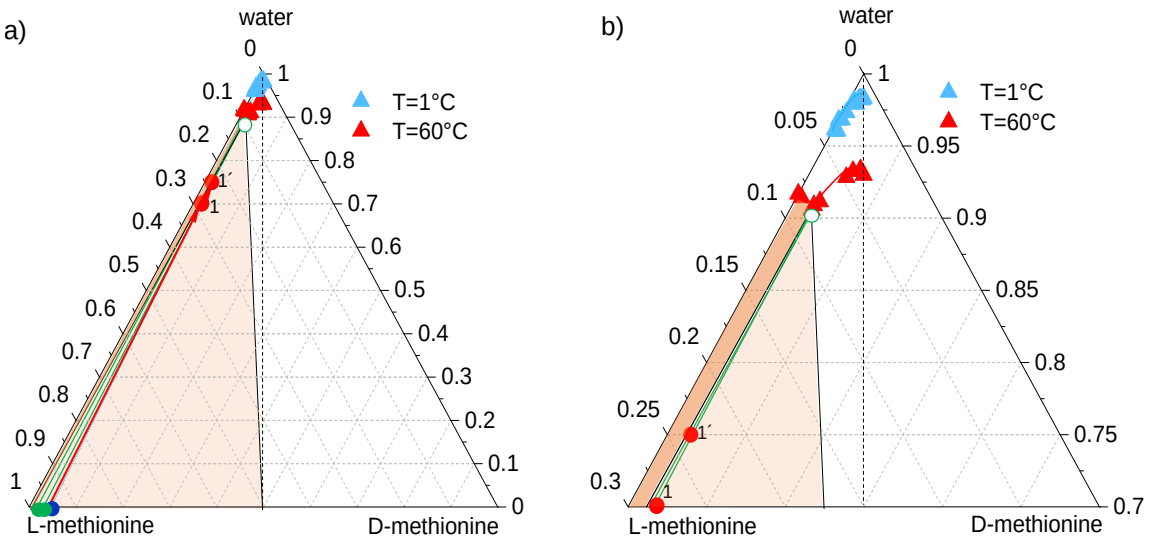

Figure A. 6 Results of the water addition (selective dissolution) experiments in the full experimental ternary phase diagram of methionine enantiomers in water (a) and magnification of the upper 30% (b). The red arrow show the trajectories of the composition during the separation processes. The green lines illustrate the final composition of the solid and liquid phases of the system in equilibrium (compare with Figure A.5a).

The second set of experiments, aimed to explore the 2-phase domain, consists in two experiments labelled 2 and 2` (Figure A.7). After the addition of a calculated amount of water to the initial enantiomerically enriched solid mixture (x_{eu}=0.94), the system is placed into the 2-phase domain, reaching a total final concentration of 0.14 g_{solute} /$g_{solution}$ for the experiment 2 and 0.11 g_{solute} /$g_{solution}$ for the experiment 2` (red dots in the 2-phase domain in Figure 5.7). The HPLC analysis confirmed the production of pure L-methionine (>99.9 %) at the solid state in both experiments 2 and 2´, while the liquid phase resulted enriched to 91.1 % and 93.3 % of L-methionine respectively for the experiment 2 and 2´ (green empty dots, Figure A.7). As demonstrated, pure enantiomer is produced when the system is located into the 2-phase domain, while the maximum achievable purity in the liquid phase is defined by the solubility isotherm at the operative temperature.

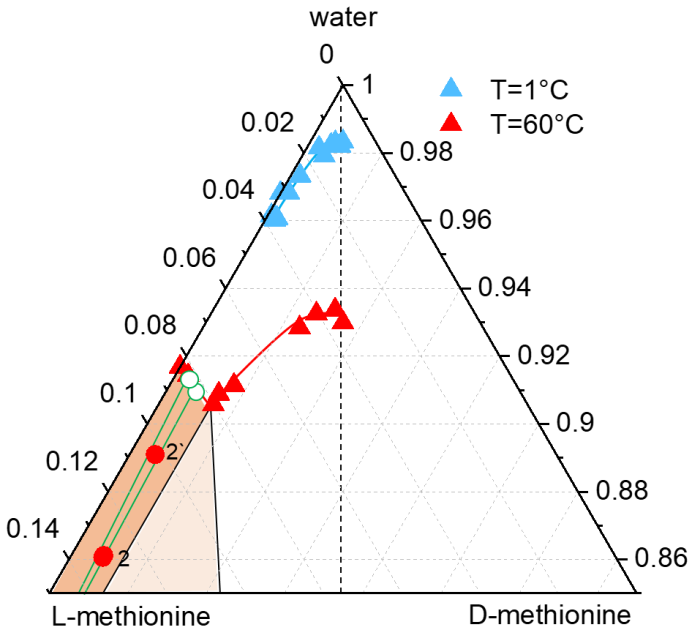

Figure A. 7 Results of the water addition (selective dissolution) experiments in the experimental ternary phase diagram of methionine enantiomers in water. Only the upper 15% and solubility isotherms at 1°C and 60°C are shown. The green lines are part of the tie lines and illustrate the final composition of the liquid phase of the system (compare with Figure A.5b).

The results presented are in agreement with the theoretical description of the process provided in Figure A.5a and b, hence demonstrating that a correct interpretation the experimental ternary solubility diagram is a powerful tool for separation of enantiomers, specifically for racemic compound forming systems exhibiting the shift of the eutectic composition in solution as a function of the temperature.

References

1. Eichelbaum, M. & Gross, A. S. Stereochemical aspects of drug action and disposition. *Advances in Drug Research* (1996). doi:10.1016/s0065-2490(96)80003-7
2. Mane, S. Racemic drug resolution: A comprehensive guide. *Analytical Methods* (2016). doi:10.1039/c6ay02015a
3. de la Torre, B. G. & Albericio, F. The pharmaceutical industry in 2018. An analysis of FDA drug approvals from the perspective of molecules. *Molecules* (2019). doi:10.3390/molecules24040809
4. De Camp, W. H. The FDA perspective on the development of stereoisomers. *Chirality* (1989). doi:10.1002/chir.530010103
5. Kagan, H. B. Asymmetric Synthesis : I - Fundamentals and Recent Advances II - Some Aspects of Asymmetric Catalysis with Transition - Metal Complexes. in *Chemical Synthesis* (1996). doi:10.1007/978-94-009-0255-8_1
6. Mosher, H. S. & Morrison, J. D. Current status of asymmetric synthesis. *Science* (1983). doi:10.1126/science.221.4615.1013
7. Green, B. S., Lahav, M. & Rabinovich, D. Asymmetric Synthesis via Reactions in Chiral Crystals. *Accounts of Chemical Research* (1979). doi:10.1021/ar50138a001
8. Gawley, R. & Aubé, J. *Principles of Asymmetric Synthesis*. *Principles of Asymmetric Synthesis* (2012). doi:10.1016/C2009-0-06104-2
9. Crosby, J. Synthesis of optically active compounds: A large scale perspective. *Tetrahedron* (1991). doi:10.1016/S0040-4020(01)80950-9
10. Kagan, H. B. & Fiaud, J. C. Kinetic Resolution. in *Topics in Stereochemistry* (2007). doi:10.1002/9780470147276.ch4
11. Keith, J. M., Larrow, J. F. & Jacobsen, E. N. Practical Considerations in Kinetic Resolution Reactions. *Advanced Synthesis and Catalysis* (2001). doi:10.1002/1615-4169(20010129)343:1<5::AID-ADSC5>3.0.CO;2-I
12. Nakano, K. & Kitamura, M. Dynamic Kinetic Resolution (DKR). in *Separation of Enantiomers: Synthetic Methods* (2014). doi:10.1002/9783527650880.ch5
13. Ahn, Y., Ko, S. B., Kim, M. J. & Park, J. Racemization catalysts for the dynamic kinetic resolution of alcohols and amines. *Coordination Chemistry Reviews* (2008). doi:10.1016/j.ccr.2007.09.009
14. Toda, F. *Enantiomer Separation Fundamentals and Practical Methods* (2004). doi:10.1007/978-1-4020-2337-8

15. Okamoto, Y. & Ikai, T. Chiral HPLC for efficient resolution of enantiomers. *Chemical Society Reviews* (2008). doi:10.1039/b808881k
16. Patil, R. A., Weatherly, C. A. & Armstrong, D. W. Chiral gas chromatography. in *Chiral Analysis: Advances in Spectroscopy, Chromatography and Emerging Methods: Second Edition* (2018). doi:10.1016/B978-0-444-64027-7.00012-4
17. Schurig, V. Separation of enantiomers by gas chromatography. *Journal of Chromatography A* (2001). doi:10.1016/S0021-9673(00)00505-7
18. Schurig, V. Chiral separations using gas chromatography. *TrAC - Trends in Analytical Chemistry* (2002). doi:10.1016/S0165-9936(02)00808-7
19. Jung, M. & Schurig, V. Extending the scope of enantiomer separation by capillary supercritical fluid chromatography on immobilized polysiloxane-anchored permethyl-β-cyclodextrin (Chirasil-Dex). *Journal of High Resolution Chromatography* (1993). doi:10.1002/jhrc.1240160403
20. Yashima, E. Polysaccharide-based chiral stationary phases for high-performance liquid chromatographic enantioseparation. *Journal of Chromatography A* (2001). doi:10.1016/S0021-9673(00)00501-X
21. Ye, J., Wu, J. & Liu, W. Enantioselective separation and analysis of chiral pesticides by high-performance liquid chromatography. *TrAC - Trends in Analytical Chemistry* (2009). doi:10.1016/j.trac.2009.07.008
22. Aboul-Enein, H. Y., El-Awady, M. I., Heard, C. M. & Nicholls, P. J. Application of thin-layer chromatography in enantiomeric chiral analysis - An overview. *Biomedical Chromatography* (1999). doi:10.1002/(SICI)1099-0801(199912)13:8<531::AID-BMC921>3.0.CO;2-Q
23. Del Bubba, M., Checchini, L. & Lepri, L. Thin-layer chromatography enantioseparations on chiral stationary phases: A review. *Analytical and Bioanalytical Chemistry* (2013). doi:10.1007/s00216-012-6514-5
24. Rajendran, A., Paredes, G. & Mazzotti, M. Simulated moving bed chromatography for the separation of enantiomers. *Journal of Chromatography A* (2009). doi:10.1016/j.chroma.2008.10.075
25. Juza, M., Mazzotti, M. & Morbidelli, M. Simulated moving-bed chromatography and its application to chirotechnology. *Trends in Biotechnology* (2000). doi:10.1016/S0167-7799(99)01419-5
26. Afonso, C. A. M. & Crespo, J. G. Recent advances in chiral resolution through membrane-based approaches. *Angewandte Chemie - International Edition* (2004).

doi:10.1002/anie.200460037

27. Xie, R., Chu, L. Y. & Deng, J. G. Membranes and membrane processes for chiral resolution. *Chemical Society Reviews* (2008). doi:10.1039/b713350b
28. Hoek, E. M. V., Tarabara, V. V., Yoshikawa, M. & Higuchi, A. Enantioselective Membranes. in *Encyclopedia of Membrane Science and Technology* (2013). doi:10.1002/9781118522318.emst131
29. Wang, Y. & Chen, A. M. Enantioenrichment by Crystallization. *Organic Process Research and Development* (2008). doi:10.1021/op700239a
30. Wang, Y. & Chen, A. Crystallization-Based Separation of Enantiomers. in *Stereoselective Synthesis of Drugs and Natural Products* (2013). doi:10.1002/9781118596784.ssd056
31. Simon, M., Wood, B., Ferguson, S., Glennon, B. & Jones, R. C. Diastereomeric salt crystallization of chiral molecules via sequential coupled-Batch operation. *AIChE Journal* (2019). doi:10.1002/aic.16466
32. Pham, X. H., Kim, J. M., Chang, S. M., Kim, I. ho & Kim, W. S. Enantioseparation of D/L-mandelic acid with L-phenylalanine in diastereomeric crystallization. *Journal of Molecular Catalysis B: Enzymatic* (2009). doi:10.1016/j.molcatb.2008.12.023
33. Coquerel, G. Preferential crystallization. *Topics in Current Chemistry* (2006). doi:10.1007/128_2006_077
34. Levilain, G. & Coquerel, G. Pitfalls and rewards of preferential crystallization. *CrystEngComm* (2010). doi:10.1039/c001895c
35. Viedma, C., Coquerel, G. & Cintas, P. *Crystallization of Chiral Molecules*. *Handbook of Crystal Growth: Second Edition* **1**, (Elsevier B.V., 2015).
36. Gal, J. Molecular chirality in chemistry and biology: Historical milestones. *Helvetica Chimica Acta* **96**, 1617–1657 (2013).
37. Knudsen, O. Lord kelvin, baltimore lectures on mathematical physics ((1884), 1904). in *Landmark Writings in Western Mathematics 1640-1940* (2005). doi:10.1016/B978-044450871-3/50139-X
38. International Union of Pure and Applied Chemistry *Rules for the Nomenclature of Organic Chemistry* **45**, (1976).
39. Cahn, R. S. An Introduction to the Sequence Rule A system for the specification of absolute configuration. *Journal of Chemical Education* **1**, 116–125 (1964).
40. Smith, S. W. Chiral toxicology: It's the same thing only different. *Toxicological Sciences* (2009). doi:10.1093/toxsci/kfp097

41. Roozeboom, H. W. B. Löslichkeit und Schmelzpunkt als Kriterien für racemische Verbindungen, pseudoracemische Mischkrystalle und inaktive Konglomerate. *Zeitschrift für Physikalische Chemie* (2017). doi:10.1515/zpch-1899-2832
42. Jaques, J., Collet, A. and S. H. Wilen. *Enantiomers, Racemates, and Resolutions* (1982).
43. Lorenz, H., Polenske, D. & Seidel-Morgenstern, A. Application of preferential crystallization to resolve racemic compounds in a hybrid process. *Chirality* (2006). doi:10.1002/chir.20327
44. Srisanga, S. & Ter Horst, J. H. Racemic compound, conglomerate, or solid solution: Phase diagram screening of chiral compounds. *Crystal Growth and Design* (2010). doi:10.1021/cg901483v
45. Galland, A. *et al.* Spotting conglomerates by second harmonic generation. in *Crystal Growth and Design* (2009). doi:10.1021/cg801356m
46. Simon, F., Clevers, S., Dupray, V. & Coquerel, G. Relevance of the Second Harmonic Generation to Characterize Crystalline Samples. *Chemical Engineering and Technology* (2015). doi:10.1002/ceat.201400756
47. Simon, F. *et al.* Enhanced second harmonic generation from an organic self-assembled eutectic binary mixture: A case study with 3-nitrobenzoic and 3,5-dinitrobenzoic acids. *Crystal Growth and Design* (2015). doi:10.1021/cg5017565
48. Nguyen, L. A., He, H. & Pham-Huy, C. Chiral drugs: an overview. *International journal of biomedical science : IJBS* (2006).
49. Willia, K. & Lee, E. Importance of Drug Enantiomers in Clinical Pharmacology. *Drugs* (1985). doi:10.2165/00003495-198530040-00003
50. Mitchell, T. B. *et al.* Subjective and physiological responses among racemic-methadone maintenance patients in relation to relative (S)- vs. (R)-methadone exposure. *British Journal of Clinical Pharmacology* **58**, 609–617 (2004).
51. Asatsuma-Okumura, T., Ito, T. & Handa, H. Molecular mechanisms of the teratogenic effects of thalidomide. *Pharmaceuticals* (2020). doi:10.3390/ph13050095
52. Kim, J. H. & Scialli, A. R. Thalidomide: The tragedy of birth defects and the effective treatment of disease. *Toxicological Sciences* (2011). doi:10.1093/toxsci/kfr088
53. Islam, M. R., Mahdi, J. G. & Bowen, I. D. Pharmacological importance of stereochemical resolution of enantiomeric drugs. *Drug Safety* (1997). doi:10.2165/00002018-199717030-00002

54. Nation, R. L. Chirality in New Drug Development: Clinical Pharmacokinetic Considerations. *Clinical Pharmacokinetics* **27**, 249–255 (1994).
55. H. Brooks, W., C. Guida, W. & G. Daniel, K. The Significance of Chirality in Drug Design and Development. *Current Topics in Medicinal Chemistry* (2011). doi:10.2174/156802611795165098
56. Myerson, A. *Handbook of Industrial Crystallization* (2002). doi:10.1016/b978-0-7506-7012-8.x5000-9
57. Mullin, J. W. Solutions and solubility. in *Crystallization* (2001). doi:10.1016/b978-075064833-2/50005-x
58. Vedantam, S. & Ranade, V. V. Crystallization: Key thermodynamic, kinetic and hydrodynamic aspects. *Sadhana - Academy Proceedings in Engineering Sciences* **38**, 1287–1337 (2013).
59. ter Horst, J. H., Schmidt, C. & Ulrich, J. Fundamentals of Industrial Crystallization. in *Handbook of Crystal Growth: Bulk Crystal Growth: Second Edition* (2015). doi:10.1016/B978-0-444-63303-3.00032-8
60. Lorenz, H. Solubility and Solution Equilibria in Crystallization. in *Crystallization: Basic Concepts and Industrial Applications* (2013). doi:10.1002/9783527650323
61. Nývlt, J. Kinetics of nucleation in solutions. *Journal of Crystal Growth* (1968). doi:10.1016/0022-0248(68)90179-6
62. Ulrich, J. & Strege, C. Some aspects of the importance of metastable zone width and nucleation in industrial crystallizers. *Journal of Crystal Growth* **237**–**239**, 2130–2135 (2002).
63. Mullin, J. W. *Crystallization (4th Ed.)*. *Oxford: Butterworth Heinemann* (2001).
64. Erdemir, D., Lee, A. Y. & Myerson, A. S. Nucleation of crystals from solution: Classical and two-step models. *Accounts of Chemical Research* (2009). doi:10.1021/ar800217x
65. Vekilov, P. G. The two-step mechanism of nucleation of crystals in solution. *Nanoscale* (2010). doi:10.1039/c0nr00628a
66. Vekilov, P. G. Nucleation. *Crystal Growth and Design* (2010). doi:10.1021/cg1011633
67. Maggioni, G. M. & Mazzotti, M. Modelling the stochastic behaviour of primary nucleation. *Faraday Discussions* (2015). doi:10.1039/c4fd00255e
68. Vetter, T., Iggland, M., Ochsenbein, D. R., Hänseler, F. S. & Mazzotti, M. Modeling nucleation, growth, and ostwald ripening in crystallization processes: A comparison

between population balance and kinetic rate equation. *Crystal Growth and Design* (2013). doi:10.1021/cg4010714

69. Gmehling, J., Wittig, R., Lohmann, J. & Joh, R. A modified UNIFAC (Dortmund) model. 4. Revision and extension. *Industrial and Engineering Chemistry Research* (2002). doi:10.1021/ie0108043
70. Gmehling, J. G., Anderson, T. F. & Prausnitz, J. M. Solid-Liquid Equilibria Using UNIFAC. *Industrial and Engineering Chemistry Fundamentals* (1978). doi:10.1021/i160068a008
71. Barrett, P. & Glennon, B. Characterizing the metastable zone width and solubility curve using lasentec FBRM and PVM. *Chemical Engineering Research and Design* (2002). doi:10.1205/026387602320776876
72. Diaz-Muñoz, G., Miranda, I. L., Sartori, S. K., de Rezende, D. C. & Alves Nogueira Diaz, M. Use of chiral auxiliaries in the asymmetric synthesis of biologically active compounds: A review. *Chirality* **31**, 776–812 (2019).
73. Lorenz, H. & Seidel-Morgenstern, A. Processes to separate enantiomers. *Angewandte Chemie - International Edition* **53**, 1218–1250 (2014).
74. Noyori, R. Asymmetric Catalysis: Science and Opportunities (Nobel Lecture 2001). *Advanced Synthesis and Catalysis* **345**, 15–32 (2003).
75. Grinberg, N. & Thompson, R. Chiral Separations by HPLC. in *Encyclopedia of Chromatography* (2020). doi:10.1201/noe0824727857-68
76. Gübitz, G. & Schmid, M. G. Chiral separation principles in chromatographic and electromigration techniques. *Molecular Biotechnology* **32**, 159–179 (2006).
77. Wang, Y. *et al.* Recent progress on chiral resolution of pharmaceuticals by crystallization. *Huagong Xuebao/CIESC Journal* (2019). doi:10.11949/0438-1157.20190718
78. Levilain, G. & Coquerel, G. Pitfalls and rewards of preferential crystallization. *CrystEngComm* (2010). doi:10.1039/c001895c
79. Kostyanovsky, R. G. Louis Pasteur did it for us especially. *Mendeleev Communications* (2003). doi:10.1070/MC2003v013n03ABEH001828
80. Collet, A., Brienne, M. josèphe & Jacques, J. Optical Resolution by Direct Crystallization of Enantiomer Mixtures. *Chemical Reviews* **80**, 215–230 (1980).
81. Sögütoglu, L. C., Steendam, R. R. E., Meekes, H., Vlieg, E. & Rutjes, F. P. J. T. Viedma ripening: A reliable crystallisation method to reach single chirality. *Chemical Society Reviews* (2015). doi:10.1039/c5cs00196j

82. Suwannasang, K., Flood, A. E., Rougeot, C. & Coquerel, G. Using programmed heating-cooling cycles with racemization in solution for complete symmetry breaking of a conglomerate forming system. *Crystal Growth and Design* (2013). doi:10.1021/cg400436r
83. Murray, J. I., Sanders, J. N., Richardson, P. F., Houk, K. N. & Blackmond, D. G. Isotopically Directed Symmetry Breaking and Enantioenrichment in Attrition-Enhanced Deracemization. *Journal of the American Chemical Society* (2020). doi:10.1021/jacs.9b11422
84. Schoen, H. M., Grove, C. S. & Palermo, J. A. The early history of crystallization. *Journal of Chemical Education* **33**, 373–375 (1956).
85. Bohm, J. The history of crystal growth. *Acta Physica Hungarica* **57**, 161–178 (1985).
86. Chen, J., Sarma, B., Evans, J. M. B. & Myerson, A. S. Pharmaceutical crystallization. *Crystal Growth and Design* **11**, 887–895 (2011).
87. Variankaval, N., Cote, A. S. & Doherty, M. F. From form to function: Crystallization of active pharmaceutical ingredients. *AIChE Journal* (2008). doi:10.1002/aic.11555
88. Hilfiker, Rolf; Raumer von, M. Polymorphism in the Pharmaceutical Industry: Solid Form and Drug Development. *Wiley.com* (2019).
89. Bernstein, J. *Polymorphism in Molecular Crystals*. *Polymorphism in Molecular Crystals* (2010). doi:10.1093/acprof:oso/9780199236565.001.0001
90. Gao, Z., Rohani, S., Gong, J. & Wang, J. Recent Developments in the Crystallization Process: Toward the Pharmaceutical Industry. *Engineering* (2017). doi:10.1016/J.ENG.2017.03.022
91. Shekunov, B. Y. & York, P. Crystallization processes in pharmaceutical technology and drug delivery design. *Journal of Crystal Growth* **211**, 122–136 (2000).
92. Davey, R. & Garside, J. *From Molecules to Crystallizers: An Introduction to Crystallization*. *Oxford Science* (2000).
93. Orehek, J., Teslic, D. & Likozar, B. Continuous crystallization processes in pharmaceutical manufacturing: A review. *Organic Process Research and Development* (2021). doi:10.1021/acs.oprd.0c00398
94. Wood, B., Girard, K. P., Polster, C. S. & Croker, D. M. Progress to Date in the Design and Operation of Continuous Crystallization Processes for Pharmaceutical Applications. *Organic Process Research and Development* **23**, 122–144 (2019).
95. Gao, Z., Wu, Y., Gong, J., Wang, J. & Rohani, S. Continuous crystallization of α-form L-glutamic acid in an MSMPR-Tubular crystallizer system. *Journal of Crystal*

Growth (2019). doi:10.1016/j.jcrysgro.2018.07.007

96. Agnew, L. R. *et al.* Continuous Crystallization of Paracetamol (Acetaminophen) Form II: Selective Access to a Metastable Solid Form. *Crystal Growth and Design* (2017). doi:10.1021/acs.cgd.6b01831
97. Lai, T. T. C. *et al.* Control of Polymorphism in Continuous Crystallization via Mixed Suspension Mixed Product Removal Systems Cascade Design. *Crystal Growth and Design* (2015). doi:10.1021/acs.cgd.5b00466
98. Briggs, N. E. B. *et al.* Seeded Crystallization of β- L -Glutamic Acid in a Continuous Oscillatory Baffled Crystallizer. *Organic Process Research and Development* (2015). doi:10.1021/acs.oprd.5b00206
99. Alvarez, A. J. & Myerson, A. S. Continuous plug flow crystallization of pharmaceutical compounds. *Crystal Growth and Design* (2010). doi:10.1021/cg901496s
100. Cascella, F., Temmel, E., Seidel-Morgenstern, A. & Lorenz, H. Efficient Resolution of Racemic Guaifenesin via Batch-Preferential Crystallization Processes. *Organic Process Research and Development* (2020). doi:10.1021/acs.oprd.9b00413
101. Petruševska-Seebach, K., Seidel-Morgenstern, A. & Elsner, M. P. Preferential crystallization of l -asparagine in water. *Crystal Growth and Design* (2011). doi:10.1021/cg101408e
102. Le Minh, T., Lorenz, H. & Seidel-Morgenstern, A. Enantioselective Crystallization Exploiting the Shift of Eutectic Compositions in Solid-Liquid Phase Diagrams. *Chemical Engineering and Technology* (2012). doi:10.1002/ceat.201100689
103. Cascella, F., Seidel-Morgenstern, A. & Lorenz, H. Exploiting Ternary Solubility Phase Diagrams for Resolution of Enantiomers: An Instructive Example. *Chemical Engineering and Technology* (2020). doi:10.1002/ceat.201900421
104. Dunn, A. S., Svoboda, V., Sefcik, J. & Ter Horst, J. H. Resolution Control in a Continuous Preferential Crystallization Process. *Organic Process Research and Development* (2019). doi:10.1021/acs.oprd.9b00275
105. Elsner, M. P., Ziomek, G. & Seidel-Morgenstern, A. Simultaneous preferential crystallization in a coupled, batch operation mode-Part I: Theoretical analysis and optimization. *Chemical Engineering Science* (2007). doi:10.1016/j.ces.2007.05.035
106. Elsner, M. P., Ziomek, G. & Seidel-Morgenstern, A. Simultaneous preferential crystallization in a coupled batch operation mode. Part II: Experimental study and model refinement. *Chemical Engineering Science* (2011).

doi:10.1016/j.ces.2010.12.035

107. Temmel, E., Eicke, M. J., Cascella, F., Seidel-Morgenstern, A. & Lorenz, H. Resolution of Racemic Guaifenesin Applying a Coupled Preferential Crystallization-Selective Dissolution Process: Rational Process Development. *Crystal Growth and Design* (2019). doi:10.1021/acs.cgd.8b01660
108. Levilain, G., Eicke, M. J. & Seidel-Morgenstern, A. Efficient resolution of enantiomers by coupling preferential crystallization and dissolution. Part 1: Experimental proof of principle. *Crystal Growth and Design* (2012). doi:10.1021/cg3009943
109. Hein, J. E., Cao, B. H., Van Der Meijden, M. W., Leeman, M. & Kellogg, R. M. Resolution of omeprazole using coupled preferential crystallization: Efficient separation of a nonracemizable conglomerate salt under near-equilibrium conditions. *Organic Process Research and Development* (2013). doi:10.1021/op400081c
110. Jiang, M. & Braatz, R. D. Designs of continuous-flow pharmaceutical crystallizers: Developments and practice. *CrystEngComm* (2019). doi:10.1039/c8ce00042e
111. Temmel, E., Gänsch, J., Seidel-Morgenstern, A. & Lorenz, H. Systematic investigations on continuous fluidized bed crystallization for chiral separation. *Crystals* (2020). doi:10.3390/cryst10050394
112. Binev, D., Seidel-Morgenstern, A. & Lorenz, H. Continuous Separation of Isomers in Fluidized Bed Crystallizers. *Crystal Growth and Design* (2016). doi:10.1021/acs.cgd.5b01513
113. Köllges, T. & Vetter, T. Design and Performance Assessment of Continuous Crystallization Processes Resolving Racemic Conglomerates. *Crystal Growth and Design* (2018). doi:10.1021/acs.cgd.7b01618
114. Galan, K., Eicke, M. J., Elsner, M. P., Lorenz, H. & Seidel-Morgenstern, A. Continuous preferential crystallization of chiral molecules in single and coupled mixed-suspension mixed-product-removal crystallizers. *Crystal Growth and Design* (2015). doi:10.1021/cg501854g
115. Sangwal, K. A novel self-consistent Nývlt-like equation for metastable zone width determined by the polythermal method. *Crystal Research and Technology* (2009). doi:10.1002/crat.200800501
116. Nývlt J., Nucleation. in *The kinetics of industrial crystallization* (1985)
117. Temmel, E., Gänsch, J., Lorenz, H. & Seidel-Morgenstern, A. Measurement and

Evaluation of the Crystallization Kinetics of l -Asparagine Monohydrate in the Ternary l -/ d -Asparagine/Water System. *Crystal Growth and Design* (2018). doi:10.1021/acs.cgd.8b01322

118. Shimura, T. & Kemp, A. I. S. Tetrahedral plot diagram: A geometrical solution for quaternary systems. *American Mineralogist* (2015). doi:10.2138/am-2015-5371
119. Jarvis, B. & Simpson, K. A Review of its Use in the Prevention of Atherothrombosis. **60**, 347–377 (2000).
120. Bianchi, S. United States Patent. **2**, (2004).
121. An, J. H., Kiyonga, A. N., Lee, E. H. & Jung, K. Simple and efficient spherical crystallization of clopidogrel bisulfate form-i via anti-solvent crystallization method. *Crystals* **9**, 1–13 (2019).
122. Saeed, A. *et al.* Developments in the synthesis of the antiplatelet and antithrombotic drug (S)-clopidogrel. *Chirality* (2017). doi:10.1002/chir.22742
123. Madivada, L. R., Anumala, R. R., Gilla, G., Kagga, M. & Bandichhor, R. An efficient and large scale synthesis of Clopidogrel: Antiplatelet drug. *Der Pharma Chemica* (2012).
124. Antic, D., Filipic, S., Ivkovic, B., Nikolic, K. & Agbaba, D. Direct separation of clopidogrel enantiomers by reverse-phase planar chromatography method using β-cyclodextrin as a chiral mobile phase additive. *Acta Chromatographica* **23**, 235–245 (2011).
125. Van Der Meijden, M. W. *et al.* Attrition-enhanced deracemization in the synthesis of clopidogrel - A practical application of a new discovery. *Organic Process Research and Development* **13**, 1195–1198 (2009).
126. Noorduin, W. L. *et al.* Scaling Up attrition-enhanced deracemization by use of an industrial bead mill in a route to clopidogrel (Plavix). *Organic Process Research and Development* **14**, 908–911 (2010).
127. Rodrigo, A. A., Lorenz, H. & Seidel-Morgenstern, A. Online monitoring of preferential crystallization of enantiomers. *Chirality* (2004). doi:10.1002/chir.20067
128. Breveglieri, F., Maggioni, G. M. & Mazzotti, M. Deracemization of NMPA via Temperature Cycles. *Crystal Growth and Design* **18**, 1873–1881 (2018).
129. Smith, G. G. & Sivakua, T. Mechanism of the Racemization of Amino Acids. Kinetics of Racemization of Arylglycines. *Journal of Organic Chemistry* (1983). doi:10.1021/jo00153a001
130. Smith, G. G. & Reddy, G. V. Effect of the Side Chain on the Racemization of Amino

Acids in Aqueous Solution. *Journal of Organic Chemistry* (1989). doi:10.1021/jo00280a017

131. Dicpinigaitis, P. V., Gayle, Y. E., Solomon, G. & Gilbert, R. D. Inhibition of cough-reflex sensitivity by benzonatate and guaifenesin in acute viral cough. *Respiratory Medicine* (2009). doi:10.1016/j.rmed.2008.12.008
132. Maher, H. M., Al-Taweel, S. M., Alshehri, M. M. & Alzoman, N. Z. Novel stereoselective high-performance liquid chromatographic method for simultaneous determination of guaifenesin and ketorolac enantiomers in human plasma. *Chirality* (2014). doi:10.1002/chir.22354
133. Albrecht, H. H., Dicpinigaitis, P. V. & Guenin, E. P. Role of guaifenesin in the management of chronic bronchitis and upper respiratory tract infections. *Multidisciplinary Respiratory Medicine* (2017). doi:10.4081/mrm.2017.260
134. Tharunkumar, B., Kalyani, P., Lakshmiprasanna, M. & Nalluri, B. N. Enantioselective analysis of guaifenesin in bulk and pharmaceutical dosage forms by chiral reverse phase HPLC-PDA method. *Indian Drugs* **55**, 36–42 (2018).
135. Yang, Y. *et al.* Separation of guaifenesin enantiomers by simulated moving bed process with four operation modes. *Adsorption* (2019). doi:10.1007/s10450-019-00110-9
136. Samokhin, A. S. *et al.* Supercritical fluid chromatography and its application to analysis and preparation of high-purity compounds. *Russian Journal of Physical Chemistry B* (2012). doi:10.1134/S1990793111080100
137. Gong, R., Lin, X., Li, P., Yu, J. & Rodrigues, A. E. Adsorption equilibrium and kinetic study of guaifenesin enantiomers on cellulose tris 3,5-dimethylphenylcarbamate packed column. *Chemical Engineering Journal* (2014). doi:10.1016/j.cej.2014.01.050
138. Fayzullin, R. R., Lorenz, H., Bredikhina, Z. A., Bredikhin, A. A. & Seidel-Morgenstern, A. Solubility and some crystallization properties of conglomerate forming chiral drug guaifenesin in water. *Journal of Pharmaceutical Sciences* (2014). doi:10.1002/jps.24104
139. Mani, N., Jun, H. W., Beach, J. W. & Nerurkar, J. Solubility of Guaifenesin in the Presence of Common Pharmaceutical Additives. *Pharmaceutical Development and Technology* (2003). doi:10.1081/PDT-120024692
140. Kaduk, J. A. Crystal structure of guaifenesin, 3-(2-methoxyphenoxy)-1,2-propanediol. *Powder Diffraction* (2004). doi:10.1154/1.1725274

141. Bredikhina, Z. A., Novikova, V. G., Zakharychev, D. V. & Bredikhin, A. A. Solid state properties and effective resolution procedure for guaifenesin, 3-(2-methoxyphenoxy)-1,2-propanediol. *Tetrahedron Asymmetry* (2006). doi:10.1016/j.tetasy.2006.10.027
142. Wagner, G., Pardi, A. & Wüthrich, K. Hydrogen Bond Length and 1H NMR Chemical Shifts in Proteins. *Journal of the American Chemical Society* (1983). doi:10.1021/ja00356a056
143. Del Bene, J. E. Hydrogen bond types, binding energies, and1H NMR chemical shifts. *Journal of Physical Chemistry A* (1999). doi:10.1021/jp9920444
144. Arnold, W. D. & Oldfield, E. The chemical nature of hydrogen bonding in proteins via NMR: J-couplings, chemical shifts, and AIM theory. *Journal of the American Chemical Society* (2000). doi:10.1021/ja0025705
145. Richardson, J. F. & Zaki, W. N. Sedimentation and fluidisation: Part I. *Chemical Engineering Research and Design* (1997). doi:10.1016/s0263-8762(97)80006-8
146. Richardson, J. F. & da, M. A. Velocity-voidage relations for sedimentation and fluidisation. *Chemical Engineering Science* (1979). doi:10.1016/0009-2509(79)85167-2
147. Intaraboonrod, K., Lerdwiriyanupap, T., Hoquante, M., Coquerel, G. & Flood, A. E. Temperature cycle induced deracemization. *Mendeleev Communications* (2020). doi:10.1016/j.mencom.2020.07.002
148. Tulashie, S. K., Lorenz, H. & Seidel-Morgenstern, A. Solubility of mandelic acid enantiomers and their mixtures in three chiral solvents. *Journal of Chemical and Engineering Data* (2010). doi:10.1021/je1006955
149. Lorenz, H., Sapoundjiev, D. & Seidel-Morgenstern, A. Enantiomeric mandelic acid system - Melting point phase diagram and solubility in water. *Journal of Chemical and Engineering Data* (2002). doi:10.1021/je0200620
150. Davey, R. J., Schroeder, S. L. M. & Ter Horst, J. H. Nucleation of organic crystals - A molecular perspective. *Angewandte Chemie - International Edition* (2013). doi:10.1002/anie.201204824
151. Kulkarni, C., Berrocal, J. A., Lutz, M., Palmans, A. R. A. & Meijer, E. W. Directing the Solid-State Organization of Racemates via Structural Mutation and Solution-State Assembly Processes. *Journal of the American Chemical Society* (2019). doi:10.1021/jacs.9b00452
152. Lorenz, H., Le Minh, T., Kaemmerer, H., Buchholz, H. & Seidel-Morgenstern, A.

Exploitation of shifts of eutectic compositions in crystallization-based enantioseparation. *Chemical Engineering Research and Design* (2013). doi:10.1016/j.cherd.2013.08.013

153. Willke, T. Methionine production—a critical review. *Applied Microbiology and Biotechnology* (2014). doi:10.1007/s00253-014-6156-y
154. Campbell, K. C. M. *et al.* Prevention of noise- and drug-induced hearing loss with d-methionine. *Hearing Research* (2007). doi:10.1016/j.heares.2006.11.012
155. Klussmann, M. *et al.* Thermodynamic control of asymmetric amplification in amino acid catalysis. *Nature* (2006). doi:10.1038/nature04780
156. Polenske, D. & Lorenz, H. Solubility and metastable zone width of the methionine enantiomers and their mixtures in water. *Journal of Chemical and Engineering Data* (2009). doi:10.1021/je9001834

Appendix

List of abbreviations

AED	Attrition Enhanced Deracemization
API	Active Pharmaceutical Ingredient
CD_3CN	Acetonitrile-d_3
CD_3OD	Methanol-d_4
CIP	Cahn–Ingold–Prelog
CNT	Classical Nucleation Theory
CPCD	Coupled Preferential Crystallization and Dissolution
CPG	Clopidogrel
DBU	1,8-Diazabicyclo[5.4.0]undec-7-en
DSC	Differential Scanning Calorimetry
FBRM	Focused Beam Reflectance Measurement
FTIR	Fourier-Transform Infrared Spectroscopy
GC	Gas Chromatography
HPLC	High-Performance Liquid Chromatography
IUPAC	International Union of Pure and Applied Chemistry
KPI	Key Performance Indicator
MFM	Mass-Flow-Meters
MSMPR	Mixed Suspension Mixed Product Removal
MSZW	Metastable Zone Width
NSAINDs	Nonsteroidal Anti-Inflammatory Drugs
PC	Preferential Crystallization
PFR	Plug Flow Reactor
Pr	Productivity
Pu	Purity
SFC	Supercritical Fluid Chromatography
SHG	Second Harmonic Generation
S	Supersaturation
SvL	Schröder van Laar
TBME	Tert-Butyl methyl ether
TLC	Thin Layer Chromatography

XRPD	X-Ray Powder Diffraction
Y	Yield

List of symbols

a	Activity coefficient
C	Concentration at the initial state
C*	Concentration at the reference state
F	Degree of freedom
G	Gibbs Free energy
H	Enthalpy
l	Liquid phase
m	Mass
N	Number of independent components
P	Number of phases at the equilibrium
R	Gas constant
r	Size of nuclei in the first stage of nucleation
r*	Critical size of nuclei
S	Supersaturation
s	Solid phase
T	Temperature
t	Time
V	Volume
x	Composition

List of Greek symbols

α	Meyerhoffer coefficient
γ	Activity coefficient
δ	Chemical shift
ρ	Density
ϭ	Surface tension

List of subscripts

cart	Cartesian
cell	Related to the densitometer cell
cryst	Related to crystallization conditions
eu	Eutectic composition
H	Related to the proton chemical shift
i	Related to the preferred enantiomer
max	Maximum
R	Related to the R enantiomer
Rac	Racemic compound
S	Related to the S enantiomer
s	Related to the surface free energy
sat	Related to saturation conditions
T	Related to the total free energy of nucleation process
V	Related to the volume free energy
0	At initial conditions

List of superscripts

f	Fusion
intersec	Intersection

List of figures

List of schemes

List of tables